Quantifying three-dimensional cell-scale mechanics in cancer using thermally responsive hydrogel probes

by

Stephanie Mok

Department of Chemical Engineering
McGill University
Montréal, Québec, Canada
October 2020

A thesis submitted to McGill University in partial fulfillment of the requirements to the degree of Doctor of Philosophy

Abstract

The combination of the mechanical properties of the extracellular matrix, the cells and their physical arrangement influences how cells sense and respond to the microenvironment. In diseases such as cancer where metastatic events led by a few cells are responsible for mortality, characterizing how local mechanics change and influence cell behavior can provide an important understanding of disease progression. In this thesis, a novel sensor to measure internal mechanics at cellular length scales, within 3D tumor tissue models was developed. Fluorescently-labelled swellable microgels, called microscale temperature-actuated mechanosensors (μTAMs), were developed as cell-sized mechanosensors that report local mechanics based on their ability to expand within a matrix. These sensors were first used in spheroid cultures and mouse models to reveal local sites of high stiffness in invasive cancers. Similar trends were observed in extended spheroid cultures of a Src inducible cell line where high stiffnesses occurred while the oncogene was constitutively expressed and there was space to grow freely. Histological examination of soft versus stiff localized areas within spheroids revealed distinct differences in morphology suggesting differences in cellular mechanical responses at these regions. Finally, the μTAMs were further developed to extend their capabilities for cell-scale viscoelastic measurements which better describe the early cell response and behavior to mechanical stress. Differences in viscoelastic behaviors at the cellular length scale were identified between invasive and non-invasive cancer spheroids where invasive tissue appear to behave more elastically than viscous behaviors in non-invasive spheroids. Overall, the development of the μTAM sensor allows us to study optically study internal tissue mechanics and has identified highly localized mechanical properties surrounding individual cells that correlate with invasive potential.

Abrégé

La combinaison des propriétés mécaniques de la matrice extracellulaire, des cellules et de leur disposition physique influence la façon dont les cellules détectent le microenvironnement et y réagissent. Dans des maladies telles que le cancer, où les événements métastatiques menés par quelques cellules sont responsables de la mortalité, la caractérisation de la façon dont les mécanismes locaux changent et influencent le comportement des cellules peut permettre de comprendre la progression de la maladie. Dans le cadre de cette thèse, un nouveau senseur a été développé, appelés mécanodétecteurs actionnés par la température à micro-échelle (μTAMs), pour mesurer la mécanique interne à l'échelle de la longueur cellulaire, dans des modèles 3D de tissus tumoraux. Des microgels expansibles marqués par fluorescence ont été mis au point en tant que mécanodétecteurs de la taille d'une cellule, qui rendent compte de la mécanique locale en fonction de leur capacité à s'elargir Ces détecteurs ont d'abord été utilisés dans des cultures sphéroïdes et des modèles de souris pour révéler les sites locaux de grande rigidité dans les cancers invasifs. Des tendances similaires ont été observées dans des cultures sphéroïdes prolongées d'une lignée cellulaire inductible par Src où des rigidités élevées se sont produites alors que l'oncogène était exprimé de manière constitutive et qu'il y avait de l'espace pour grandir librement. L'examen histologique des zones localisées molles et rigides des sphéroïdes a révélé des différences morphologiques distinctes, suggérant des différences dans les réponses mécaniques cellulaires de ces régions. Enfin, les μTAM ont été développés pour étendre leurs capacités de mesures viscoélastiques à l'échelle cellulaire, ce qui permet de mieux décrire la réponse cellulaire précoce et le comportement aux contraintes mécaniques. Des différences dans les comportements viscoélastiques à l'échelle de la longueur cellulaire ont été identifiées entre les sphéroïdes cancéreux invasifs et non invasifs où les tissus invasifs semblent se comporter de manière plus élastique que les comportements visqueux des sphéroïdes non invasifs. Dans l'ensemble, le développement du senseur μTAM nous permet d'étudier optiquement la mécanique interne des tissus et a permis d'identifier des propriétés mécaniques très localisées entourant les cellules individuelles qui sont en corrélation avec le potentiel invasif.

Acknowledgments

This work was supported by grants from the National Sciences and Engineering Council, the Canadian Institutes for Health Research, and the Canadian Cancer Society, and scholarships from McGill Engineering Doctoral Award, and the Alexander Graham Bell Canada Graduate Scholarship.

I would like to thank my supervisor, Christopher Moraes, for giving me a chance to take a foray into the engineering world, and to my "Team Ontario" friends for providing all the support I needed to survive my first year here. To Wontae, thank you for all the time you have given to teach me basic engineering concepts and pushing me to just do the math. To Sanya and Ray, thank you for all your patience with my grumpy days and accompanying me on the fun adventures of discovering the wonders a new city.

Thank you Avital for helping me get adjusted in a new environment and introducing me to teaching opportunities outside of the department. To my TA friends, Tung, Bin, Alexandra, and Sherif, it has been fun to share these teaching experiences with you all and thank you for all the good times both inside and outside those 301 labs.

During my time here, I have had the privilege of meeting many wonderfully talented and amazing people at McGill. Thank you Sarah for barging into my life and showing me the wonders of escaping into the wilderness when I need a break from everything. To Sonya, thank you for making this "a more pleasant experience" with your frank and delightful conversations, and all the secrets we will take to the grave. To Frank, thank you for sharing the experience of consuming the ghost pepper I grew. I will never forget the physical pain we shared.

To my Sainte-Famille roommates of present and past, thank you for being a socially enriching part in my life. I can never express how much I enjoyed our living experiences together, from the small things like coming home to a lit house to the bigger things like sharing meals and lively discussions with one another. I especially want to thank Ashley for remaining unfazed by all my shenanigans over the years, and Ioana for joining us in weathering through quarantine together.

Finally, to my family, thank you for accepting my decision to move away and pursue this challenge even though it meant a few more years away from you all.

Table of Contents

List of Figures

List of Tables

Preface

This thesis is written in manuscript-based format. It contains one book chapter in submission (Chapter 1), one published article (Chapter 2) and two manuscripts in preparation (Chapter 3 and 4).

First author publications originating from this thesis

1. Probing tissue mechanics at the cellular length-scale in cancer microenvironments
   S Mok, CM Boghdady, and C Moraes
   Chapter in submission for book titled "Micro and Nano Systems for Biophysical Studies of Cells and Small Organism" to be published Nov 2021 by Elsevier

2. Mapping cellular-scale internal mechanics in 3D tissues with thermally responsive hydrogel probes
   S Mok, S Al Habyan, C Ledoux, W Lee, KM MacDonald, L McCaffrey, and C Moraes
   Nat Commun 11, 4757 (2020). doi.org/10.1038/s41467-020-18469-7

3. Time and growth evolution of stiffness in cancer tumor models
   S Mok, CM Boghdady, L McCaffrey, and C Moraes
   Manuscript in preparation

4. Local viscoelastic measurements using thermoresponsive mechanosensors within cancer spheroids
   S Mok, B Campbell, N Kalashnikov, and C Moraes
   Manuscript in preparation

Additional publications

1. Thinking big by thinking small: advances in mechanobiology across the length scales
   S Mok, and C Moraes
   Integrative Biology, Volume 8, Issue 3, March 2016, Pages 262–266, doi.org/10.1039/c6ib90008a

2. Dispersible hydrogel force sensors reveal patterns of solid mechanical stress in multicellular spheroid cultures
   W Lee, N Kalashnikov, **S Mok**, R Halaoui, E Kuzmin, AJ Putnam, S Takayama, M Park, L McCaffrey, R Zhao, RL Leask, and C Moraes
   Nat Commun 10, 144 (2019) doi.org/10.1038/s41467-018-07967-4

3. Micropocket hydrogel devices for all-in-one formation, assembly, and analysis of aggregate-based tissues
   L Zhao, **S Mok**, and C Moraes
   Biofabrication 11 (4), 045013 (2019) doi.org/10.1088/1758-5090/ab30b4

4. Functional Redundancy between β1 and β3 Integrin in Activating the IR/Akt/mTORC1 Signaling Axis to Promote ErbB2-Driven Breast Cancer
   T Bui, J Rennhack, **S Mok**, C Ling, M Perez, J Roccamo, ER Andrechek, C Moraes, and WJ Muller
   Cell Reports 29 (3), 589-602. e6 (2019) doi.org/10.1016/j.celrep.2019.09.004

5. Mechanobiological regulation of placental trophoblast fusion and function through extracellular matrix rigidity
   Z Ma, L Sagrillo-Fagundes, **S Mok**, C Vaillancourt, and C Moraes
   Sci Rep 10, 5837 (2020). doi.org/10.1038/s41598-020-62659-8

Co-Authorship Statement

In this section, contributions of each author are described for the manuscripts presented in this thesis.

Manuscript 1 (Chapter 1): Probing tissue mechanics at the cellular length-scale in cancer microenvironments

Stephanie Mok – researched, wrote, and edited the review, drew and prepared figures

Christina-Marie Boghdady – edited the manuscript, contributed drawn figures

Christopher Moraes – edited the manuscript

Manuscript 2 (Chapter 2): Mapping cellular-scale internal mechanics in 3D tissues with thermally responsive hydrogel probes

Stephanie Mok – formulated idea behind the study, designed and conducted experiments, analyzed all data, drafted and edited the manuscript

Sara Al Habyan – performed injections into animal models and ex vivo tumor imaging

Charles Ledoux – performed finite element simulations

Wontae Lee – assisted with mechanical characterization of polyacrylamide gels and data analysis

Katherine N MacDonald – assisted with experiments

Luke McCaffrey – assisted with experiment design, provided reagents, materials, animals and analysis expertise

Christopher Moraes – formulated idea behind the study, assisted with experiment design and analysis expertise, provided reagents and materials, edited the manuscript

Manuscript 3 (Chapter 3): Time and growth evolution of stiffness in cancer tumor models

Stephanie Mok – formulated idea behind the study, designed and conducted experiments, analyzed data, drafted and edited the manuscript

Christina-Marie Boghdady **–** assisted with data analysis

Luke McCaffrey **–** provided reagents and materials

Christopher Moraes **–** assisted with experiment design and analysis expertise, provided reagents and materials, edited the manuscript

Manuscript 4 (Chapter 4): Local viscoelastic measurements using thermoresponsive mechanosensors within cancer spheroids

Stephanie Mok – formulated idea behind the study, designed and conducted experiments, analyzed data, drafted and edited the manuscript

Benjamin Campbell – performed finite element simulations, assisted with data analysis

Nikita Kalashnikov – assisted with finite element simulations and analysis expertise on viscoelastic behavior and modeling, edited the manuscript

Christopher Moraes **–** formulated idea behind the study, assisted with experiment design and analysis expertise, provided reagents and materials, edited the manuscript

Chapter 1

1 General Introduction and Literature Review

The following chapter begins with a comprehensive review of the relevant background and literature on measuring mechanics within the cellular microenvironment, with a specific focus on cancer mechanics and mechanobiology. The main text from section 1.1 is a chapter contribution towards a book titled “Micro and Nano Systems for Biophysical Studies of Cells and Small Organism” to be published in November 2021 by Elsevier. Following this, the overall rationale and objectives of the thesis are presented.

1.1 Probing tissue mechanics at the cellular-length scale in cancer microenviroments

1.1.1 Abstract

Tissues are mechanically complex composite structures, in which an organized collection of cells in various configurations, interwoven within a complex extracellular matrix maintain mechanical integrity and function. Cellular activity in response to these local mechanical properties can drive considerable changes in the tissues over time. Given the importance of tissue mechanics in maintaining tissue homeostasis and in progressing disease phenotypes, understanding the relationship between the local mechanical microenvironment and cell behavior is therefore crucial to predict tissue health. Specifically, measuring complex mechanics at length-scales similar to those of a cell, in realistic and living tissues presents considerable challenges. In this chapter, we discuss conventional and emerging techniques to measure tissue mechanics in the cellular microenvironment, with a specific focus on measurements to better understand cancer

1.1.2 Introduction and current challenges in biomechanical characterization

Cells are the basic unit of life and their proper function has major implications for development, health, and disease. The principal lens through which biologists view cellular systems is though the central dogma of molecular biology: reading genetic information stored in the nucleus to producing molecular signaling pathways that guide cell behavior. However, it becoming more apparent that beyond biochemical signals, cells can sense and respond to their physical surroundings [1–3], and these mechanical stimuli are implicitly present in virtually all cell and tissue cultures. For example, anchorage-dependent cells must be adhered onto a surface to survive [4], or and some cells benefit from cell-cell contacts to remain viable [5]. These mechanical conditions surrounding the cell are well-established to influence cell structure and function [6].

Mechanical conditions arise within tissues through several mechanisms, and are essential for tissue function. A spatial distribution of intrinsic stress is essential maintain and stabilize tissue architecture, while also transducing mechanical cues from the microenvironment into biochemical responses [7]. The mechanical elasticity of the cell and surrounding tissue components dictates how local stresses result in deformations leading to functional changes. Direct deformation of the cell can alter both gene expression and molecular signaling. Most prominently, nuclear dysmorphia can alter gene accessibility and even damage the genome [8–10]. The stability of the nuclear envelope has also been associated with changes in stiffness of the surrounding tissue, highlighting the importance of maintaining a narrow working range of appropriate mechanical properties for proper function [11]. Mechanosensory mechanisms rely on the external rigidity as cells generate internal stress by pulling on their surroundings to trigger signaling cascades [12,13]. Therefore, an understanding of where and how forces are generated, reacted upon, and resisted may reveal new strategies to assess tissue health and disease progression in diseases such as cancer.

The most prominent feature of mechanically-influenced biological systems in recent years has been the mechanical rigidity of tissues. These factors are particularly important in considering human health, as tissue function is reliant on appropriate tissue mechanics, which can span 100s of pascals in the brain and lung to gigapascals in bone [14]. Proper tissue function relies on maintaining the tissues within a narrow range of appropriate mechanical properties, and deviations from this range are common signs of disease [15]. To quantify these tissue mechanics, early strategies used classical mechanical measurement techniques like rheometry, tensile testing, and mechanical indentation to characterize biological tissues [16,17]. However, biological samples are highly heterogeneous composites of different cells and extracellular matrix proteins, and classical characterization methods provide only a lumped measurement that fails to distinguish between these individual contributions. Tissues are carefully organized to maintain structure and fulfill specialized functions, and changes in cell shape, ECM organization, and overall tissue patterns accompany disease progression [18]. These visually-observable changes suggest that local alterations in the tissue's material properties evolve concurrently with local cell behavior. Therefore, quantifying these properties and resolving spatiotemporal mechanical profiles within 3D tissues is critically important to understand triggers for pathogenic development, and this has now been shown to be particularly relevant in the context of cancer [19,20].

In terms of tissue function, spatial distribution of stresses maintain and stabilize tissue architecture, while also transducing mechanical cues from the microenvironment into biochemical responses [7]. The elasticity of the cell and overall tissue dictates how local stresses result in deformations leading to functional changes. Gene expression and molecular signaling can both be altered by direct deformations of the cell. Most prominently, nuclear dysmorphia can alter gene accessibility and even damage the genome [8–10]. The stability of the nuclear envelope has also been associated with changes in matrix stiffness, highlighting the importance of maintaining a narrow working range of appropriate mechanical properties for proper function [11]. Mechanosensory mechanisms

are reliant on the rigidity of the environment as cells require force transmissions from pulling on the surroundings to trigger signaling cascades [12,13]. Therefore, an understanding of where and how forces are generated, reacted upon, and resisted may reveal new metrics on assessing tissue health and disease progression, like in cancer.

Conventional macroscale characterization techniques for testing millimeter- and centimeter-scale samples lack the resolution needed to characterize local mechanical differences within cellular constructs. Since these measurements capture mechanically dominant properties only, they neglect heterogeneity that exists within tissues. For example, with tensile testing or indentation-based methods, local soft spots would be masked by an overall stiff tissue, effectively limiting the ability to capture soft regions in the tissue. In the context of diseased tissues like cancer, the overall tumor tends to be stiffer than normal surrounding tissue, but cancer cells themselves are well documented to be significantly softer than normal cells [21,22]. Thus, the resolution and length scale of acquired mechanical measurements need special consideration according to the study in question. Furthermore, while individual cells are components in a more complex tissue, they acutely sense and respond to mechanics at the nano and micro length scale, which may differ from the global average of the whole tissue [14]. Such mechanical cues provided by the extracellular microenvironment will guide cells in development, differentiation, and disease progression [19,23,24]. Cells must first sense these cues to trigger a response, and they do so by extending stiff exploratory motile structures and retracting them to probe the mechanics of their local environment [25]. Depending on the adhesions the cell can form with the existing extracellular proteins and the traction force magnitude it can exert on its surroundings, a cell will react and adapt to these mechanical cues by physically and compositionally remodeling their environment [1,26,27]. Hence the local microenvironment surrounding a cell plays a disproportionately important role in maintaining or driving higher-order structural changes in the tissue. Therefore, quantifying the mechanical cues that a cell experiences within its local microenvironment requires measurement tools that apply forces at micro- and nano- length scales.

In addition to this requirement for high-resolution measurements, cells in vivo typically exist in a three-dimensional context. Cell morphology, cytoskeletal organization, and even survival against cytotoxic drugs have been shown to be different in 2D culture versus 3D culture environments [28–30], indicating the importance of this microenvironmental parameter on cell function. While flat 2D culture systems impose a flat cell morphology and defined polarity, these phenotypes may differ from those found in their native 3D conformation. Moreover, cells express different behaviors in 2D and 3D when it comes to collective rotation, geometric cues, and topographical cues. Monolayers of cells confined in 2D micropatterned circular islands rotate as whole sheets [31,32] whereas cells cultured in 3D have shown more spatially complex rotational movement [33]. 2D cultures also lack the fibrous topography within the true ECM, where cells tend to migrate along the orientation of the fibers. Although grooved or protein patterned surfaces can be fabricated on tissue culture plastic, cells cultured in naturally extracted 3D matrices can alter and realign the fibers which plays a key role in homeostasis and disease progression [34]. 3D studies can hence be physically and physiologically more realistic compared to 2D cultures on hard plastic.

Measuring mechanics at the length scale of individual cells, within large, living, and undamaged biological tissues remains a difficult task. Most conventional techniques require inducing some type of tissue damage, like sectioning, but is ultimately detrimental to mechanical studies. Slicing tumors to expose internal surfaces to study mechanics has been shown to release internal stress [35], which significantly reduces a tissues' internal resistance to applied deformation. Such discrepancies have been quantified by mechanical testing on sections of resected tumors, measuring stiffnesses between 0.2 to 20 kPa [35,36], while compression testing of intact tumors shows stiffnesses of up to 60 kPa [37]. The mismatch between these studies demonstrates that maintaining 3D tissue integrity is essential when characterizing internal tissue mechanics. Furthermore, damaging tissues for mechanical studies prevents spatiotemporal monitoring of mechanical properties because the sample is destroyed after measurement.

1.1.3 Potential impact in cancer mechanobiology

Cancer is an abnormal proliferation of cells that may result in benign, non-invasive tumors. However, they can become deadly when cancer cells gain an invasive ability to move away and colonize distant sites from the primary growth. This phenomenon is known as metastasis when it occurs between organs and is the main cause of death for individuals diagnosed with cancer. Understanding both the biochemical and physical cues that encourage cell invasion is critical in gaining insight in the metastatic mechanism and preventing it from occurring. The molecular genetics and signaling pathways that drive malignant transformation have been extensively studied [38] and are beyond the scope of this chapter. However, much less is known regarding the mechanical changes underlying this disease. While molecular biomarkers are currently the most used for cancer diagnosis and prognosis, physical biomarkers play an equally important role in cancer progression and can contribute to detect predictive markers of early malignant transformation events. The best way to treat cancer is to eradicate all the cancer cells as early as possible, with earlier detection yielding better prognostic outcomes. Mechanics may be helpful in classifying benign tumors from malignant ones to avoid unnecessary aggressive treatments that would have negative quality of life impacts for an otherwise harmless growth.[39,40] This is due to the instructive role of biophysical characteristics of the cancer microenvironment in determining the phenotype of tumor cells [41]. Normal tissue architecture creates microenvironments that exert suppressive forces on tumors and prevent metastasis, but its destabilization can promote disease progression [42,43]. In order to develop physical markers, we need a better understanding of the mechanical changes occurring throughout the disease, which requires the design and implementation of appropriate measurement techniques to characterize these changes. In this section, we highlight a selection of mechanical measurements that can be done on tumors and/or cancer

cells, and illustrate how biophysical changes in the cancer microenvironment can prompt tumorigenic behavior.

In terms of mechanical properties, tumours stiffen their environment and are stiffer than their healthy tissue counterparts [15,44,45]. Aside from increasing cellular mass, overall tumour stiffening can be attributed to higher fluid pressures from a leaky blood vasculature, as well as desmoplastic stromal response, which consists of an increase in extracellular matrix protein deposition and crosslinking [46–48]. The distribution of such compressive forces within the tumour and how they are felt by individual cells remains unclear, despite observing phenotypical changes resulting from this mechanosensing. Differences in bulk tumour stiffnesses have been measured between benign tumours and tumours that have higher instances of metastases [49]. These differences in stiffness can also be seen at the cellular level where cancer cells with high migratory and invasive potential have been shown to be much more compliant (less stiff) than their benign counterparts. Various single cell and tissue monolayer studies have quantified these observations using magnetic tweezers and atomic force microscopy as measurement techniques [50,51].

Throughout tumour growth, the extracellular matrix is remodeled and stiffened through increased deposition of specific matrix proteins and proteases, as well as matrix protein fiber realignment by the cells themselves [52]. This remodeling alters the biochemical and mechanical properties of the tumour environment and is implicated in promoting malignant transformation in breast cancer [20,53]. Additionally, tumour growth-induced solid stresses lead to a stiffening of the environment around the primary tumour [47,54,55], which in turn generates compressive stresses that stiffen local cells and may limit overall tumour outward growth (Figure 1.1A) [56,57]. Interestingly, this compressive force in cancer cells also promotes invasive behavior [58–60]. Furthermore, invading cancer cells have been shown to be soft themselves despite that other cell types within the tumour, such as fibroblasts, have been shown to match the stiffness of their culture substrate [49–

51,56,61]. Therefore, tumour cells likely undergo dynamic changes in internal stiffness in response to external compressive forces throughout the overall development and progression of the disease.

In terms of cancer progression, there are a number of physical barriers and forces a malignant cell must overcome to leave its original site to travel and establish itself in a distant part of the body (Figure 1.1B). The key step in initiating this invasive process lies in cellular reprogramming that creates a mobile phenotype. Cellular shape and mobility are stabilized by the cytoskeleton, which is the protein structure that maintains mechanical support and organelle organization. Continuous cytoskeletal reorganization enhances cellular mobility [62] and may be the reason why malignant cells have been found to be much softer than their benign counterparts [63]. In fact, the metastatic potential of a cancer cell has been shown to be inversely correlated with cell stiffness in both patient tumor cells and cancer cell lines [51].

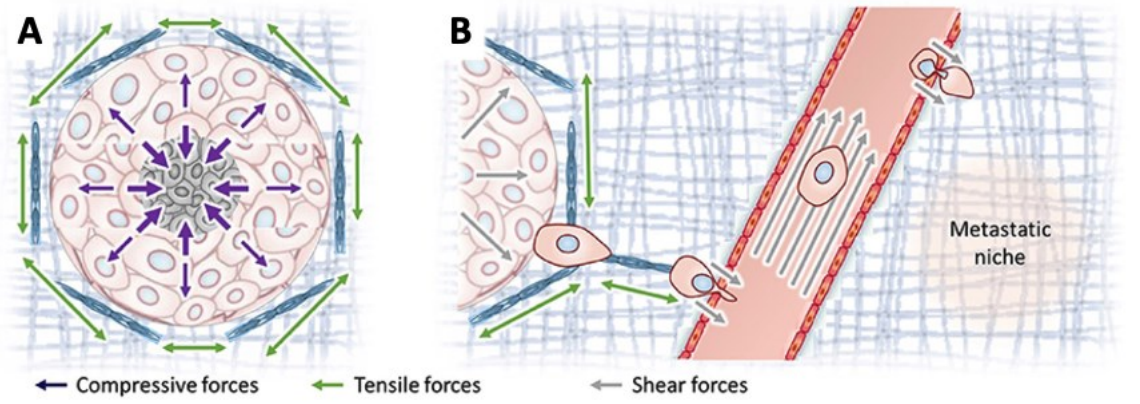

Figure 1.1. Solid mechanical forces present during tumor expansion (A) and metastasis (B).
Reproduced from Northcott JM, Dean IS, Mouw JK and Weaver VM (2018) Feeling Stress: The Mechanics of Cancer Progression and Aggression. Front. Cell Dev. Biol. 6:17. doi: 10.3389/fcell.2018.00017.

From a diagnostic point of view, spatiotemporal patterns in tissue stiffness can be indicative of cancer formation and development. Tumours are highly heterogeneous tissues. Recognizing this variation may help with diagnosis by guiding biopsy targets towards areas of the tumour where malignancy is more likely to develop. This way, the most aggressive parts of the tumour can be sampled and a more insightful prognosis can be made. Moreover, a higher degree of variation in spatial stiffness may be indicative of areas with higher malignant potential. Their irregular tissue structure, composition, and shape result in a varying mechanical landscape at the cellular scale, yielding a higher potential of fostering a local invasive phenotype. The ability to characterize and detect these variations may help predict potentially problematic areas where irregular changes in the mechanical properties can provide early indicators for disease development.

1.1.4 Contributors to tissue stiffness in the cellular microenvironment

The main load-bearing components of the cellular microenvironment consist of the ECM and neighboring cells mechanically coupled together through specialized adhesions. The composition and ECM-to-cell ratio varies according to tissue type. For example, connective tissues largely consist of ECM with few cells, but in epithelial tissues where the ECM is sparse, the cells themselves support mechanical loads. The ECM does not only provide mechanical stability and structure, but also contributes to regulating fluid pressure within blood and lymphatic vasculature [54,64]. In this section, we discuss how structural components within the ECM and cells distribute and resist mechanical stresses within the tissue (Figure 1.2). Understanding the composition and structure of the cellular microenvironment provides insight on the mechanisms for force generation and transmission through biological tissues, elucidating different mechanical behaviors under varying study conditions.

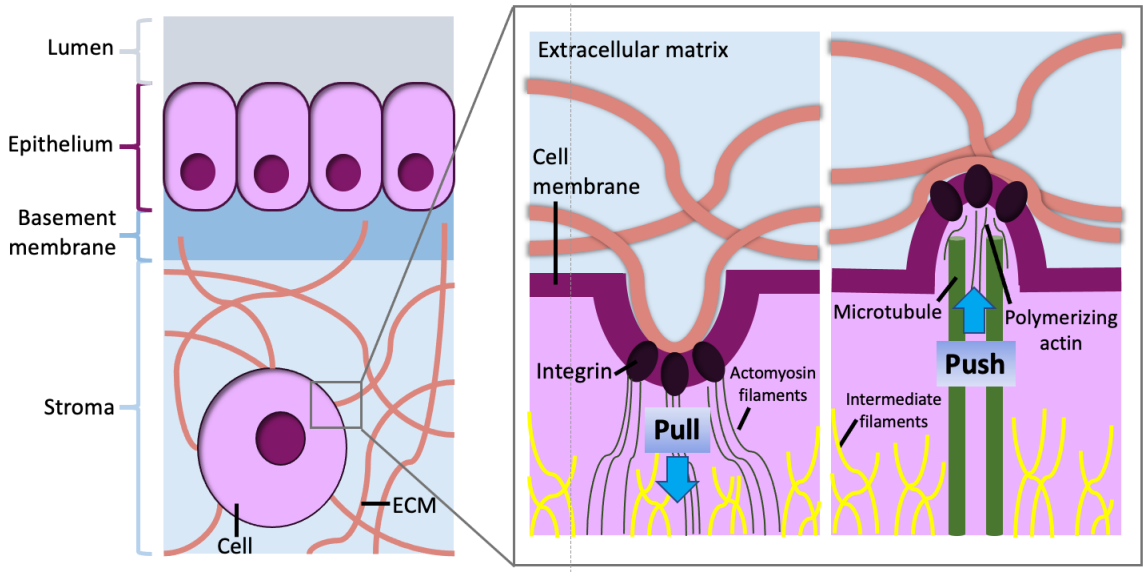

Figure 1.2. Cells mechanically interact with the extracellular matrix.
Cells create pushing and pulling forces using multiple components of their cytoskeleton. Figure based on explanations from Chaudhuri et al., (2020) [65].

Extracellular matrix

The tensile strength of tissues is mostly provided by fibrillar collagen in the extracellular matrix. At the molecular level, collagen is a long triple-stranded helical structure with three collagen polypeptide chains woven together like rope to form tropocollagen (1.5 nm in diameter) [66]. Multiple tropocollagens can then be assembled into collagen fibrils (10-300 nm) which can further bundle together to make collagen fibers (0.5 to 3 µm) [67]. Collagen within the tissue is produced by fibroblast cells. Typically these matrix components are secreted by the cells in a naïve form and assembled into complex aggregates extracellularly [68]. Fibroblasts will then pull and move over deposited collagen fibrils to orient and compact them into patterns best suited for the tissue. The type of collagen, its quantity, crosslinking pattern, and organization in the ECM will alter its material properties [69]. Fibroblasts also secrete other matrix components to create a hydrating gel to fill the spaces between the collagen fibril network. This gel consists of

proteoglycans linked to glycosaminoglycans forming large molecules within the collagen meshwork, which creates an innate swelling pressure [70]. This provides additional material strength for resisting compression, which in turn is balanced by the tension in the collagen fibrils.

Once the structural support is in place, cells can interact and adhere to the ECM through integrin receptors spanning the cell membrane which connect the cell's actin cytoskeleton to the extracellular matrix [71]. This link is facilitated by fibronectin proteins that have binding sites for both collagen in the ECM and integrin receptors on the cell. Not only do integrins transmit passive stresses, they can also react to stress for outside-in cell signaling pathways by induced conformational changes of the intracellular domain [13]. To initiate this transmission, the cell must first bind to the ECM and pull on it [26]. A minimum amount of tensile force across the receptor between the ECM anchorage and the cell's contractile force is needed to activate downstream responses [72]. These changes can expose activation sites for other molecules to stabilize the interaction by forming mature focal adhesions. Additionally, direct cell behaviors can be directed through downstream signaling pathways responsible for anchorage dependent cell survival and ECM remodeling [73,74].

Cytoskeleton

The cytoskeleton is an intracellular protein network composed of three main types of protein filaments supporting external physical stresses experienced by cells: actin microfilaments, intermediate filaments, and microtubules [75]. Actin filaments are ~7 nm in diameter are highly concentrated underneath the cell membrane, in what is called the actin cell cortex. There, actin filaments are crosslinked for cellular structure, shape, and mechanical stability [76]. Adjacent cells can join their actin cytoskeletons through adherens junctions to create actin rings of power for cytokinesis, epithelial cell extrusion,

and wound closure through a purse-string-based mechanism [77]. Actin filaments are also essential for cell generated forces as they can form small contractile bundles with myosin proteins in the cytoplasm in a similar mechanism to muscular contraction [78]. These bundles allow cells to extend stiff yet motile exploratory structures and retract them, similar to a prodding motion, to test their microenvironment [79].

Then, intermediate filaments are most prominent within the cytoplasm of cells experiencing high levels of mechanical stress [80]. By knocking out intermediate filament genes of cells, they were found to be unable to resist physical stresses, resulting in cell degeneration and mechanic instability within the tissue [81]. These filaments at 10 nm in diameter provide mechanical support by stretching and distributing locally applied stresses to keep cells intact together, especially against shear stresses [82]. These stresses are distributed across the tissue through desmosomes that join adjacent cells through intermediate filaments. Similarly, in hemidesmosome junctions, intermediate filaments are attached to a specialized ECM sheet called the basal lamina and is exclusive to epithelial tissues [83,84].

Lastly, microtubules are the largest type of cytoskeletal filament and are best known for their role in chromosome segregation during cell division [85]. Microtubules are rigid hollow tube structures, 25 nm in diameter, composed of tubulin dimers [86]. This configuration means they are best suited for bearing compressive forces within cells and tissues [87]. They can also generate pushing forces by microtubule polymerization which pushes against the cell membrane in the direction of elongation. Conversely, pulling forces can be generated by depolymerization or by molecular motor proteins running along the filament [88]. Considered the intracellular highway, these filaments dictate the paths which motor proteins, like kinesins and dyneins. can move along to organize organelles, proteins, and vesicles within the cellular interior [89].

1.1.5 Overview of mechanical characterization theory

Solid mechanical forces result in stresses at different length scales from the molecular level to the multicellular tissue scale. These forces can originate from external sources or within the tissue itself from cell-generated forces which can undergo coordination up to the tissue scale. Additionally, hydrostatic fluid pressures may also generate biologically relevant forces within tissues, but active distinct mechanical pathways from conventional solid stresses, and are not considered in this review. Solid mechanical stresses are defined as a pressure: the ratio of the force to the area it is applied upon.

$$Stress, \sigma = Force/Area$$

Depending on the material properties of the molecule, cell, or tissue, these forces are integrated to result in strains or deformations. Mechanically, deformations refer to the relative change in size of a body due to exerted force where L_0 is the initial size and L is the size post-deformation. This deformation is often referred to as strain and is dimensionless.

$$Deformation, \epsilon = \frac{L - L_0}{L_0}$$

The essential components of mechanical material analysis are an ability to apply a force, and to observe a deformation. The conventional techniques to achieve this includes tensile, compressive, shear and torsional deformations to test the material. Young's modulus (E) is a measure of stiffness in units of N/m or Pa and can be determined from tensile or compressive tests. Tensile tests place a material under extensional tension while compressive tests place the material under compressive loads, both of which result in a stress and strain normal to the loaded surface. Linear elastic properties can be described using Young's modulus of a material which is defined by the slope of stress plotted against strain. Elastic materials undergo strain but maintain their original shape when the applied force is removed, irrespective of the time under stress (Figure 1.3A). Shearing a material

can be used to obtain a shear modulus (G) where the stress and strain are parallel to the cross-section and has an angular component. For isotropic materials that respond equally to all externally applied forces no matter their orientation, Young's modulus and shear modulus can be related through Poisson's ratio (v) where $E = 2G(1+v)$. However, biological materials are frequently anisotropic, meaning that their mechanical properties can depend on the orientation of the applied stress and require more extensive characterization [90].

Biological tissues can also be viscoelastic, meaning that their response to an applied force will have elastic resistance to deformation under stress as well as a viscous resistance to flow (Figure 1.3B). While the elastic response is near instantaneous, the viscous properties of a material can only be determined by considering the dynamic deformation of a material under load. Viscoelastic characteristics can be described through stress relaxation and creep behaviors as well as hysteresis seen from the stress-strain curve. Unlike purely linear elastic materials which store energy efficiently, the viscoelastic samples dissipate the energy, resulting in prolonged recovery and irreversible deformations. Stress relaxation can be measured by maintaining an applied strain deformation and measuring the decreasing restorative force over time. Conversely, creep studies monitor the increasing strain of the material over time while maintaining a constant applied force. Viscoelastic measurements typically require dynamic testing to obtain both a storage modulus (E') and loss modulus (E'') that respectively describe the elastic and viscous behaviors of the material. Generally, the loss modulus represents the permanent structural change or energy dissipated within the material or tissue as a result of the applied stress. Similarly, shear equivalent moduli can be obtained to describe this as well. Viscoelastic behaviors can also be described using spring-and-dashpot systems with elastic (spring) and viscous (dashpot) parameters arranged in various configurations. Examples include the Maxwell model, the Kelvin-Voigt model, or the standard linear solid model which is a combination of the two. Thus, characterizing the mechanics of biological tissues relies on an array of features including stiffness, force, and viscoelasticity. Their

quantification requires the design and implementation of particular techniques which will be discussed in the following section.

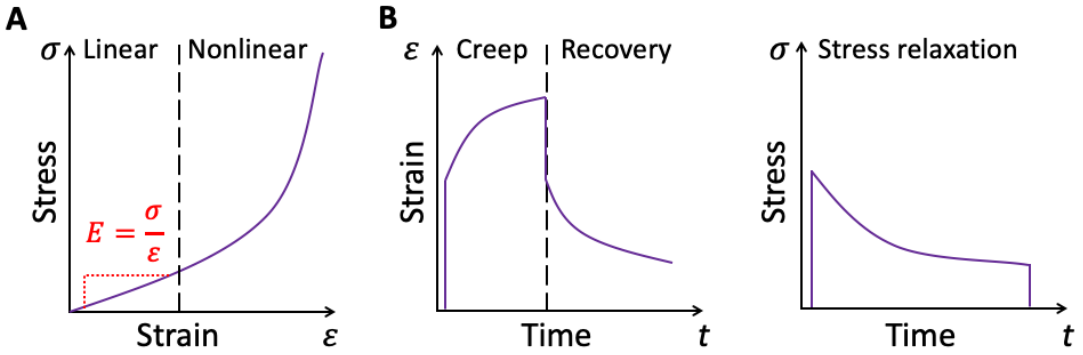

Figure 1.3. Mechanical behaviors of elastic and viscoelastic materials.
(A) Stress strain curve for an elastic material. Young's modulus, E, can be described by the slope of the linear region. (B) Characteristic material responses of a viscoelastic material showing creep during applied constant stress, and stress relaxation for a constant strain.

1.1.6 Techniques to measure solid mechanics in cells and tissues

In this section, we review a variety of techniques currently used to measure solid mechanical properties of biological material. We find it useful to categorize these techniques based on the biological complexity of the system being studied, and the spatial length scale at which the measurements are taken. A summary of these techniques has been presented in Figure 1.4 and Figure 1.5, as a guide to rapidly identify the most appropriate technique for a specific biological question. We then also describe the specifics of these techniques, with a specific focus on measurements made in the context of cancer, in each of the following subsections.

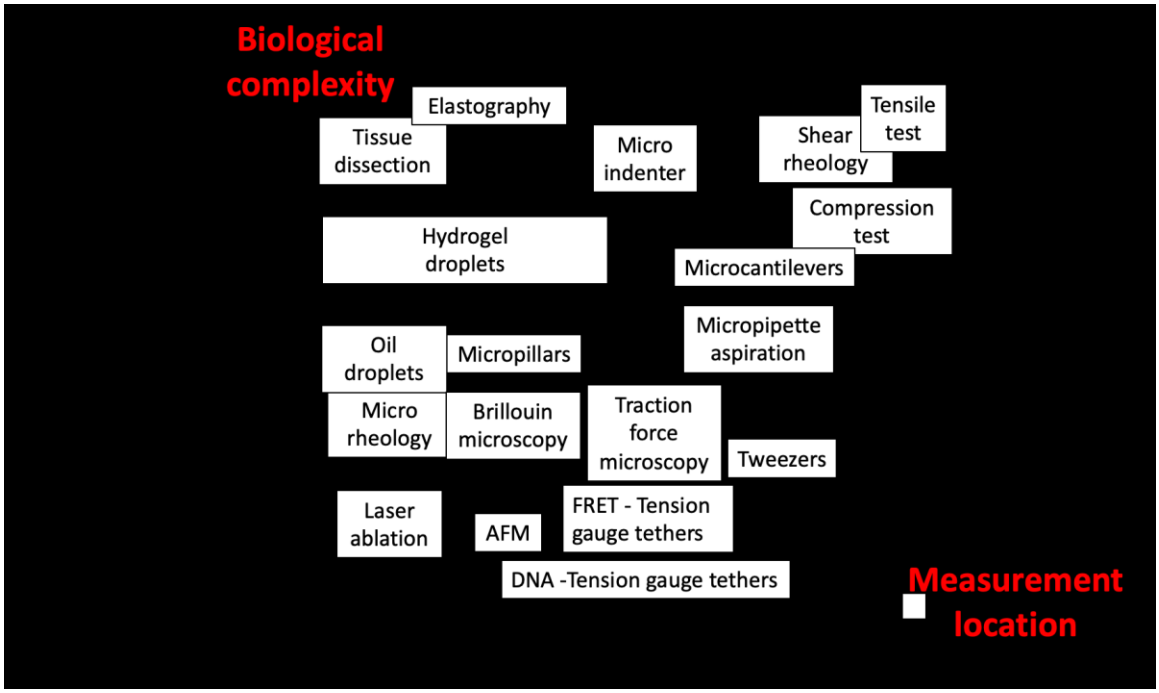

Figure 1.4. Overview of selected techniques used to study soft tissues based on measurement location and biological complexity.

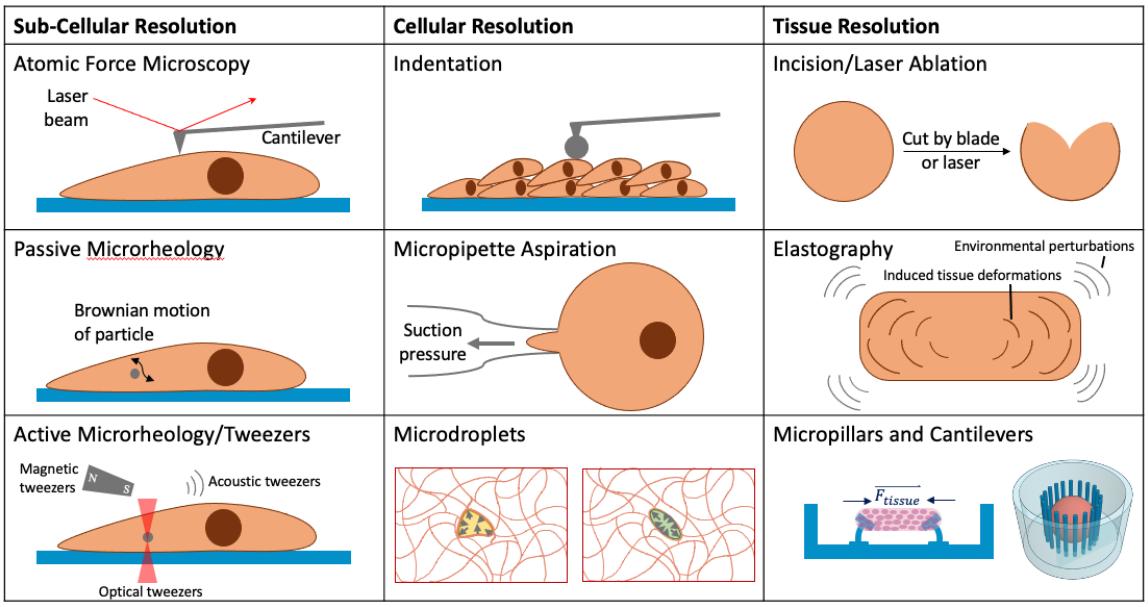

Figure 1.5. Schematic overview of selected techniques.

Microdroplet, cantilevers and micropillar figures based on works by Campas et al., (2014) , Legant et al, (2009), and Aoun et al., (2019) respectively [91–93].

Indentation

"Pressing" upon a material is perhaps the most intuitive way to determine its' mechanical properties. With indentation techniques, mechanical properties are measured by deforming the surface of a sample with a probe using a defined force. Knowing the applied force and measuring the displacement of the probe indenting the sample, stiffness can be determined. To extract a stiffness modulus descriptor, indentation curves are assessed by plotting indenter load as a function of indentation depth. The shape of this curve is largely determined by mechanical properties of the sample, and thus the sample's stiffness can be quantified. Indentation tests have been done on trimmed millimeter-sized tumor tissues derived from cancer cell line inoculated animal models and clinical samples of breast cancer. Indentation measurements show the plasticity of these tissue, which may enable cancer invasion by allowing permanent deformations to form in dilating pores [94].

Probe geometry must be appropriately designed and selected to accurately measure samples. Glass-based microindenters can be microforged by melting the glass tip of a micropipette, yielding a probe 10 μm in diameter used to profile the changes in the viscoelasticity of individual cells [95]. Probe geometries can be spheres, flat cylinders, cones, and even needles [96], but an appropriate model based on the indenter shape is needed to calculate stiffness from the experiment [16]. Probe sizes range from millimeters to micrometers for the purposes of studying tissue mechanics, depending on sample size and stiffness. Indentation depths and the speed will also affect the apparent stiffness measured and must be reported. Biological tissues pose certain considerations for adapting indentation technology to measure their stiffness: the effect of capillary forces when working with submerged or wetted tissues [97], a non-flat or not-well defined surface to make even contact with the probe, and adhesive forces between the indenter and tissue.

Atomic force microscopy

Atomic force microscopy is similar to the indentation method described above, except the probe can be fabricated to have micron-to-nanometer scale dimensions, and attached to a cantilever which bends and deflects as the probe moves along the surface of the material while scanning. A detector records the deflection and motion of the cantilever using optical beam deflection. AFM can operate in several ways but the most common one used for biological samples is the tapping mode for force mapping or force scanning [98], Force-distance curves plotting cantilever deflection against z-distance provides stress-strain curves to calculate Young's modulus and adhesion of tissue surface measurements with nanometric resolution (Figure 1.6). In addition to these mechanical properties, AFM can simultaneously provide high-resolution and non-destructive imaging of surfaces, generating topographical information of the sample. AFM can also be used for force spectroscopy to measure forces between individual interacting molecules and as a nanoindentor, similar to indentation testing, but with a sharp nanometer sized probe.

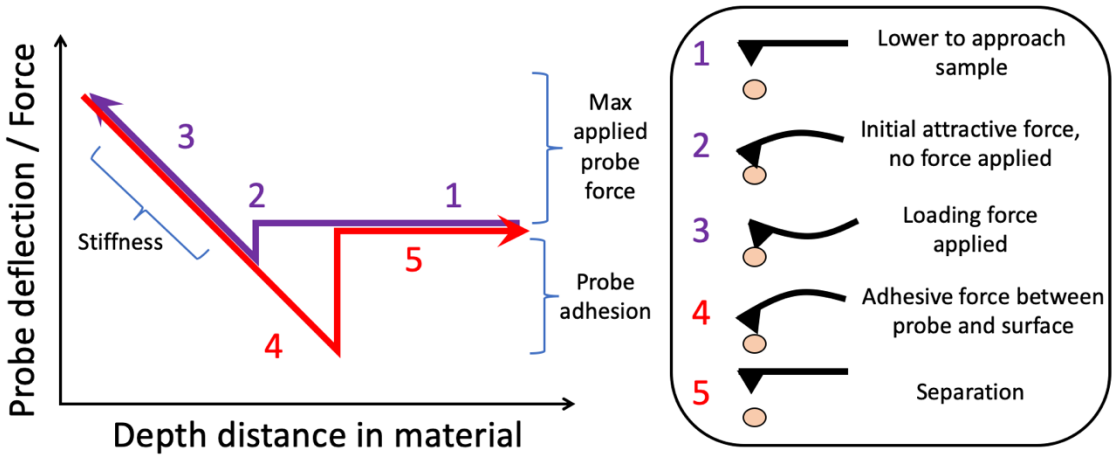

Figure 1.6. Force distance curve for AFM.
Force distance curve for AFM. Key events during the approach (#1-3, in purple) and retraction (#4-5, in red) of the cantilever probe are numbered and described. The probe is

vertically lowered onto a sample (1) and experiences a “snap in” or “jump in” region (2) where the cantilever is attracted to the surface without any load being applied. Loading force is applied as the cantilever is lowered further into the surface of sample and is deflected upwards (3). Stiffness and elasticity can be analyzed from this region. As the cantilever is pulled away from the sample, adhesive forces between the probe and sample causes the cantilever to bend downwards (4) before separating (5).

The cellular and subcellular resolution of its mechanical measurements have shown that despite overall tissue stiffening in cancer, individual cancer cells tend to be softer than normal cells [36,99]. While this may seem like contradictory measurements, tissue stiffness is not only regulated by cellular stiffness. In combination with fluorescence microscopy to label and distinguish between cells and ECM, force mapping of tissue sections show that the ECM, specifically collagen, stiffen during tumor progression [44].

AFM has been widely used because of its broad capabilities but its biggest limitation is that it can only be used to study exposed tissue surfaces. Although tissues can be cut to expose internal surfaces, slicing releases internal stress which alters the apparent stiffness of the interior tissue [35]. This limits the applicability of this technique in quantifying spatial profiles of mechanical properties in 3D tissues to better understand their function and architecture.

Tissue incisions and laser ablation

Making tissue incisions can be a robust and simple technique to infer the tension and solid stresses of the overall tissue. The tissue stresses released by cutting it can be quantitatively evaluated in how the tissue relaxes or retracts from the cut margins as a deformation. After this tension is released, compressive forces that were within the tissue will manifest as bulges, the dimensions of which can be used to calculate the original tissue internal stresses. Macro-scale mechanics of tumours have been studied using this technique to show

that tumours experience growth induced solid stresses stored within neighboring cells and the ECM as tumour expansion compresses its surroundings [100]. The stress build-up is inversely proportional to the stiffness of the ECM and reducing the ECM content can reduce solid stress accumulation [37]. Finer, microscale mechanical characterization can be done using strategic cuts to release solid stresses in a controlled way and creating a 2D map of quantified stresses using high-resolution ultrasound imaging [35]. In this system, stress induced deformations manifest as depressions where areas were under tension and as protrusions where areas were under compression.

While this technique requires considerable manual dexterity and experimental skill, laser ablation presents an alternative strategy, by using a high-powered laser to locally create incisions at the cellular or subcellular levels. Under a microscope, retraction velocities can be measured after laser incision, where higher stresses are correlated with higher velocities [101]. Thus, this technique is best suited for quantifying tensional forces at the cellular or sub-cellular scale. However, it cannot be used to resolve temporal variations in properties within the same sample since it is destructive to the studied tissue.

Micropipette aspiration

Micropipette aspiration has been used to study the surface tension properties of cells and cell aggregates. Similar to AFM, micropipette aspiration is limited to surface measurements but still has versatile applications. A typical experimental set up involves using the micropipette to apply a known suction pressure onto a cell or surface, and monitoring the bulge geometry of the surface at the suction tip. The suction pressure can be generated by an adjustable water reservoir or pump. In an adjustable water reservoir, suction or aspiration pressure (P) is determined by the relationship between the height difference (h) of the micropipette and the water level in the reservoir, along with the specific weight of water (pg) where P=pgh. Equilibrated or dynamic deformation of the

surface can be measured optically to determine stiffness, surface tension, and viscosity using biomechanical models [102].

This technique is particularly versatile in that it is also possible to hold a cell or tissue in place with one micropipette while spatially manipulating the sample or probing it with another micropipette (Figure 1.7). With this type of set-up, micropipettes can be used to hold or mount microscopic samples for microindentation or cantilever-based studies similar to force probing [103]. By incorporating the ability to move the micropipette around, adhesion forces can be measured by using micropipette suction to hold and manipulate cells interacting with ECM, effectively quantifying cell-ECM interactions. These types of experiments have shown that cell adhesion area scales with detachment force [104]. Additionally, studies on cell-cell adhesions have been done by having two pipettes each holding one of two cells in contact and opposition [105]. Here, one pipette remains fixed while the other moves to provide a pulling force in an attempt to pull both cells apart. The suction force on the moving pipette is incrementally increased until the cells are pulled apart to determine their adhesion force [106]. Cell-cell adhesions have been shown to mechanically couple actin cortexes, therefore coupling the tension between cells to drive morphogenesis [107]. While this technique is limited in throughput, microfluidic devices for higher-throughput micropipette aspiration have been designed to increase the efficiency of these studies [108].

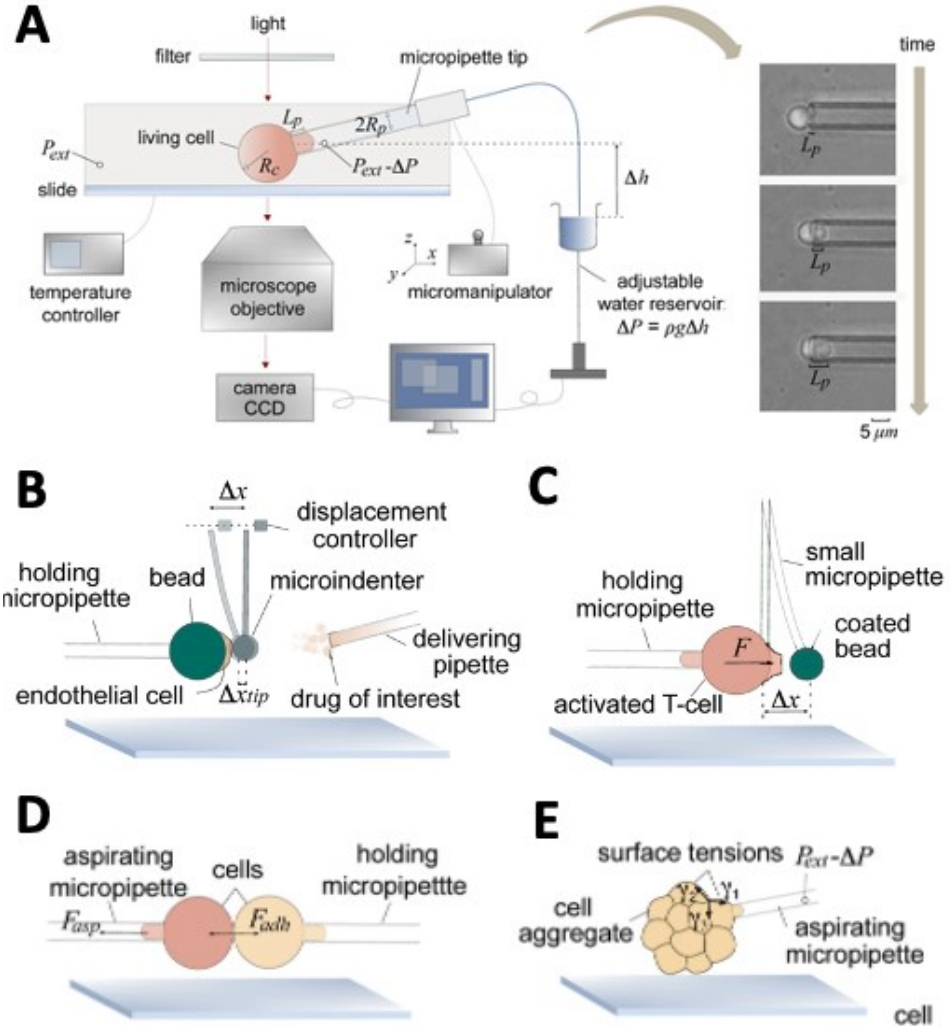

Figure 1.7. Micropipette aspiration applications.
(A) Experimental setup for typical micropipette aspiration system. (B-E) Selection of schematics for micropipette aspiration based techniques. (B) Micropipettes can be used to hold a cell or cell aggregates with a microindenter force tool to deform samples. (C) Micropipette immobilized samples can also measure cell pulling and pushing forces by measuring the deflection of a small micropipette or cantilever. (D) Dual-pipette aspiration can be used to quantify intracellular forces between samples. (E) Surface tension can be mapped across surfaces of cell aggregates. Adapted from Biophysical Journal; Vol 116; Blanca González-Bermúdez, Gustavo V. Guinea, Gustavo R. Plaza; Advances in Micropipette Aspiration: Applications in Cell Biomechanics, Models, and Extended Studies, Pages 587-594, Copyright (2019), with permission from Elsevier.

Tweezers – particle traps

Tweezing methods represent an active form of micromanipulation for biomechanical characterization. Its essence relies on the ability to trap and manipulate microspheres with a known force and precision. The method of trapping and manipulation differs between the types of tweezers, modifying the types of experimental set-up required. Low force outputs on the scale of pNs also means particularly high resolution and sensitivity to very low ranges of stiffness measurements. Trapped particles can be manipulated extra-cellularly or intra-cellularly for microrheological measurements of shear moduli or matching active cellular forces to quantify them. Optical, magnetic, or acoustic methods can each be used to create these tweezing platforms.

Optical tweezers

Optical tweezers use laser light through an objective to trap microparticles close to the focus point of the beam. Once a particle is trapped within the optical trap, its position can be manipulated by changing the focus of the laser beam. The trap behaves like a linear Hooke's spring near the focus and can be used measure and generate forces from 10s of fN to 100s of pN [109]. The k value of the spring, also known as the stiffness of the optical trap, depends on the calibration of the optical trap, with higher stiffnesses resulting in stronger holds on the microparticles. Movement of the trapped particle can be manipulated in three dimensions with the movement of the laser and its focus. Typically, polystyrene or silica microspheres are used as they can be functionalized with adhesion molecules necessary for cell binding and manipulation. A variety of configurations exist using single or multiple bead traps in static or dynamic approaches to measure forces and displacements. Static traps holding beads in place provide a resistive force against active biological motions such as motor protein movements in kinesin [110]. Dynamic

configurations manipulate the movement of the trapped bead to apply a known force and can be used to perform active microrheology at the cell scale within 3D tissues [111].

Optical tweezers work best for in vitro settings although in vivo uses have been possible, even by trapping small organelles with the right calibration. Trap calibration is dependent on the physical properties of the particle being trapped (shape, size, refractive index) and the homogeneity of the material surrounding it. Difficulties in implementing this system within living 3D tissues arise from tissue heterogeneity since calibration of the optical tweezers needs to be done in situ. Also, the scale of force output for this method largely limits it to measuring molecular forces. However, optical trapping can be adapted to create optical stretching systems, where two laser beams trap individual particles and deform single cells [112]. This works well in microfluidic systems to characterize single cells flowed through a channel in suspension for higher throughput analysis and has been used to study differences in stiffness between normal and cancerous cells [113].

Magnetic tweezers

Magnetic tweezers trap and manipulate multiple magnetic micro particles within a magnetic field generated by permanent magnets or electromagnets. Particle sizes can range from 100 nm to 100 μm and can be functionalized for cellular or extracellular adhesion. The magnetic force is controlled by the size and shape of the magnet, its magnetic orientation and its distance from the magnetic micro particle. Effectively, this means that a custom setup must be built to generate a specific force to be applied for a biological question, complexifying initial experimental set-up. However, a unique method called magnetic twisting cytometry (MTC) is made possible by magnetic tweezers because of their ability to generate twisting forces, and thus apply torque to micro particles by oscillating magnetic fields [114]. To create this torque, two sets of coils are required: one for magnetizing and one for twisting [115]. This is a type of active microrheology where

the torqueing of the trapped bead is used to measure the mechanics of individual cells on their surface [116]. Shear viscoelastic moduli of cells can thus be obtained with MTC by twisting micro particles on the exterior of the cell membrane.

Acoustic tweezers

Additional to light and magnetic waves, sound waves can be used to trap particles in a similar fashion. Many variations of acoustic tweezers are used to hold or manipulate particles and even cells [117]. Acoustic tweezers can induce 3D translational and rotational movements of multiple particles at once and is often used in applications involving cell sorting or patterning [118]. Its ability to easily manipulate many particles simultaneously makes it ideal for high-throughput application, such as force spectroscopy for single-molecular force measurements [119,120].

Microrheology – Passive and active

Microrheology involves particle tracking of many small tracer particles, which can be designed from the nanometer to micron scale. Tracer particles are suspended or injected into a matrix of interest, including intracellular or extracellular spaces, and their motions are tracked to study the local environment at short length scales. In passive microrheology, there is no external force application, and the movement of the particles is driven by thermal energy or Brownian motion as well as any fluctuating forces in the environment. Their motions will also differ depending on the environment's architecture: particles freely floating in a liquid medium will diffuse differently from those entrapped in a fibrous network. Considerations on the relative size of the tracers to the pore sizes of the matrix will also determine whether the particle is probing bulk or local properties. Due to the passive nature of this method, it is mostly used to study the linear response region of a

viscoelastic material. Alternatively, active microrheology consists of adding an externally controlled force to drive particle movement and is more suited in studying stiffer materials. Such induced forces can come from optical and magnetic tweezers as discussed previously [121].

In either type of microrheology, the mean square displacement (MSD) of the particles describes their local mechanics. Microscopy or dynamic light scattering are typical observation techniques to track their movements, but alternative methods are required to extract the MSD when particles are too small to resolve optically. Diffusing wave spectroscopy has better spatial resolution than microscopy or light scattering methods, effectively better suited to track smaller particles. Once MSD data is acquired, the generalized Stokes-Einstein relation can be used to extract the shear, storage, and loss moduli. Since these are internal measurements, intracellular properties can be studied in response to imposed microenvironmental changes. In cancer, microrheology has been used to measure adaptive changes within intracellular mechanics in response to matrix stiffness [61].

Elastography

Elastography is a medical imaging method to map the stiffness of tissues [122,123]. There are many ways to perform this at different length scale resolutions but common ones include the use of ultrasound or magnetic resonance imaging. At the core of each method, a distortion is created within the tissue, and an observation is made on how the tissue responds to infer the mechanical properties of the tissue. These distortions can include pushing, deforming, or vibrating the tissue surface which can be achieved by acoustic radiation force impulses with ultrasound, or even distortions from normal physiology such as a pulse. Stiffness can be traditionally calculated based on the applied force and resulting strain. Alternatively, calculating differences in how fast mechanical waves propagate

through the tissue also quantifies stiffness, where waves travel faster in stiffer tissues in comparison to soft tissues. Optical elastography provides the means to adapt traditional elastography to micron scale mapping of stiffness in vivo tissues. This adaptation results in greater sensitivity than conventional elastography, allowing it to provide higher resolution spatial profiles of tissue stiffness [124,125].

Brillouin microscopy

Brillouin microscopy is an example of optical elastography suited to study viscoelastic properties of cells and tissues non-invasively in 3D [126]. Microscopy captures the Brillouin light scattering phenomenon which occurs when light interacts with a material. Elastic vibrational waves cause light to scatter in different directions and are affected by material stiffness (E). While other techniques yield Young's modulus (E), this technique reads out the longitudinal modulus (M) that can be related back to E by Poisson's ratio, v, by $M = E(1 - v)/[(1 + v)(1 - 2v)]$. Thus, Brillouin microscopy is a non-invasive method used to map mechanical properties of cells in 2D and 3D microenvironment without physical contact [127].

Micropillar and microcantilever deformation

Microfabricated structures can often be fashioned to be compliant to cell-generated forces since they are commonly made of PDMS and other elastomeric materials. Micropillars can be designed with varying dimensions of heigh and diameter at high aspect ratios to alter the stiffness felt by cells or microtissues bending the pillars. An array of these structures can be used to study traction forces in cells [128,129]. Forces exerted by growing spheroids can be measured by arranging the micropillars in a circle to surround a spheroid place within it. As the spheroid grows the outward forces can be measured based on the deflection

of the micropillars(Figure 8) [93]. Similarly, microtissues can be cultured in situ between two larger microcantilever pillars to study their contraction force by observing the extent of pillar deflection (Figure 1.8) [92]. These pillars can be actuated by incorporating magnetic particles on or within the pillar to tug on the microtissues like a tensile tester [130]. This mechanism also provides mechanical stimulus to the microtissues to study their effects on tissue contractility [131,132]. To facilitate higher throughput studies and enhance stretching magnitude, micropillars can also be designed with vacuum actuation to study cytoskeletal remodeling under dynamic stretching [132].

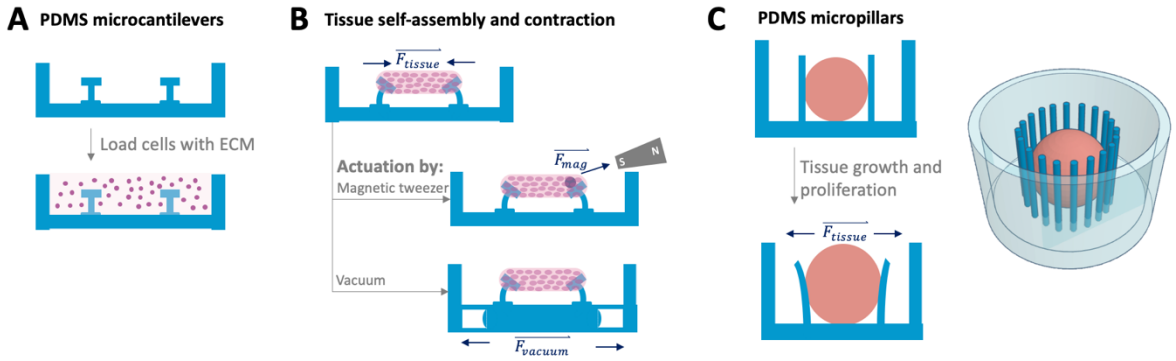

Figure 1.8. Schematic of microcantilevers and micropillars to measure microtissue mechanics.
(A) Microcantilevers are made of PDMS by microelectromechanical systems (MEMS) technology. A solution of cells in uncrosslinked ECM is cast in the well. (B) The cells self-assemble to form a functional and contractile microtissue around the cantilevers. Beam deflection and geometry are used to calculate the contractile force of the tissue. This construct can be actuated to apply forces and measure stiffness by incorporating a magnetic nickel particle and using magnetic tweezers to spatially manipulate the bead. Vacuum actuation is also possible for higher throughput applications. Figures are based on works by Legant et al., (2009), Zhao et al., (2013), and Walker et al., (2018) [92,130,133]. (C) Micropillars are also made of PDMS by MEMS technology. A multicellular aggregate is loaded within the array of beams. As the tissue grows and proliferates, the beams deflect, providing a quantification of the tissue's expansion forces. Figures are based on experiments by Aoun etal., (2019) [93].

Liquid and Hydrogel Microdroplets

A relatively recent development that seems particularly promising in measuring cellular-scale tissue mechanics involves liquid and hydrogel deformable structures. Stresses and stiffness can be measured within 3D tissues using oil droplets with magnetic particles or hydrogel microbeads that are incorporated into cell aggregates during tissue formation or injected within tissues (Figure 1.9). Magnetic particles suspended in oil can be actuated under a magnetic field to move the oil droplet within zebrafish embryos, actively probing tissue stiffness and viscosity [134]. They can also be passively deformed to measure anisotropic stresses [135]. This stress distinction is made due it the incompressibility of oil, which hydrogel microbead systems circumvent. Microbeads made of polyacrylamide or alginate are compressible and can measure isotropic stresses like mechanical pressure and tensile stresses [136,137]. Magnetic particles have also been incorporated into alginate hydrogels to function similarly to the magnetic oil droplets but are several millimeters in diameter and involve using nanoparticles [138]. Hydrogel microbeads made of a polyacrylamide derivative, N-isopropylacrylamide, can be used to generate local forces within tissues to non-invasively measure stiffness in 3D tissues without damaging the tissue. The mechanism behind this comes from the thermoresponsive nature of the material such that a slight temperature drop below body temperature conditions results in the force actuation of the microgel.

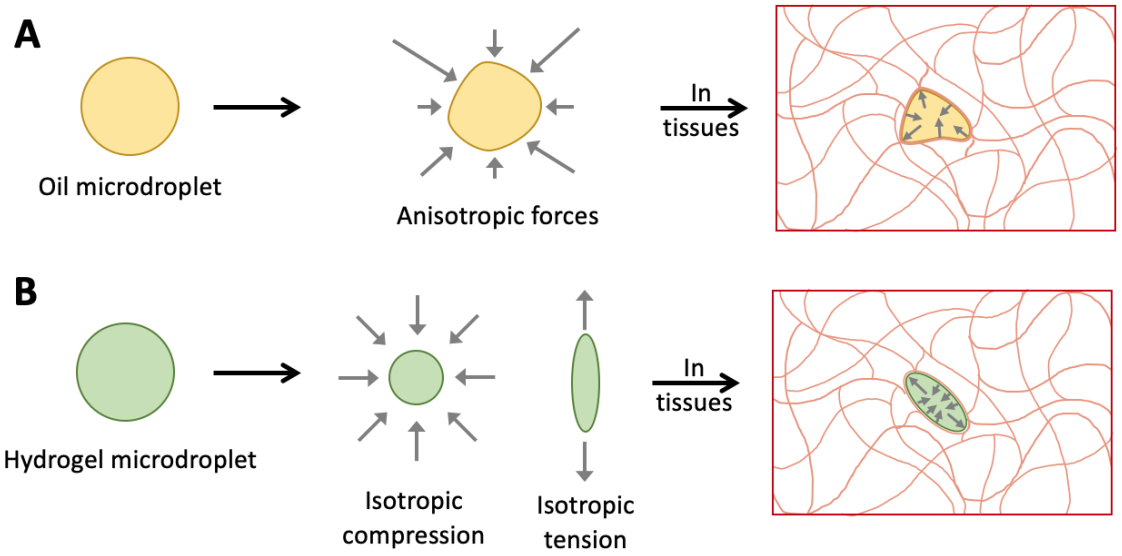

Figure 1.9. Microdroplets as mechanical sensors.
(A) Oil microdroplets deform non-uniformly under anisotropic stresses. They are injected into tissues to quantify cell-generated anisotropic forces and characterize cellular-scale tissue mechanics. (B) Hydrogel microdroplets deform uniformly under isotropic stresses. They are incorporated into tissues to quantify cell-generated isotropic stresses like tension and compression to characterize cellular-scale tissue mechanics. Figure based on works by Campàs et al., (2014), and Lee et al., (2019) [91,139].

1.1.7 Picking the right technique for the right purpose

Given the wide variety of commonly available and specialized designer techniques available for mechanical characterization of biological tissues, it can often be challenging to select the most appropriate metric for specific cases. This selection is particularly important, as comparison measurements on the same cell line source show orders of magnitude differences in material responses, depending on the force loading profile of the technique used [140]. To both highlight and resolve this problem, a summary of techniques and their relative resolutions and length scales has been included in Table 1. Summary of techniques., and in this section we present a short discussion on experimental considerations to be made in selecting and interpreting the results from a particular technique.

Table 1. Summary of techniques.

Method	Spatial scale	How it works	Length scale	Force range	Pros	Cons
Tensile testing	Global	· Apply pulling forces pointing outwards from the tissue	mm to cm	N	· Obtain overall tissue mechanics, · Easy to obtain and understand data	· Large sample volumes · Sensitivity difficult for soft tissue ranges · Assumes homogenous material
Compression testing	Global	· Apply pushing forces pointing inwards from the tissue	mm to cm	N		
Shear rheometry	Global	· Apply forces acting tangential to the surface of the tissue	mm to cm	N		
Tension gauge tether	Surface	· Ligand receptors immobilized to a tether (dsDNA or PEG) that requires different amounts of (known) forces to rupture · Observe whether there is cell spreading over a range of surfaces attached with tension tethers at one tension tolerance	10-100 nm	10-100 pN	· Measure molecular force across single integrins · Can decouple tension from stiffness	· Requires characterizing of each tension gauge and testing over multiple tension tolerance to determine one value
FRET-based tension sensors	Internal, surface	· Insert molecular spacer with known rigidity (spring constant) in between donor and acceptor of FRET system · Fluorescence intensity depends on distance which measures elongation of molecular spring for tension	10- 100 nm	1-100 pN	· Provide spatial and temporal maps of subcellular tensions	· Unfavorable signal-to-noise ratio in complex 3D tissues

2D and 3D traction force microscopy	Surface	· Gel of known elastic modulus containing dispersed fluorescent microbeads · Cell apply force, position of microbeads change · Track displacement to measure strain field and direct mapping of mechanical stresses	100 nm to 10 μm	100 pN to 100 nN	· Quantitative map of stresses generated by cell	· Calibrated in linear elastic regime · Only small deformations permitted · Mechanical constrain imposed by surrounding gel on growing tissue
Microindenter and microplates	Surface	· Application of a controlled force (or strain) at the surface of cell or tissues while monitoring its response (deformation/force) over time	100 μm to 10 mm	μN	· Quantitative measurements of forces and mechanical properties	· Contact with surface of sample · Global average of selected tip, tip geometry influences · Requires relatively flat tissues for accuracy
Atomic force microscopy and cantilevers	Surface	· Calibrated beam or cantilever that deflects in contact with surface of material · Measure deflection · Knowing mechanical properties of cantilever, can quantify forces and mechanical properties	10 μm	nN	· Quantitative measurements of forces and mechanical properties in vivo and in situ · Spatial mapping of elasticity assuming samples does not change over the time of the scan	· Requires contact with surface of sample · Time for spatial mapping several minutes · Obtaining elastic modulus requires fitting the data to models involving several assumptions

Laser Ablation	Surface	· Microdissection to measure retraction speed of ablated structure · Initial retraction velocity of ablated structure provides information for tension state before ablation · Probe tension but not compressive loads	10 nm to mm	pN to nN	· Easy integration to microscope set up (add a laser)	· Need to estimate some material properties for quantification · Better suited for isotropic and homogenous system like epithelial monolayers (2D)
Tissue Dissection and relaxation	Global, internal	· Ex vivo dissection of large tissue explants with a blade · Observe response (deformation) after dissection	4 mm to cm	mN	· Global tissue mechanics (average tension state, mechanical properties, surface tension)	· Only on large explants · No local information · Cells exposed to surface may reorganize to a non‑native state
Micropipette aspiration	Surface	· Local aspiration of a portion of a cell or tissue · Observe deformation (length of aspirated portion) over time · Measure force and material properties using static and dynamic response of system	2-50 μm	~100 nN	· Quantitative measurements of force (stress) and other mechanical properties · Applicable for in vivo and in/ex vivo	· Requires constant contact with sample · Surface measurements only (no internal)
Optical tweezers	Internal, surface	· Focused laser beam on a bead to control its movement and to apply controlled forces within sample	0.5-2 μm	fN to 100 pN	· Beads have controlled physical properties	· Difficult to calibrate in situ of in vivo if material lack homogeneity (which most tissues do)

		· Measure the response of the bead for quantitative measurement of mechanical properties and forces			· For highly localized measurements	
Magnetic tweezers and twisting cytometry	Internal, surface	· Apply controlled net force on magnetic bead within a gradient of magnetic field · Measure the response of the bead for quantitative measurement of mechanical properties and forces	10 – 50 μm	pN to nN	· Can provide quantitative measurements of force, torque, and mechanical properties with proper calibration	· Require steep gradient of magnetic field for tissue scales (difficult to generate) · Calibration within living tissue difficult
Acoustic tweezers	Surface	· Acoustic radiation forces from sound waves move particles or cells	10 μm	fN to pN	· Simultaneously apply forces to many microspheres (high throughput); · Can move particles or cells within any medium · Spatial movements of cells in 3D possible	· Limited force application range on cell surfaces · Better suited for sorting applications
Microrheology	Internal, surface	· Micro-sized beads injected in cells · Track motion of beads by thermal noise or active fluctuating forces inside cell · Characterize distribution of bead motion	100 nm to 10 μm	pN to nN	· Quantitative measurements for in vivo and in situ	· Passive system assumes only thermal fluctuation drives diffusive motion within cell (not necessarily true) · Cannot probe at larger supracellular scale

Micropillar arrays and microcantilevers	Surface, global	· Measure traction forces of a cell laying upon a bed of microfabricated post by observing the deflections of the posts and knowing micropost stiffness · Also scalable to engineered tissues deflecting microcantilever posts	100 nm to 10 μm	100 nN to 10 μN	· Quantitative measurements of mechanical force · Pillar dimensions can be varied for different length scale measurements	· Requires microfabrication preparation using SU‑8 photolithography (technically challenging) · in vitro only (single cell or engineered tissue studies)
Oil droplet-based sensors	Internal	· Cell-sized oil microdroplets microinjected between cells in a tissue · Knowledge of its interfacial tension and reconstruction of its shape in 3D allow quantitative measurement of mechanical stresses surrounding the droplet	30-100 μm	nN	· Quantitative measurements of endogenous stresses in vivo and in situ · spatial and temporal measurements within simple embryonic organisms	· Microinjection at site · Can measure quantitative anisotropic stresses but cannot measure isotropic stress (tissue pressure) due to incompressibility of oil
Hydrogel droplet-based sensors	Internal	· Cell-sized microgels integrated or injected within in vitro and in vivo animal model system · Fluorescent imaging deformations on the microgel or by the microgel provides information on local force and stiffness	10-50 μm	1 μN to N	· Can measure isotropic stresses generated within 3D complex tissues (mutlicellular spheroids) · Variants can remotely produce local strains to probe internal stiffness	· Fluorescent readout within tissue limited by optical depth of microscope

Elastography	Internal	· Induce distortion in the tissue (deforming, pushing, or vibrating) by probe, ultrasound, or normal physiological processes · Observe the tissue's response to deformation by conventional medical imaging techniques like ultrasound or magnetic resonance	100 µm to 10 mm	N/A - readouts based on frequency shifts	· Quantitative spatial mapping of stiffness within soft tissues in clinical settings · Techniques can be tailored to map a wide range of stiffness scales (soft tissues to musculoskeletal tissues)	· Limited depth of penetration when mapping stiffnesses within the human body · Temporal mapping possible, but with limited spatial dimensions
Brillouin microscopy	Internal	· Light scatter from laser source off solid components within sample is captured by a spectrometer · Frequency shifts from scattered light provide material density and refractive index to characterize material property	100 nm to µm (light/acoustic wavelength)	N/A - readouts based on frequency shifts	·No sample labeling required ·Possible to obtain both elastic and viscous properties through the complex modulus' real and imaginary parts respectively · Can create 3D image reconstruction based on shifts in frequency	· Material property given as complex longitudinal modulus (M) that is different from Young's modulus and tends to readout much higher values · Proper quantification to separate real and imaginary parts of M require exact knowledge of local refractive index and material density

To select appropriate techniques, it is critical to clearly establish the insight required from the experiment, and the advantages and limitations of the chosen technique. For example, one technique may be best suited to measure a specific material property like stiffness and less accurate for another like viscosity. Techniques that share the same physics on how the tissue is deformed produce similar modulus values and differences can be accounted for based on the shape geometries of the probe used. The handling of the material and the binding of treated surfaces for mounting samples can also contribute to variation in these measurements. Furthermore, the analysis involved in transforming raw data into the material properties can create differences depending on the assumptions used to fit the measurements to a particular model.

Bulk measurements obtained from rheology and tensile/compressive testing provide an averaged value of the overall sample (Figure 1.4). They also assume a degree of homogeneity within the material which is problematic with tissues since they are typically heterogeneous, especially at the large volumes which are required for these measurement techniques. Measuring live matter is also particularly difficult in bulk measurement techniques and often requires explanted material (removed from the body) which may not be feasible considering the amount required. The mechanical properties of the tissue may be different outside the living organism as well since cell hypoxia and death begins soon after removal.

Techniques such as atomic force microscopy, nanoindentation and micropipette aspiration, take surface measurements and recognize tissue heterogeneity by taking local measurements (Figure 1.4). They have the capacity to map material properties such as the stiffness of live samples through consecutive point measurements much like line by line printing. However, this has limited capabilities for live 3D tissue where mechanical properties at the surface may not reflect internal properties. When considering local mechanical measurements, surface mechanical properties of the tissue will also differ from

internal mechanical properties as well since tensile forces over solid stress will be more apparent near the surface of the tissue compared to the interior.

Displacement based measurements produced by techniques like magnetic or optical tweezers have the capacity to take mechanical measurements within 3D tissues (Figure 1.4). Quantitative measurements by these techniques require the application of controlled forces or knowing some property of the substrate material that the tracking beads are suspended in. Unfortunately, these techniques often require specialized equipment and complex analyses to generate meaningful data. Furthermore, the scale of measure for these techniques are often subcellular which may not be the appropriate scale to consider when studying tissue mechanics in relation to tissue health. The forces that the cell experiences are the forces that it responds to.

1.2 Rationale

Changes in the mechanical properties of cells and their extracellular matrix are related to changes in tissue health. The effects of matrix stiffness, and compressive mechanical forces experienced by cells, are especially important in regulating the stability of the breast duct architecture as well as triggering an invasive transformation in ductal breast cancer [47,58]. The development of these tumors presents a complex and dynamic mechanical environment, with forces being generated during tumor growth in a confined tissue duct. Monitoring tumor-matrix mechanics may provide an important indicator of the likelihood of developing a life-threatening metastatic cancer in the future. However, current techniques are unable to monitor tissue stiffness during cancer development without disrupting the tissue architecture, or killing the cells with fixatives, thereby altering the three-dimensional environmental mechanics [141]. Furthermore, they are restricted in their ability to spatially resolve cellular-scale stiffness variations in 3D tissues, which would be critical to characterize the stiffness a cell would experience in situ. Hence, there is a need for techniques to study cell-environment mechanics, in real-time without disrupting living tissue architecture.

1.3 Objectives

The specific aims to accomplish this thesis are:

(1) to engineer smart-material probes to monitor local stiffness within engineered tissues;

(2) to measure and track stiffness evolution within 3D engineered models of breast cancer;

(3) to extend the capabilities of the smart-material probes to measure local viscoelasticity within cancer spheroids.

Overall, this body of work aims to develop smart material sensors that will allow us to study living cell mechanics throughout their growth and without disrupting tissue architecture or fixing the cells. More broadly, the engineered technology will enable rapid and real-time stiffness measurements in model culture systems, enabling mechanical characterization with unprecedented resolution and sensitivity to uncover novel perspectives on the role of tissue microenvironment mechanics. Irregular changes in these mechanical elements may provide early indicators for deviations of normal physiology and health.

Chapter 2

Local tissue mechanics influences cell behavior but are difficult to measure at the cell scale. Current techniques available have shown that local stiffness can vary broadly between a few pascals to hundreds of kilopascals depending on the method used to assess this. There are specific limitations to current methods that I aimed to improve upon: the first was the ability to measure internal cell-scale stiffnesses within intact tissues, and the second was to reconcile the large differences in stiffness magnitudes reported by different techniques. Using microgels made of thermoresponsive N-isopropylacrylamide hydrogels, I designed, characterized, and established the use of a novel cell-scale stiffness sensor to study the local cellular microenvironment. This work was published in Nature Communications on September 21, 2020, and reproduced here with permission. In this manuscript, I described the model used to relate hydrogel expansion to external stiffness and then use this model to study the differences in microscale stiffness that arise from spheroids generated from different formation techniques and different breast cancer cell lines. Furthermore, I demonstrated the use of this tool in long term animal studies and show differences in stiffness heterogeneity between tumors of different ages.

2 Mapping cellular-scale internal mechanics in 3D tissues with thermally responsive hydrogel probes

2.1 Abstract

Local tissue mechanics play a critical role in cell function, but measuring these properties at cellular length scales in living 3D tissues presents considerable challenges. Here we present thermoresponsive, smart material microgels that can be dispersed or injected into tissues and optically assayed to measure residual tissue elasticity after creep over several weeks. We first develop and characterize the sensors, and demonstrate that internal mechanical profiles of live multicellular spheroids can be mapped at high resolutions to reveal broad ranges of rigidity present within a tissue, which vary with subtle differences in spheroid aggregation method. We then show that small sites of unexpectedly high rigidity develop in invasive breast cancer spheroids, and in an *in vivo* mouse model for breast cancer progression. These focal sites of increased intratumoral rigidity suggest new possibilities for how early mechanical cues that drive cancer cells towards invasion might arise within the evolving tumor microenvironment.

2.2 Introduction

Exquisitely structured tissues and organs arise from a homogenous blastomere through spatial patterns of cell proliferation, migration, and differentiation, in concert with matrix secretion and remodeling [3,23,142,143]. Mechanical features of the local microenvironment are critical regulators of these cellular processes [144–151], and tissue stiffness is now well-established to drive fate-function relationships during development [24,152]; disease progression [22,153–155] and tissue homeostasis [156–158]. However, our technical ability to monitor and characterize tissue mechanics at the cellular length scale during tissue development remains severely limited, and could be critically important in elucidating biophysical mechanisms of tissue morphogenesis and disease.

Conventional mechanical characterization techniques provide only a limited view of tissue rigidity, particularly at the meso-length scale of individual cells. Macroscale measurement tools such as tensional or shear rheometry cannot capture local mechanical variations around cells [159], while high-resolution tools such as atomic force microscopy are ideally suited for sub-cellular nanoscale measurements, and are limited to measuring near-surface stiffness in two-dimensional or cut tissue sections. Although non-contact techniques such as ultrasound elastography or magnetic cytometry [160–162] provide limited remote access to address these issues of scale, they cannot mimic a cell's ability to interrogate the surrounding tissue by applied deformations with stroke lengths of 10s of microns [26,163].

Serwane *et al.* recently developed an intriguing strategy to measure tissue mechanics with injectable, cell-sized, magnetic oil droplets, that deform in response to applied magnetic fields to quantify local tissue mechanics in soft tissues such as zebrafish embryos [134]. This powerful approach provides unique insight into highly local evolution of tissue mechanics during development, but the small droplet volumes allow only very low magnetic actuation forces, limited stroke lengths, and can only measure stiffnesses of < 1 kPa. Moreover, oil droplets also split apart during large scale morphogenesis, limiting the monitoring period. Finally, this technique requires specialized equipment and expertise

for simultaneous magnetic and optical probing, which limits experiments to small, thin, transparent, tissues that can stimulated with a uniform magnetic field. To circumvent some of these limitations, we build upon recent materials-based strategies using poly N-isopropylacrylamide hydrogels that have been used generate local deformations within porous materials [159].

Microscale temperature-actuated mechanosensors (μTAMs) can measure a wide range of residual tissue elasticities within 3D biomaterials, at the length-scales of individual cells, in engineered tissues or animal models. μTAMs are spherical, thermoresponsive hydrogels that remain compact at tissue culture temperatures, but swell when cooled by a few degrees. By measuring the degree to which they expand, the residual elasticity after creep of the surrounding tissue can be inferred (Figure 2.1 A). In this work, we first develop the design principles to optimize hydrogel formulations for soft tissue measurements; and then demonstrate that μTAMs can be integrated into engineered tissues and animal models. These studies reveal that significantly different internal residual elasticities arise in multicellular aggregates based on aggregation method; and that highly localized hot spots of considerably elevated intratumoral rigidity emerge during establishment of a metastatic breast tumor.

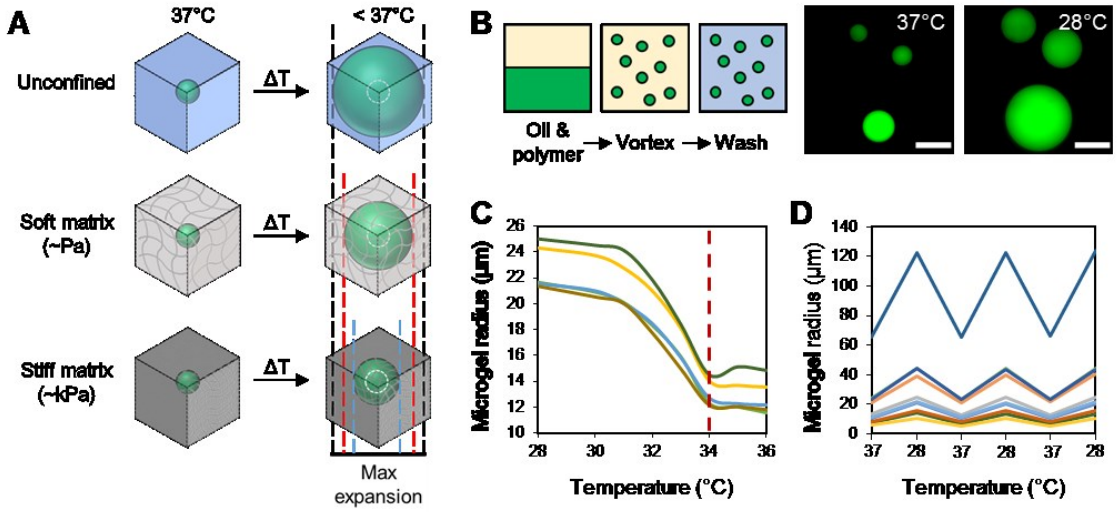

Figure 2.1. Conceptual overview of using µTAMs to measure local residual elasticity. (A) Poly N-isopropylacrylamide (PNiPAAM) hydrogel droplets reversibly expand and collapse based on temperature. PNiPAAM microgels can be compacted at tissue culture temperatures of 37 °C and embedded in tissues of interest, where they will keep their contracted state while the tissue is maintained in culture conditions. Reducing the temperature below the lowest critical solution temperature triggers the microgels to expand. The degree of expansion permitted depends on the rigidity of the surrounding porous material. The expansion ratio of the sensor can hence be used to determine highly localized measurements of internal tissue residual elasticity after creep, at or near tissue culture conditions. (B) To fabricate the hydrogels, an oil/water vortex emulsion technique is used to produce polydisperse spherical microscale temperature-actuated mechanosensors (µTAMS). (C) Swelling transitions between expanded and compacted states occur at 34°C, which can be (D) reproducibly observed over multiple temperature cycles. Different colors represent individual microgels in panels C and D. Scale bar = 50 µm. Representative images are consistent over three batches of µTAMs.

2.3 Results

2.3.1 Design and characterization of μTAMs.

Poly N-isopropylacrylamide (PNiPAAM) hydrogels are tunable, biocompatible, thermoresponsive materials that remain compact at 37 °C, but reversibly swell at slightly lower temperatures when solute interactions favour hydrophilic domains of the polymer [164,165]. To form PNiPAAM gels into μTAM probes, microspherical droplets of hydrogel formulations were polymerized with a fluorescent label [139], in an oxygen-free, oil/water vortex emulsion (Figure 2.1B). This produces polydisperse hydrogel particles with expanded diameters that range from 10 to 100 μm (Supplementary Fig. 1), which is comparable to the size and mechanical sensing range of many adherent cells when compact [166]. The fabricated μTAMs retain their ability to reversibly shrink above a lower critical solution temperature of ~34 °C [167] (Figure 2.1C &D). The thermoresponsive diameter change was independent of μTAM size, and tunable based on the hydrogel formulation (Supplementary Fig. 2). Free expansion in solution was tunable between 1.92 ± 0.05 and 3.4 ± 0.18 for the polymer formulations tested. To confirm suitability in tissue culture conditions, we tested μTAM expansion in physiologic protein-rich conditions, as long-chain molecules in the cellular milieu may molecularly crowd and interfere with the polymer-water interactions necessary for expansion. Free expansion ratios of non-functionalized μTAMs were not significantly altered in even 100% fetal bovine serum (FBS; Supplementary Fig. 2), which contains supraphysiologically high levels of soluble protein [168].

μTAMs require an adhesive matrix protein coating to support integration into tissues, which may impact their expansion characteristics through transport limitations or mechanically restrictions. Collagen I was selected as a candidate coating for all described experiments, as it is the most abundant matrix in the tissues studied. Standard sulfo-SANPAH crosslinking chemistry [139] produced a monomeric collagen coating on the μTAM surface, and did not significantly affect the free expansion ratio in standard culture conditions (Supplementary Fig. 2). We did observe a small but non-significant increase in

expansion variability in the 100% FBS condition, likely arising from collagen interactions with supraphysiologically high concentrations of albumin present in FBS [168]. Since *in vivo* interstitial albumin levels are an order of magnitude lower than in this extreme case [169], this mechanism is unlikely to impact swelling behaviour in tissues. Together, these results confirm the suitability of PNiPAAM for repeated expansion cycles *in situ.*

2.3.2 Design and characterization principles for μTAM hydrogel formulations.

To select the appropriate hydrogel formulations and model deformation, we required a conceptual framework with which to design μTAMs for tissues of different rigidity ranges. Theoretically, a complete molecular simulation from first principles could determine the stored energy density of various hydrogel formulations, but such approaches would require a combination of multiscale structural, thermodynamic and molecular-interaction simulations with supporting characteristic measurements. As a first approximation, we instead reasoned that the dimensional expansion of compacted μTAMs is a balance between mechanical energy stored in the compressed sensors, and the mechanical work required to deform the surrounding material during expansion. Compacted μTAMs can hence be conceptualized as springs that are pre-loaded by thermodynamic expulsion of water prior to embedding in the tissue. Reducing the temperature releases this pre-strain, and the springs return to a new equilibrium position that is influenced by the rigidity of the surrounding material (Figure 2.2A).

To develop finite element computational models, we approximated the stored energy density as proportional to microgel rigidity and the degree of initial compressive pre-strain. This approximation does treat any non-linear stiffening effects as a single lumped parameter, but should still provide insight into design criteria for desirable PNiPAAM properties. Simulated spherical μTAMs of defined stiffness were isotropically pre-strained and placed within an encapsulating linear elastic material. When the pre-strain is released, a characteristic negative sigmoidal curve for μTAM expansion is produced as

a function of encapsulating tissue stiffness (Figure 2.2B). This is reasonable, as µTAM expansion should asymptotically approach the free expansion ratio in sufficiently soft tissues, and the completely compressed size in excessively stiff tissues. Increasing the mechanical rigidity of the µTAMs while maintaining the pre-strain levels increases the stored strain energy, shifting the sigmoidal measurement curves to provide greater sensitivities for stiffer tissues. Similar results were observed when increasing the pre-strain while maintaining µTAM mechanical rigidity. Hence, tuning the µTAM expansion ratio and mechanical rigidity can together be theoretically used to optimize stored mechanical energy in the sensors, to make measurements with desired sensitivities to tissue stiffness.

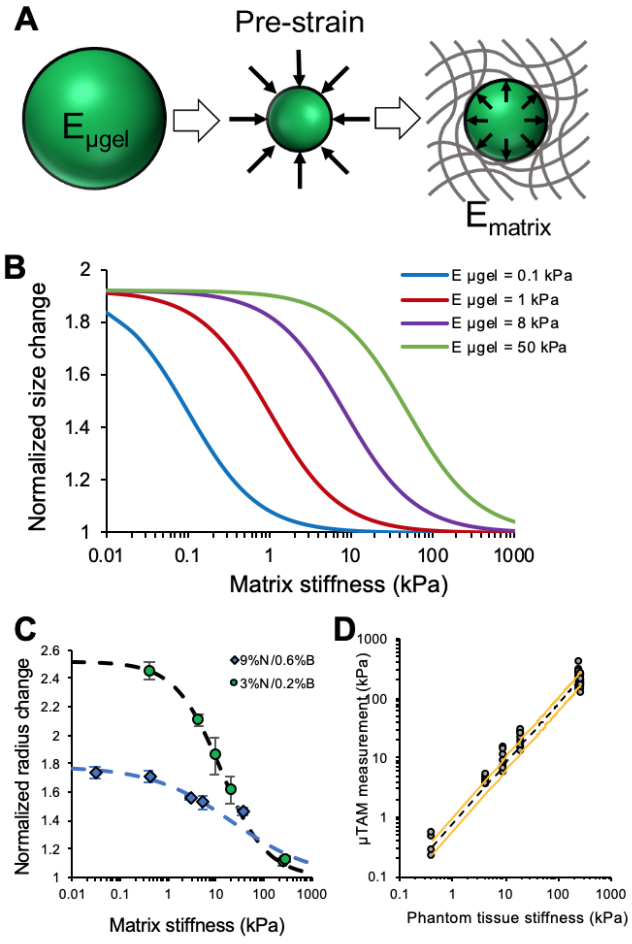

Figure 2.2. Modelling and characterization of µTAM expansion.
(A) µTAMs can be modelled as pre-strained springs when compacted, which then deform the surrounding matrix when the pre-strain constraint is removed. (B) Simulations using

this conceptual approach indicate that μTAMs sensitivity to the stiffness of the surrounding matrix can be tuned based on stored strain energy in the μTAM, which depends on μTAM rigidity over the actuation stroke length and applied pre-strain. A characteristic sigmoidal curve is observed with maximized measurement sensitivities in distinct measurement regimes. (C) Empirical characterization data demonstrates similar sigmoidal behaviors base on μTAM polymer formulation (Supplementary Table 1; data presented as mean +/- SD; n = 6 to 11 μTAMs). Dashed line shows simulated data from a sigmoidal data fit with iteratively optimized parameters (Supplementary Table 3). (D) Multiple μTAM measurements of residual matrix elasticity are compared against rheological measurements of matrix stiffness to determine the precision of each measurement. A linear relationship between matrix stiffness (black dashed line) and measurement precision (yellow bounding lines) was observed, and used as a model to estimate the error in all subsequent measurements.

2.3.3 Sensor calibration and validation in engineered tissues

To experimentally test the trends expected through simulation, we encapsulated μTAMs in stiffness-tunable polyacrylamide tissue phantoms (Supplementary Table 2). Polyacrylamide exhibits linear elastic mechanical properties over a large strain range [139], making it an ideal phantom material for these tests. Although the PNiPAAM formulations had similarly high mechanical stiffness in their compacted states, we were unable to independently tune the expanded stiffness and expansion ratio of the μTAMs (Supplementary Fig. 3), making it difficult to predictively tune the lumped strain energy parameter underlying the model. However, low- and high- polymer content formulations were tested, and demonstrated the expected negative sigmoidal curve for increasing tissue stiffness (Figure 2.2C). Based on these experimental results, we selected the 3% NiPAAM/0.2% bisacrylamide μTAM formulation for all described experiments, as it displayed the highest measurement sensitivity within the expected stiffness ranges for soft tissue. We then determined the error associated with each individual μTAM measurement by comparing the μTAM-reported residual elasticity with the known stiffness of the tissue phantom, and empirically found that measurement errors can be modelled as linearly increasing with measurement values (Figure 2.2D).

To verify that the μTAMs work as expected in an engineered tissue, we embedded them in multicellular spheroids (Figure 2.3A&B), which are commonly used to model three-dimensional, diffusion-limited, and high-cell density tissues [170]. A model T47D cell line suspension was mixed with μTAMs, and formed into spheroids by aggregation [171]. As a first demonstration of μTAM stiffness sensing, we measured sensor expansion before and after tissue crosslinking through paraformaldehyde fixation, which we verified would not affect μTAM operation (Supplementary Fig. 4A). Embedded μTAMs remained circular in both their compacted and expanded states, in both live (soft) and fixed (stiff) tissues, indicating that the expansion force generated is sufficiently large to overcome small gradients of residual elasticity that may exist around each sensor (Supplementary Fig. 4B). All measurements were taken after μTAMs reached their equilibrium sizes (~30 minutes, Supplementary Fig. 4C), and hence all measurements reported are of residual elasticity after viscous tissue creep. The average residual rigidity increased significantly after fixation, demonstrating that the sensors function as expected (Supplementary Fig. 4D, E). These results confirm that water transport, even within densely crosslinked spheroids, is sufficient to swell the μTAMs, and that the μTAMs function as expected in an externally manipulated biological model system.

2.3.4 Internal spheroid mechanics differ with cell aggregation method

Since spheroid architecture can be internally heterogeneous, we asked whether μTAMs can be used to determine whether spheroid fabrication methods affect internal tissue mechanics. We hence formed 400-500 μm diameter spheroids containing 1-3 μTAMs from HS-5 fibroblasts (Supplementary Fig. 5A-B), using an aqueous two-phase system (ATPS) that confines cells to a small phase-separated liquid volume [172]; and a micropocket-based system in which cells passively settle into and aggregate in hydrogel cavities (Figure 2.3A) [171]. These two techniques both rely on cell-driven aggregation and compaction within confined volumes, and should hence produce reasonably similar structures. No significant differences in internal cell density patterns were found in H&E-stained

histology sections of the two spheroid types (Supplementary Fig. 5C-E). However, in the ATPS-formed spheroids, circumferential cell alignment increased (Supplementary Fig. 5F-G) and was accompanied by a distinctive f-actin ring structure at the spheroid periphery (Figure 2.3B). We then asked whether μTAMs might capture mechanical differences arising from these observed structural differences (Figure 2.3C). Significant mechanical heterogeneity is observed across the spheroids in both cases, with measurements ranging from 0 to 13 ± 2.7 kPa in micropocket spheroids and 0 to 22 ± 4.6 kPa in ATPS spheroids (Figure 2.3D), with no clear spatial patterns observable based on position within the spheroid. This broad range of residual stiffness likely reflects heterogeneity of internal architecture at these length scales within the spheroids, which is quite consistent with histology sections and with previous reports of cell heterogeneity within spheroids [136,139]. When pooled together, spheroids formed through ATPS-induced aggregation exhibited significantly higher internal residual rigidity than those formed via micropocket-based aggregation (Figure 2.3E).

Hence, conceptually similar fabrication methods produce spheroids with distinct internal tissue mechanics, and while the cause of these subtle differences remain uncertain, they may arise from small osmotic compressive pressures exerted by the dextran on the spheroids in the ATPS method [64,173]. Speculatively, these differences could spatially influence cell behaviour within the spheroid, which may contribute to explaining why biological findings vary considerably between research labs that use spheroids formed via slightly different methods [174]. In general, these experiments establish the utility of μTAMs in spatially characterizing internal mechanical rigidities that arise in 3D tissues.

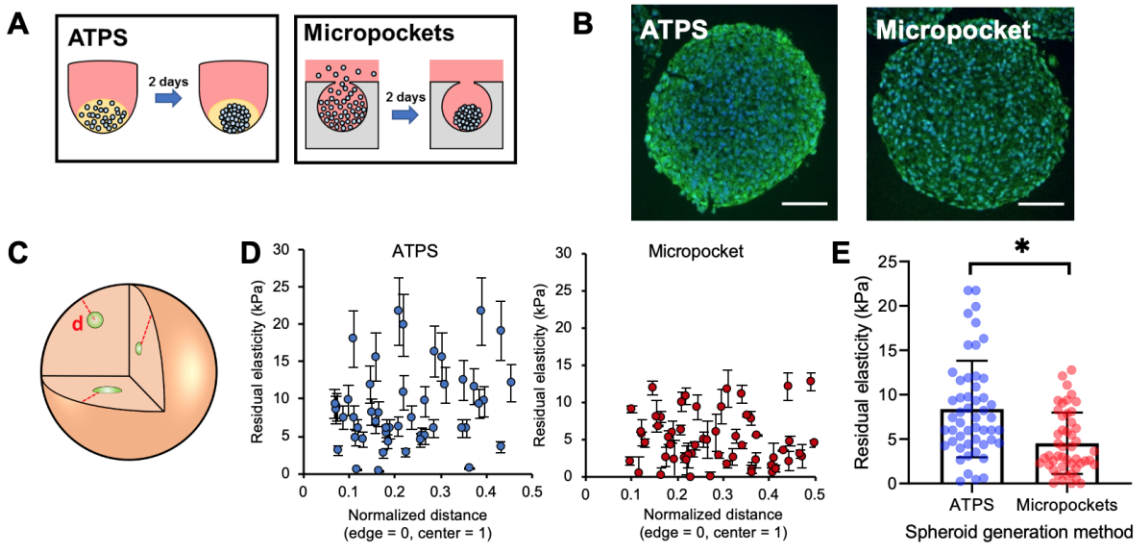

Figure 2.3. Distinct internal spheroid mechanics arise based on tissue formation technique.
(A) HS-5 fibroblast spheroids can be formed using a printable aqueous two-phase system (ATPS), in which cells are confined within a small droplet of immiscible liquids or by confining cells within a small cavity in a hydrogel where they passively aggregate. (B) These techniques produce grossly similar spheroids, with subtle distinctions in internal architecture as assessed by tissue sectioning and staining (green = f-actin; blue = nuclei; scale bar = 100 μm). (C) PNiPAAM microgels can be randomly incorporated into 3D multicellular spheroid cultures during the tissue formation process. (D) Pooled μTAM measurements across multiple spheroids show no obvious patterns of internal residual elasticity based on spatial location within the spheroid. Data presented as measurement +/- expected error. (E) Significant differences are observed in average internal rigidity between the two formation techniques. Data presented as mean +/-SD. n = 48 and 56 individual μTAM readings across 30 ATPS and 40 micropocket spheroids respectively for panels D and E over 3 independent experiments. * denotes p = 0.0022 for in an unpaired two-tailed t-test. Representative spheroid images from one of the three independent HS-5 spheroid generating experiments of each method.

2.3.5 Internal stiffness levels of engineered tumors vary with cell type

We next asked whether μTAMs could resolve conflicting reports regarding the stiffness of metastatic and non-metastatic cancer tumors. Invasive cancer cells themselves are well-established to be more mechanically compliant than non-invasive cell types [51], and compliant tumors are associated with local recurrence and metastasis [35,49]. However,

clinical evidence suggests that metastatic likelihood increases with tissue stiffness [175,22], and external mechanical stiffness is known to promote cell migration and invasion *in vitro* [52,176,177]. Other studies suggest that the internal stiffness of invasive tumors is more heterogeneous than quiescent tumors [36]. In all cases, these observations were made using either bulk mechanical characterization, or through surface mapping of cut tissue sections which is known to release mechanical stress [35]. Here, we aimed to use the μTAMs to characterize the internal mechanical heterogeneity of live engineered tumors generated from differently aggressive breast cancer cell lines.

Using the micropocket-formation method, we produced similarly-sized spheroids with embedded μTAMs from human metastatic breast cancer cell lines (Figure 2.4A, Supplementary Fig. 6) that we have previously established to be non-invasive (T47D) and invasive (MDA-MB-231) in collagen hydrogels over 2 days in culture [171]. While the residual internal elasticity of the spheroids did vary within spheroid populations, this was not correlated with spatial position within the spheroid (Figure 2.4B). The average residual elasticity was significantly greater in invasive spheroids (Figure 2.4D), and reached unexpectedly high values at some sites (295 ± 62 kPa). Grubb's test confirmed that these readings were not outliers, and nearly a third of the measurements fall into a high-rigidity regime (Figure 2.4C). Hence, some fraction of cells within the invasive spheroids experience extremely high local rigidities, perhaps resolving the contradictory needs for high-stiffness to prime the mechanical invasive machinery of invasive cell types, while allowing the cells to be sufficiently soft to invade through the surrounding matrix.

Although these observations of residual elasticity within spheroids is significantly higher than previously reported, these results are quite consistent with previous studies. Fresh metastatic tumor tissue sections probed by atomic force microscopy were found to be quite heterogenous, containing stiffer regions (up to 16 kPa), compared to non-invasive tumors [36]. The internal mechanical stress state of tissues can be very high when measured in live samples [178], and tissue sectioning is well-established to release these stresses and disrupt the active contractility of cells [35], which would otherwise increase

rigidity in non-linear biological materials [179]. Our findings demonstrate the extent of this effect, further supporting the need for mechanical measurements without disrupting live tissue architecture. Furthermore, non-disruptive live techniques such as quantitative ultrasound have previously demonstrated internal tumor stiffness measurements up to 150 kPa [180], albeit at considerably lower spatial resolutions. It is therefore likely that these measurements reflect highly focal and considerably larger rigidities that are blurred over a larger region. Hence, the measurements obtained with this technique are reasonable, and suggest that mechanical stimuli that promote invasion within tumors may be provided by small groups of cells within the spheroid population.

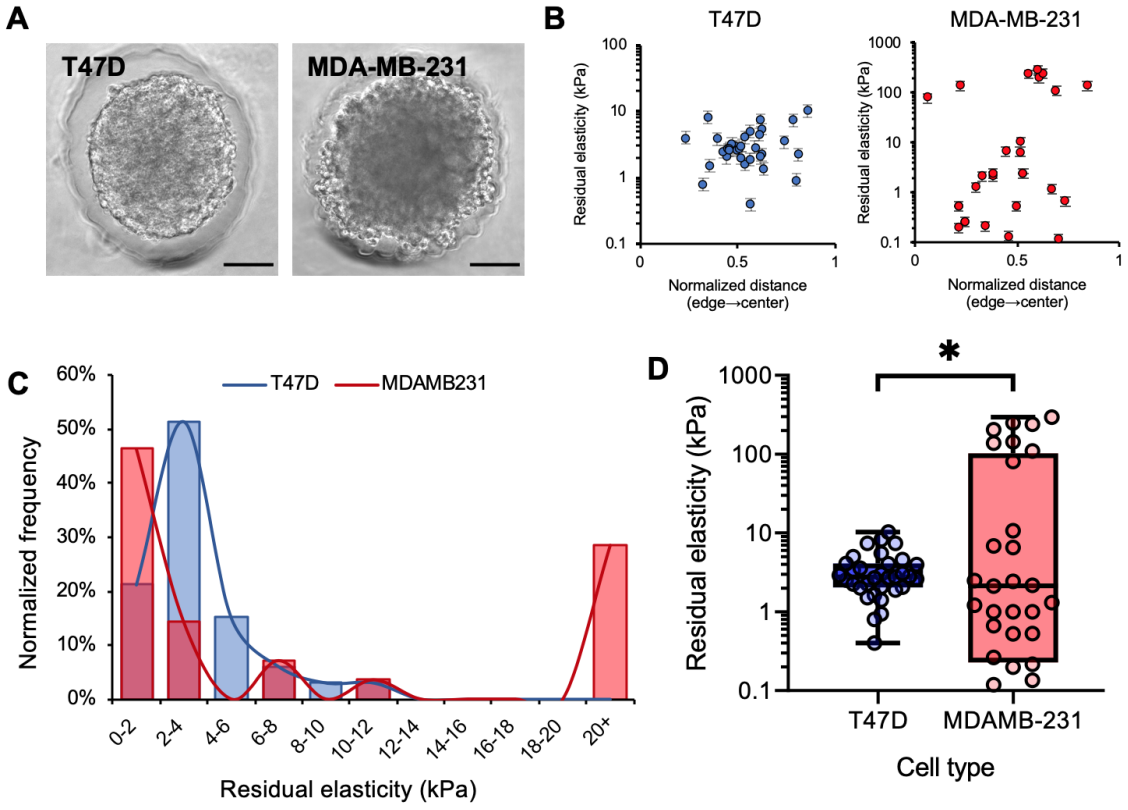

Figure 2.4. Residual elasticities within engineered tumors varies based on cell type. (A) Spheroids generated from aggressively invasive MDA-MB-231 and less aggressive T47D metastatic breast cancer cell lines. Scale bar = 100 µm. (B) Spatial variation of internal residual elasticity in tumor spheroids of each cell type (data presented as measurement +/- expected error, pooled from 25-27 spheroids with 1-2 µTAMs embedded in each). (C) Histogram of measurement data demonstrates that a significant fraction of µTAMs in the MDA-231 spheroids register high residual rigidities. (D) The average

residual elasticity within spheroids are significantly different based on cell type. Box plots indicate the median and 25th to 7th percentiles, and the whiskers span the range. * p = 0.0074 (unpaired two-tailed t-test, n = 33 and 28 μTAM stiffness measurements respectively for T47D and MDA-MB-231 spheroids for all panels over one set of experiments).

2.3.6 Long-term measurements of internal tumor rigidity in animal models

We then asked whether our findings extend to in vivo models. Previous studies have demonstrated that tumors can macroscopically soften, stiffen, or stay the same compared to adjacent normal tissue [49], but whether this reflects macroscale tumor organization or microscale rigidity remains unclear. Furthermore, the surrounding stromal tissue stiffens with disease progression [52], and it is challenging to eliminate those contributions when macroscopically probing live whole-tumor mechanics. Therefore, measuring mechanics within the living tumor itself, at length scales and stroke lengths relevant to individual cancer cells may yield new insights into tumor mechanobiology.

We injected immune-competent BALB/c mice with collagen-functionalized μTAMs and a 4T1 metastatic cancer cell line that has been well-established to initially form local tumors in the mammary fat pad and spontaneously transition through the metastatic cascade with invasion to distal sites over time [181]. We confirmed that tumours grew rapidly in the mammary fat pad, degrading mammary gland tissue architecture by replacing fat tissue and lymph nodes with solid tumour, and that within 3 weeks, a heterogeneous architecture indicative of advanced disease was observed (Figure 2.5C; Supplementary Fig. 7). While initially clustered along a well-defined wound track after injection, uTAMs dispersed within the tumor as the disease progressed (Figure 2.5B). No signs of additional fibrosis or inflammation were observed between sham animals injected with PBS only, and those injected with PBS and μTAMs, suggesting excellent biocompatibility of the μTAMs (Supplementary Fig. 8).

Mice were sacrificed weekly, and the excised fat pads were immediately placed in a PBS bath to control tissue temperature for stiffness measurements (Figure 2.5A). Only those μTAMs away from the excision wound edge were selected for analysis, to avoid measurements in regions affected by tissue stress release. These sensors were fully incorporated into the tumour tissue and retained their ability to swell and compact with temperature changes (Figure 2.5D). Although the mean measurements of internal tumor rigidity did not change significantly over 21 days, we observed a significantly different distribution of measurements as the tumor progressed from day 7 to day 21 (Figure 2.5E; * $p = 0.022$), with some sites stiffening between 25 and 50 kPa. The probability of measuring these high values in the sham control experiment are between 0.25% and 1.5%, based on descriptive z-score statistics. Certain regions within the mouse tumors were therefore much more rigid than the overall tumour by day 14, which matches both our findings that local mechanical heterogeneity increases in invasive engineered tumors (Figure 2.4), and observations of increasing architectural heterogeneity and stromal organization as the tumor overtakes normal tissue (Figure 2.5C).

While it must be recognized that injection-based models may create tumor architectures that are different from spontaneously-arising tumors, these results do demonstrate that significant differences in mechanical heterogeneity accompany tumor progression *in vivo*, and correlatively suggests that highly-focal sites of rigidity may be sufficient to provide a mechanical stimulus for disease progression. More broadly, in diseases such as cancer where only a few aggressive cells are required to initiate metastasis, the ability afforded by μTAMs to study highly localized mechanical microenvironments could ultimately provide an improved understanding of subpopulation-driven transitions between quiescent and malignant tumors.

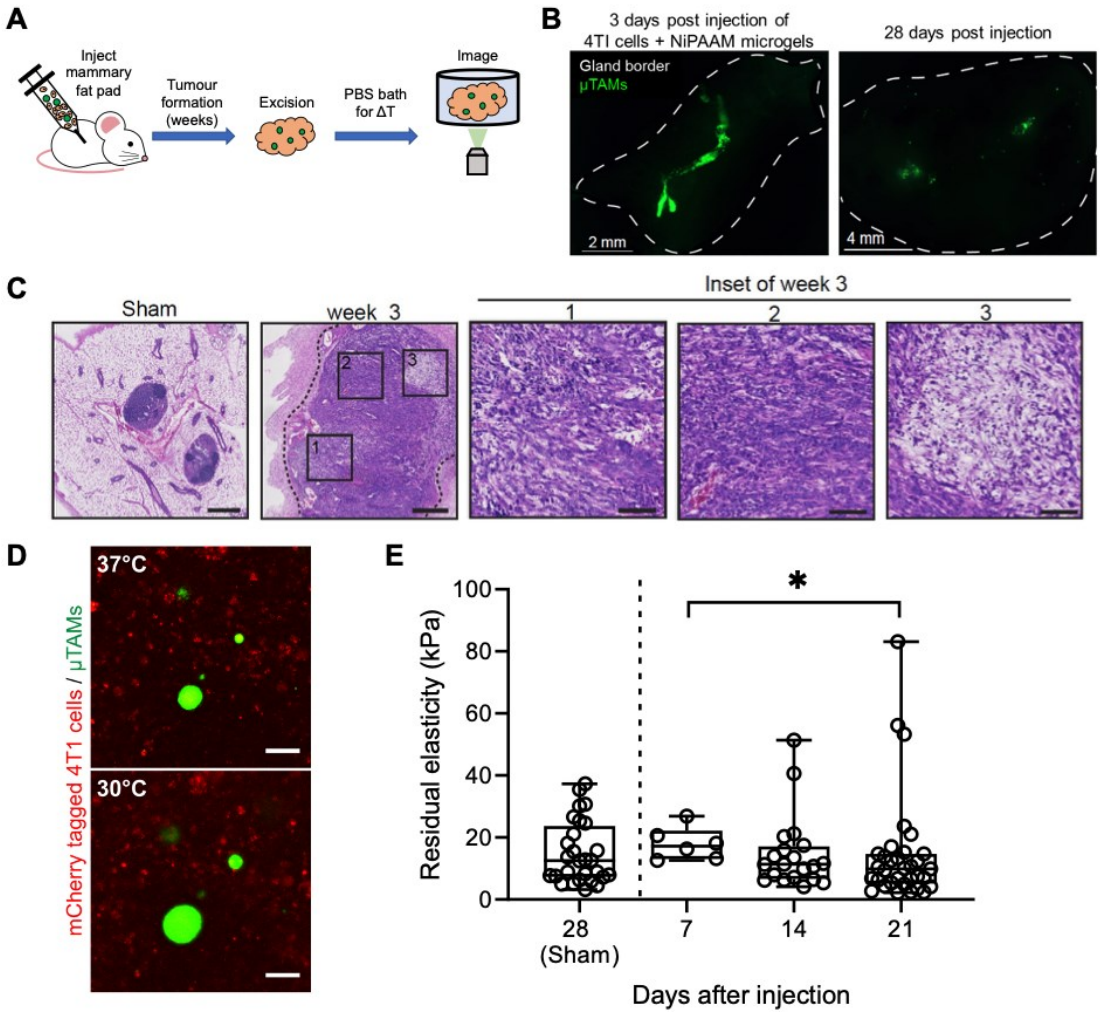

Figure 2.5. Measurements of residual internal tumor elasticity in cancer mouse model.

(A) µTAMs were co-injected with mCherry-labelled T41 breast cancer cells into the mammary fat pads of female mice, and allowed to form tumors over several weeks. At various time points, tumors were excised and imaged in a temperature-controlled saline bath. (B) µTAMs are initially clustered together after injection, but disperse as the tumor develops over several weeks. (C) H&E stained tissue sections of excised fat pads at week 3 shows recovery of normal tissue architecture immediately around the needle injection site (sham, no cancer cells), and an absence of normal architecture in the tumor model. (Insets) Considerable variability in tissue cellularity is observed in distinct regions of the tumor after 3 weeks. (D) µTAMs are interspersed with mCherry-labeled 4T1 cells in the mammary fat pad, and change size when the temperature is decreased (Scale bar = 50 µm). (E) Comparison of residual elasticity within tumors indicates an increasing number of high-rigidity measurements as the cancer progresses towards metastasis, and a significant difference in measurement distributions between Day 7 and Day 21 of tumor progression. Box plots indicate the median and 25th to 7th percentiles, and the whiskers span the range.

n = 28, 6, 20, and 33 individual μTAM stiffness measurements in sham, post-injection day 7, 14 and 21 respectively. (* p = 0.022 by non-parametric two-tailed Mann-Whitney test to compare the distribution of ranks between groups). Box plots indicate the median and first to third quartile, whiskers span the range. Representative images derived from 6 animal replicates for each time point with both left and right intraductal mammary injections to generate separate tumors.

2.4 Discussion

μTAMs provide an opportunity for high spatial-resolution measurements of residual elasticity after creep in a wide range of living, three-dimensional tissues. Rather than measurements of global tumor mechanics, as has previously been reported [37,55], the tunable size of these sensors allows interrogation of mechanical properties at multiple length scales relevant to that of a biological cell, enabling an improved understanding of the local microenvironment that cells would experience. Furthermore, whereas sensitive analysis techniques as atomic force microscopy [182] and microrheology [183] may capture these spatial resolutions they do not approximate the stroke lengths generated by real cells, and hence measure mechanical properties of the material in a strain regime that may or may not be relevant to cellular mechanosensing and microenvironmental interrogation.

The proof-of-concept experiments developed here together demonstrate that at these cell-relevant length scales, the mechanical microenvironment in 3D tumors is far more heterogeneous than generally expected, and our findings together suggest that microscale 'hot spots' of rigidity develop as tumors progress towards an invasive, pre-metastatic phenotype. Given the well-established sensitivity of cancer cells to rigidity of the local microenvironment [44,52,184], these studies broadly demonstrate that fine spatial resolution is necessary to describe the mechanical evolution of tumors as diseases progress.

μTAMs present some limitations that require careful consideration. First, the measurements obtained with this technique cannot be quantitatively compared with those obtained from more conventional approaches, for materials that exhibit non-linear mechanical properties, such as viscoelastic tissues[185]. Our current measurements of residual elasticity after creep can only be used to extract a stiffness modulus for materials that deform without a time-dependent component. Similarly, more advanced measurements that capture both mechanical stiffness and applied strain, such as internal solid stress[35] also cannot be extracted. Second, μTAMs may be sensitive to confounding local factors such as pH. This is unlikely to affect the present experiments, as PNiPAAM

does not behave significantly differently between pH 5-8 [186], and tumors have internal pHs between 7.0 and 7.2 [187], but should be considered carefully for other tissues. Third, the requisite thermal cycling could itself influence tissue stiffness. Although previous studies have demonstrated that cellular rigidity is not significantly affected between 21°C and 37°C [188], repetitive expansion of the sensors may theoretically induce local structural changes via damage mechanisms. To mitigate these issues in this study, we only make single measurements from each μTAM, and additional studies would be required to determine if local stress changes affect the biological systems. Fourth, the presence of these sensors itself may affect cell behavior, as they do provide a foreign, hard surface in their compacted state. In our experiments, the hard surface presented by compacted μTAMs recapitulate microcalcification that occurs naturally in breast cancer[189]. Hence the differential responses between tissues and across timepoints in our experiments still allows us to conclude that focal stiffening is associated with invasive phenotypes. More broadly, the ability to functionalize the surface with candidate matrix molecules provide further opportunities to minimize any foreign body response.

We envision broad utility for this technology in understanding cell-scale stiffness evolution in tissues, particularly given some simple future design modifications. Developing polymer engineering strategies to tune stored strain energy through independent manipulation of expansion ratio and sensor stiffness would enable precise manipulation of actuation force and stroke length, to better simulate mechanical interrogation by specific cell types and tune the sensors for various applications. While thermal activation was a relatively easy first step, other smart material triggers may be introduced that are faster and less disruptive, particularly for in vivo imaging. Finally, incorporating alternative imaging agents such as MRI or X-ray contrast agents would facilitate deep tissue imaging, allowing us to develop a tissue-scale cellular perspective of the local mechanical microenvironment during the highly complex processes of development and disease progression.

2.5 Methods

Unless otherwise stated, all cell culture materials and supplies were purchased from Fisher Scientific (Ottawa, ON), and chemicals from Sigma Aldrich (Oakville, ON).

µTAMs fabrication

Separate solutions of 6% (w/v) polyglycerol polyrincinoleate surfactant (PGPR 4150; Palsgaard, 90415001) in kerosene; 1% (w/v) ammonium persulfate (APS) in phosphate buffered saline; and a prepolymerized PNiPAAM solution following Table S1 (excluding 1% APS) were each prepared in individual glass test tubes with 1-2 mL of each solution in their respective tubes. Volumes within the test tubes are fairly flexible, provided there is a matched or excess volume within the kerosene tube to create a bath. A magnetic stir bar was placed within the kerosene test tube. To purge the system of oxygen, a rubber septum stopper were used to seal each tube and nitrogen gas was bubbled through each liquid for at least 20 minutes using a 25G non-coring needle, with a second needle to vent the tubes to atmosphere. Microspherical gels were formed by drawing the desired amount of 1% APS solution into a syringe and dispensing it into the sealed test tube containing PNiPAAM components. The mixture was immediately vortexed and transferred into the kerosene bath with another syringe. An emulsion was made by vortexing the kerosene/PNiPAAM mixture for 5 to 10 seconds. Droplets were prevented from coalescing by gentle magnetic stirring for 20 minutes as the µTAMs polymerized. To facilitate washing and recovery of the µTAMs, the emulsion was aliquoted into several 1.5 mL microcentrifuge tubes. Each washing step included centrifugation at 14,800x g for 3 minutes, supernatant aspiration and µTAM resuspension with the appropriate solution. The µTAMs were first washed with fresh kerosene three times to remove the PGPR4150 surfactant, and then with PBS three times to recover the microgels in an aqueous phase. Finally, µTAMs were stored at 4°C in PBS overnight to allow gels to swell to equilibrium before further use.

µTAMs surface functionalization

µTAMs were suspended in a 0.05 mg/mL solution of sulfoSANPAH (GBiosciences # BC38) in PBS and irradiated under 36 W UV light for 4 minutes. The solution was aspirated and the µTAMs were washed once with PBS before being incubated in 0.05 mg/mL solution of collagen I (Advanced Biomatrix PureCol #5005B) in PBS overnight at 4°C. Gels were then washed with PBS and stored at 4°C. Prior to embedding or injection into tissues, µTAMs were UV sterilized for 45 minutes (36W UV source).

Stiffness-tunable tissue phantoms

Polyacrylamide hydrogels were fabricated on glass coverslips with embedded µTAMs to calibrate sensor measurements. Hydrogel-releasing hydrophobic glass slides were prepared by coating RainX onto 75 x 50 mm glass slides. Glass coverslips were silanized to bind polyacrylamide by immersion in a 0.4% 3-(Trimethoxysilyl) propyl methacrylate (MPS) in acetone for 5 minutes, washed with fresh acetone for 5 minutes, and air dried.

To embed µTAMs into polyacrylamide tissue phantoms, polyacrylamide pre-gel solutions were made according to Table 2 with a small volume of PBS replaced by an equal volume of µTAMs in PBS. The complete pre-gel solution with PNiPAAM microgels was pipetted onto a hydrophobic glass slide in multiple 127 µL drops to produce a 0.5 mm thick gel when a silanized 18 mm round coverslip was place on top of each drop. The solution was left to polymerize on a slide warmer set to 45°C for 10 minutes. This ensures that µTAMs enter the tissue in their compacted state. After polymerization, the coverslips with the attached hydrogel were peeled off the glass slide with tweezers and placed in a multi-well plate. All hydrogels were washed 3 times with PBS and left to equilibrate overnight in a 37°C incubator before thermal cycling and imaging.

Cell culture

Human HS-5 fibroblasts (ATCC CRL-11882); and T47D (ATCC HTB-133) and MDAMB-231 (ATCC HTB-26) breast cancer cell lines were cultured in Dulbecco's modified eagle media with 10% fetal bovine serum (FBS) and 1% anti/anti (complete media). Cells used for mice experiments were Mouse 4T1 (ATCC CRL-2539), which were cultured in RPMI 1640 (Wisent) with 10% FBS, 1% sodium bicarbonate, 0.5% sodium pyruvate and 0.5% HEPES. When the cells reached at least 80% confluence (70% for 4T1 cells to maintain tumorigenic characteristics), they were detached using 0.25% trypsin-EDTA and either subcultured into a new culture vessel at a 1:10 ratio or used as a single cell suspension for experiments.

Spheroid formation via aqueous two-phase systems

Spheroids formed via aqueous two-phase systems (ATPS) were grown in a non-adhesive 96-well round bottom plate following previously published techniques using a robotic liquid handler (Gilson PipetMax, Mandel, Guelph ON)[172,190]. Briefly, a 0.2% (w/v) solution of Pluronics F108 in PBS was pipetted into each well and incubated for 1 hour at room temperature (23°C). The solution was aspirated, and the wells rinsed with reverse osmosis (RO) water before air drying. Plates were sterilized under UV light for 45 minutes prior to use. Stock solutions of 6% (w/v) polyethylene glycol (PEG) in complete media; and diluted to 5.4% in water prior to use. A cell-laden dextran (DEX) solution was prepared by mixing 85 µL of a 15% (w/v) dextran in PBS solution with 15 µL of a 17 x 10^6 cells/mL suspension of HS-5 fibroblasts. To incorporate PNiPAAM microgels into the spheroids, 1-3 µL of the functionalized microgel suspension was mixed into the cell-laden dextran depending on the desired microgel to spheroid ratio. 50 µL of the PEG solution was dispensed into each well of the non-adhesive 96 well-plate, and 1 µL of cell-laden DEX was carefully dispensed slightly above the bottom of each well. The plates were carefully transferred to a cell culture incubator (5% CO_2, 37 °C) for 1 hour before adding 75 µL of complete media and growing the spheroids for two days.

Spheroid formation via micropocket hydrogel cavities

Spheroids were formed in polyacrylamide micropockets using previously published protocols[171]. Polyacrylamide micropockets were cast using the 12 % acrylamide/0.24% bis-acrylamide formulation. Approximately 125 µL of the prepolymer polyacrylamide solution was dispensed over a 3D printed mold containing ~200 spherical structures of 0.5 and 1 mm diameters across the surface area of a 12 mm coverslip to generously fill the mold. An MPS-treated 18 mm coverslip was placed on top of the mold, and the hydrogel was allowed to polymerize for 10 minutes. The polymerization grafted the polyacrylamide hydrogel to the coverslip, which was then gently separated from the 3D printed mold, and washed 3 times in PBS. Gels were stored at 4 °C in PBS to equilibrate overnight, and sterilized under UV light for 45 minutes. PBS was aspirated prior to loading the micropocket gels with cells. A mixture containing 100 µL of a 15 x 10^6 cells/mL suspension of the desired cell type with 1 µL of functionalized µTAM suspension was distributed over each hydrogel. The cells were left to settle into the micropockets for 5 minutes before submerging the entire polyacrylamide micropocket device in complete media. Spheroids then formed over 2 days in a standard cell culture incubator (5% CO2, 37 °C).

Mouse breast cancer model

Mice were housed at the Goodman Cancer Research Center animal facility in adequate enclosures as described in the Canadian Council on Animal Care guidelines for mice. Specifically, the rooms go through a 12 hour light/dark cycle from 7 am to 7 pm and ambient temperatures were set to 22°C with humidity kept at 40%. Up to 5 adult mice are kept in each cage dressed with a bedding of corn and Enviro-dri (Cedarlane; Burlington, ON). Cages are supplied with enough food for 2 weeks with weekly top ups and water is freely available through water bottles fitted with animal drinking valves in the cages.

All procedures were performed in accordance with the animal care guidelines by the Canadian Council on Animal Care after obtaining ethics approval from the Animal Resource Centre of McGill University. For each replicate, a set of 4 female BALB/c mice (Charles River) at 8-10 weeks of age were randomly allocated a condition (sham, week 1, week 2 or week 3). Mice were anesthetized under isoflurane gas, as the 4th and the 9th mammary fat pads were injected using a 22G needle (Becton Dickinson) attached to a Hamilton syringe. Each gland was injected with a suspension of mCherry-labelled 4T1 cells at 5 x 10^5 cells/mL with different concentrations of µTAMs in 25 µl of sterile PBS. The 4T1 tagged cells were generated using lentivirus and the lentivector pWPI-mCherry. Sham condition mice were injected only with a suspension of µTAMs in 25 µl of sterile PBS and left for 3 weeks

Mice were euthanized by cervical dislocation under isofluorane anesthesia. At the indicated time points, injected mammary fat pads or tumors were surgically isolated and immediately rinsed in sterile PBS. Tumors exceeding 5 mm in thickness were sectioned to layers 4 ±1 mm in thickness to facilitate bead visualization and rinsed 10 times in sterile PBS. Tissue was immersed in sterile PBS in a 2-well chambered cover glass (Nunc™ Lab-Tek™) for immediate imaging.

Temperature-controlled imaging and µTAMs size analysis

Polyacrylamide phantoms, and multicellular spheroids were mounted in a Chamlide imaging chamber and submerged with 300 µL of PBS before being placed on a controlled stage warmer (Ibidi). Images were taken on an Olympus IX-73 microscope under epifluorescence (Olympus, X-CITE 120 LED), with an sCMOS Flash 4.0 Camera and Metamorph software (version 7.8.13.0), and automated stage (Zaber) to record and return to specified positions. Samples were mounted in a live-cell imaging chamber (Ibidi), and imaged initially at 37°C and during cool-down to room temperature at 30 minute intervals to ensure temperature equilibration and complete sensor size change. Live mouse tissue

explants were imaged with an LSM700 laser scanning confocal microscope with a 20 x 0.8NA objective lens and ZEN software (Zeiss) in a temperature-controlled environmental chamber. The tissue was then incubated at 37˚C for 1 hour, and the same positions were re-imaged using the same imaging parameters. Images were deconvolved using the iterative deconvolve 3D plugin [191] and a point spread function generated by imaging 0.19 μm green TFM beads in identical imaging conditions as the μTAMs.

μTAMs that were damaged (missing chunk or fragment), in contact with an adjacent sensor, or partially exposed outside of given tissue were excluded from measurements. μTAMs that were less than 10 μm in diameter were excluded from stiffness analysis to reduce measurement error. All μTAM images were analyzed in FIJI by manually drawing a fitted ellipse around the μTAM and measuring the Feret's diameter for the microgel size, as well as shape descriptors for the circularity of the μTAM which was calculated within the software as:

$$circularity = \frac{4\pi \times Area}{\sqrt{Perimeter}} \qquad (1)$$

Conversion between μTAM size change ratio was done using the modelling curve and the iterated best fit values for parameters specified in Supplementary Table 3:

$$\frac{D_{30}}{D_{37}} = \alpha - \frac{\alpha - 1}{1+\left(\frac{E_{matrix}}{E_{bead}}\right)^{-B}} \qquad (2)$$

where D_{30}/D_{37} is the observed expansion ratio between the μTAM diameter at 30 °C (expanded) over its diameter at 37 °C (compacted), α is the expansion ratio of μTAMs in free solution, E_{matrix} is the apparent stiffness of the matrix, E_{bead} is the apparent stiffness of the μTAM, and β is a lumped parameter estimated by curve fitting that captures friction, surface penetration, and other losses.

Shear rheometry for bulk characterization of hydrogels

The stiffness of each polyacrylamide and PNiPAAM gel formulation was measured using a parallel plate shear rheometer (Anton-Paar, MCR 302) in strain-controlled mode. Hydrogels fabricated for shear rheology were made by sandwiching 113 μL of the complete pre-gel solution (compositions provided in Supplementary Table 2) between two 12 mm coverslips treated with MPS as described earlier. After 10 minutes, the sandwiched polymerized hydrogels were placed in a multi-well plate and submerged in PBS. After three washes, the gels were left to swell overnight at 4°C. During testing, excess PBS was dried off the top and bottom of the samples, and adhesively mounted between rheometer plates. Storage and loss moduli were recorded over a strain sweep that was run from 1 to 50% at 10 Hz and verified to be plateau within this range. The moduli values were reported as an average of all the readings. Young's modulus (E) was calculated using $E = 2G(1 + \nu)$ where G is the average storage modulus, and ν is the Poisson's ratio of the hydrogel which was assumed to be 0.5 based on literature[192].

Histology and staining

Spheroids were fixed in 4% paraformaldehyde solution for at least 24 hours at 4°C. Spheroids in the micropockets were extracted and transferred using a clipped P1000 pipette tip placed directly over the chamber opening. Spheroids formed by ATPS were pipetted directly with a clipped pipette tip. Spheroids were collected into a 1.5 mL microcentrifuge tube with PBS embedded in paraffin blocks. Tissue blocks were sectioned at 4 μm and mounted on charged glass slides for histology.

For staining, the tissue sections were deparaffinized in xylene for 15 minutes and rehydrated using a decreasing ethanol gradient at 100%, 90% and 80% for 2-minute intervals. Slides were washed twice with PBS for 5 minutes, and permeabilized in 0.1% Triton-X solution for 5 minutes, before two additional PBS washes. Tissue sections were blocked with 1% BSA in PBS for 30 minutes at room temperature (23°C). An actin cytoskeletal and nuclear staining mixture of FITC-conjugated phalloidin (1 μg/mL) and

hoescht 33258 (1 μg/mL) in 1% BSA was applied for 20 minutes. The slides were washed twice in PBS and once with water before coverslip mounting using Fluoromount Aqueous Mounting Media and sealing with clear nail polish.

Histological section image analysis

All image analyses were performed using FIJI [193]. The cross-sectional area of the circular spheroids were segmented into 5 annuli of equal area. Cell density in each anulus was quantified with an automated nuclear count by thresholding the image to isolate the nuclei and performing a particle analysis count with a minimum of particle size of 20 μm^2. Nuclear orientation was analyzed by determining the difference between the expected angle for a circumferentially aligned nucleus (Θ_{expt}) and the angle of the nucleus itself as determine by the particle analysis on FIJI. To get Θ_{expt}, the angle at the center of a circle (Θ_r) was calculated by taking the tangent angle between the X and Y distance of the nucleus to the center of the spheroid. Θ_{expt} was calculated by assuming spherical symmetry in the spheroid and taking the absolute value of $\Theta_r + 90°$ if $\Theta_r > 0°$ or $\Theta_r - 90°$ if $\Theta_r < 0°$.

Statistical analysis

Z-scores were used to assess the probability of obtaining measurements compared to a control population. For non-normal distributions, log transformations were used to first obtain normal distributions, which were confirmed via Shapiro-Wilks tests. Comparative data analyses of populations were performed without pre-specifying a required effect size. Datasets that were normally distributed, with similar variances between compared groups were analyzed using unpaired t-tests, one-way, or two-way ANOVA to test for significance which was set at $\alpha = 0.05$. Post-hoc pairwise comparisons were conducted using the Bonferroni method. Datasets that were not normally distributed were analyzed using the nonparametric Mann-Whitney test to compare the distribution of ranks between two

groups, with significance values set at $\alpha = 0.05$. All statistical analyses were performed using GraphPad Prism v8.0.2 (San Diego, CA).

Finite element modelling of μTAM expansion

Simulations were performed using the open-source software package FEBio[194] with the pre-strain plugin [195] to apply compressive loads to simulated μTAMs prior to release within an encapsulating matrix of defined stiffness. 3D spherical geometries were used to simulate the μTAMs (unit radius) embedded in a 10x larger encompassing sphere, to simulate an infinitely large matrix. The model was meshed with hexahedral elements, and a mesh size sensitivity analysis was performed. Less than 1% variation was observed in deformation for a mesh element size of 0.16 at the μTAM/matrix interface, for an r-ratio of 1.57. Fixed displacement boundary conditions were applied to the outer matrix surface, and a tied contact interface was defined at the μTAM/matrix interface. Linear elastic material properties and initial pre-strain of the μTAMs were defined and modulated based on experimental data. Analyses were conducted using a dynamic large deformation structural mechanical analysis, and data is reported as a fold change in μTAM size for matrices of various mechanical stiffness.

Data Availability

Select μTAM characterization data and all μTAM stiffness measurements from spheroid and animal experiments are provided in supplementary tables. Additional data supporting the findings of this manuscript are available upon reasonable request from the corresponding author.

2.6 Acknowledgements

We thank Profs. Richard Leask and Milan Maric (McGill University) for rheometer access and expertise; Dr. Clement Ma (Harvard University) for consultation on statistical methods; and the Goodman Cancer Research Centre Histology Facility for assistance with processing, embedding and section tissue samples. This work was supported by the Canadian Cancer Society (Grants # 704422, 706002) and the Canadian Institutes for Health Research (Grant # 01871-000) to C.M. and L.M., and the NSERC Discovery RGPIN-2015-05512 (C.M.). We gratefully acknowledge support from NSERC Canada Graduate Scholarship-Doctoral to S.M, Postgraduate Scholarships-Doctoral to W.L, and the Canada Research Chairs in Advanced Cellular Microenvironments to C.M.

2.7 Author Contributions

S.M and C.M. formulated the idea behind the study. S.M., L.M, and C.M. designed experiments. S.M. and K.M conducted μTAM empirical characterization. S.M performed experiments in spheroid cultures, and conducted stiffness analysis for all experiments. C.L. performed finite element simulations. S.A. performed μTAM injections into mice and imaging of ex vivo tumors. S.M. and W.L. performed mechanical characterization and data analysis/fitting. L.M., and C.M. provided reagents, materials, animals, and analysis expertise. S.M and C.M. drafted the manuscript. All authors edited the manuscript.

2.8 Supplementary Materials

2.8.1 Supplemental Figures

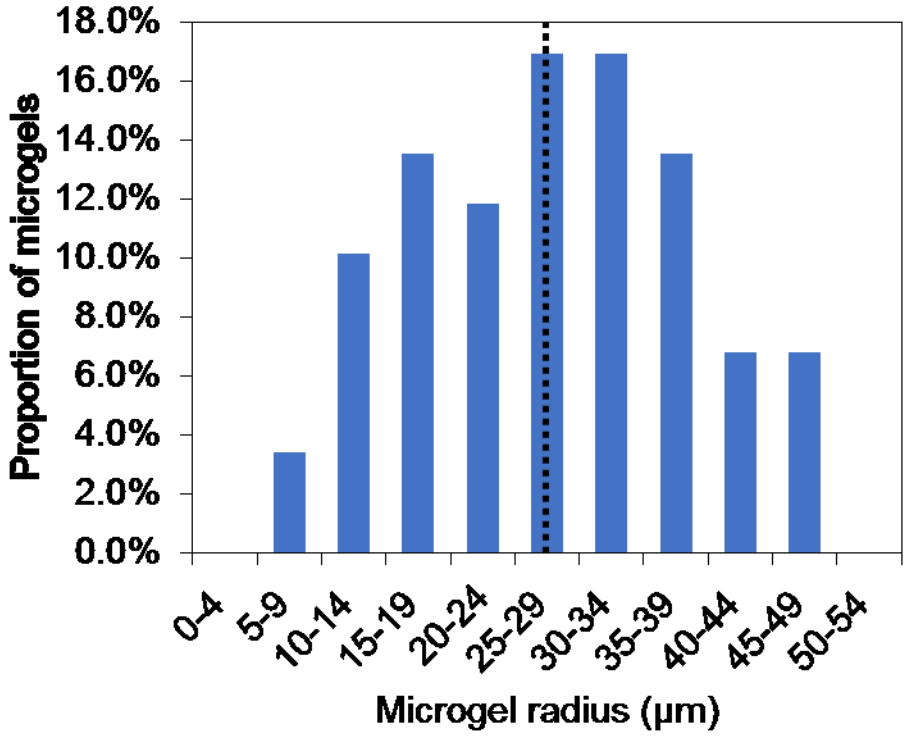

Supplementary Figure 1. NiPAAM microgel size distribution at room temperature. Polydispersed microgels fabricated using the oil/water emulsion technique show a normal distribution of sizes with a mean radius (dotted line) of 27±11 µm. Data reported for µTAMS in expanded state (n=59).

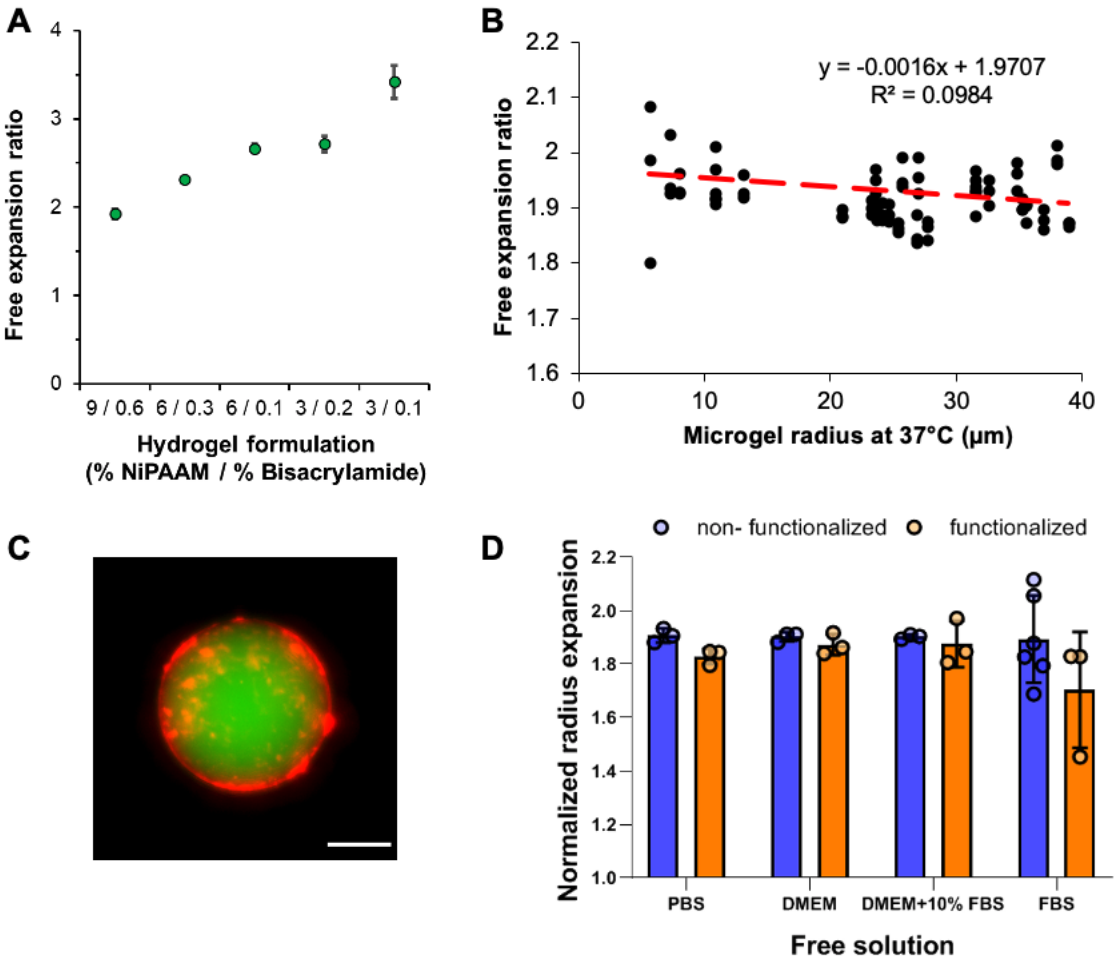

Supplementary Figure 2. Unconfined thermoresponsive free expansion of µTAMs in solution. (A) The free expansion ratio between the measured diameters of microgels in their expanded and contracted state varies for various tested hydrogel formulations (n= 10, 11, 11, 8 and 9 individual µTAMs in order shown on graph). Data points show mean +/- SD. (B) Free expansion ratios are independent of microgel size (data presented for PNiPAAM formulation 9N0.6B (see Suppl. Table S1). Red dashed line indicates linear trend where y= 0.-0016x +1.9707, R^2 = 0.0984; n = 26). No correlation was observed between PNiPAAM microgel size and expansion ratio. Increased variability for smaller microgel sizes can be attributed to increased measurement error percentage under the selected imaging conditions . (C) Representative image of a µTAM (green) functionalized with type I collagen (red). Scale bar = 25 µm. (D) Comparison of free expansion ratios for native and surface functionalized microgels in solutions with varying fetal bovine serum (FBS) protein content. Functionalization with collagen I has no statistically significant effect in PBS, DMEM, complete media (DMEM + 10%FBS), or 100% FBS, but some increased variability is observed in protein-rich suspensions. (Data presented as mean ± standard deviation, statistical analysis conducted by two-way

ANOVA, not significant p = 0.56, 0.47 and 0.09 for the interaction between solutions and surface coating, within solutions, and within coatings; n = 3 for PBS, DMEM, DMEM+10% FBS, and functionalized gels in FBS; n= 6 for non-functionalized gels in FBS). Representative images from three collagen I staining experiments from two separate µTAM samples.

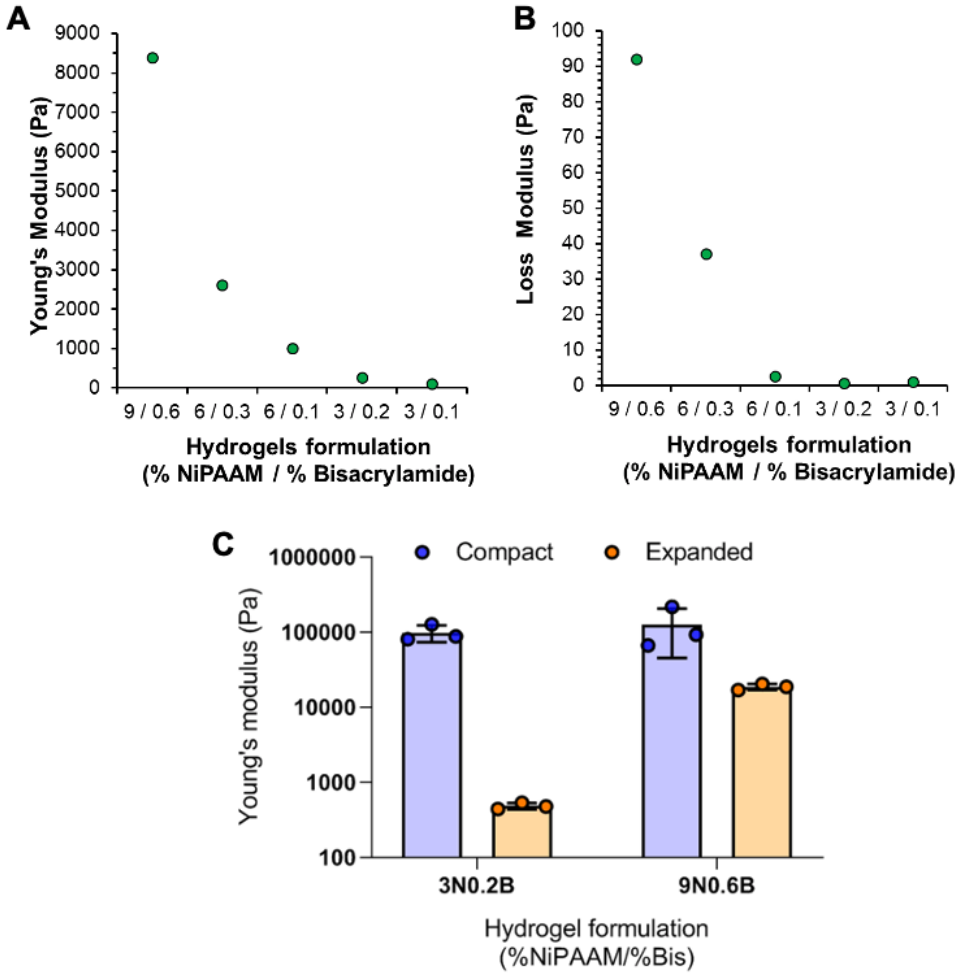

Supplementary Figure 3. Mechanical characteristics of PNiPAAM obtained via shear rheology. (A) PNiPAAM hydrogel storage modulus and (B) loss modulus. Loss moduli were minimal, indicating strongly linear elastic materials behavior. (C) PNiPAAM stiffness at the compact (>34 °C) and expanded (<34 °C) hydrogel state indicate that stiffness changes dramatically between the compact and expanded state depending on PNiPAAM formulation. Data reported as mean ± SD for n = 3.

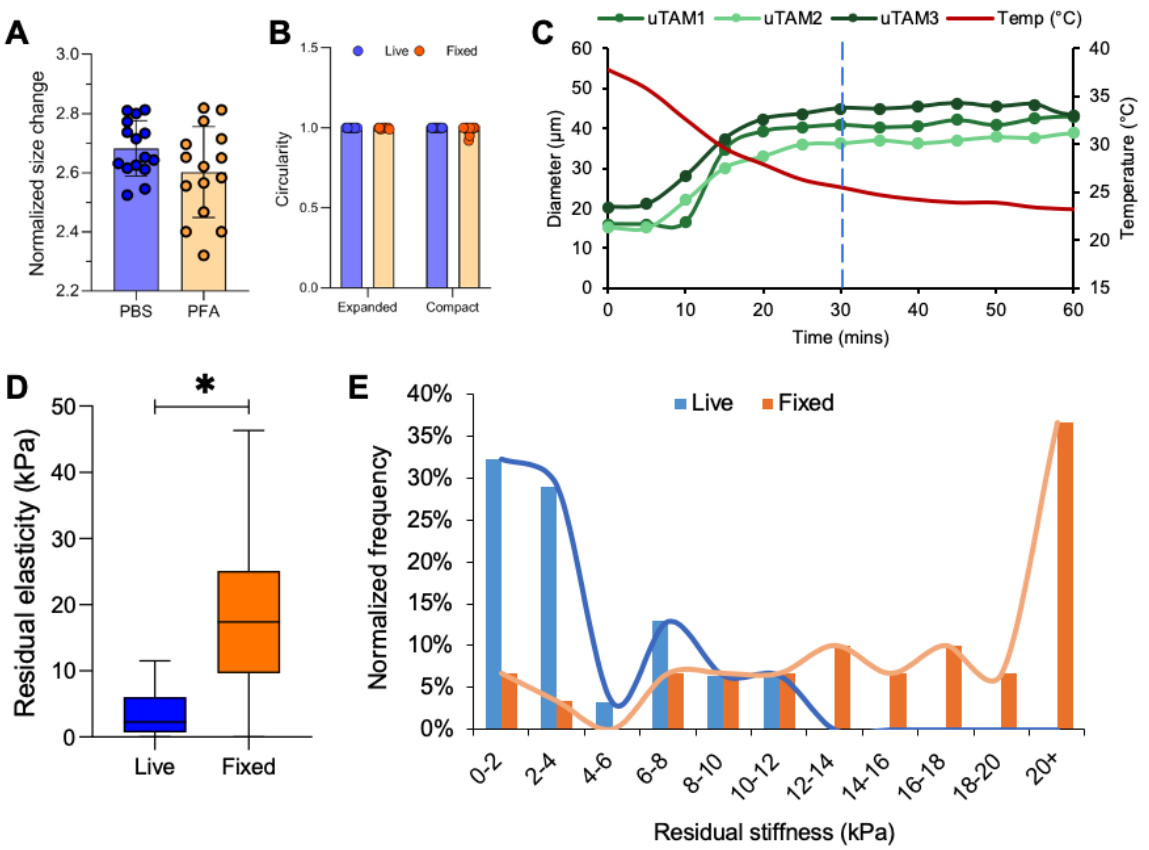

Supplementary Figure 4. Residual elasticity distribution within engineered T47D multicellular aggregates before and after fixation. T-47D mammary-derived ductal carcinoma cells formed spheroids over 2 days within polyacrylamide micropockets and fixed with 4% paraformaldehyde overnight at 37°C. (A) Fixation does not affect free µTAM swelling characteristics. (n = 15 µTAMs readings for each condition). (B) Circularity of µTAMs within live and fixed tissues. No significant differences ($p = 0.061$) in circularity between compact and expanded µTAMs in either tissue condition are seen based on a two-way ANOVA. Data reported for n = 16 and 17 for live and fixed tissue condition respectively in each µTAM state. (C) µTAM size change over time within T47D spheroids during cooling on our microscope stage. Temperature and size measurements were recorded every 5 minutes for an hour to ensure that 30 minutes was adequate time for µTAM expansion to equilibrate, thereby ensuring residual elasticity around the µTAM is measured. (D) Stiffness in fixed spheroids is significantly stiffer than its live pre-fixed state (n = 33 and 30 individual µTAM readings in live and fixed spheroids respectively; 30 live spheroids and 11 fixed spheroids were measured). Asterisks denotes $p < 0.0001$ according to unpaired two-tailed t-test with Welch's correction. (E) Histogram of residual elasticity distributions between live and fixed spheroids. Data from panels A, B and D are presented as mean +/- SD.

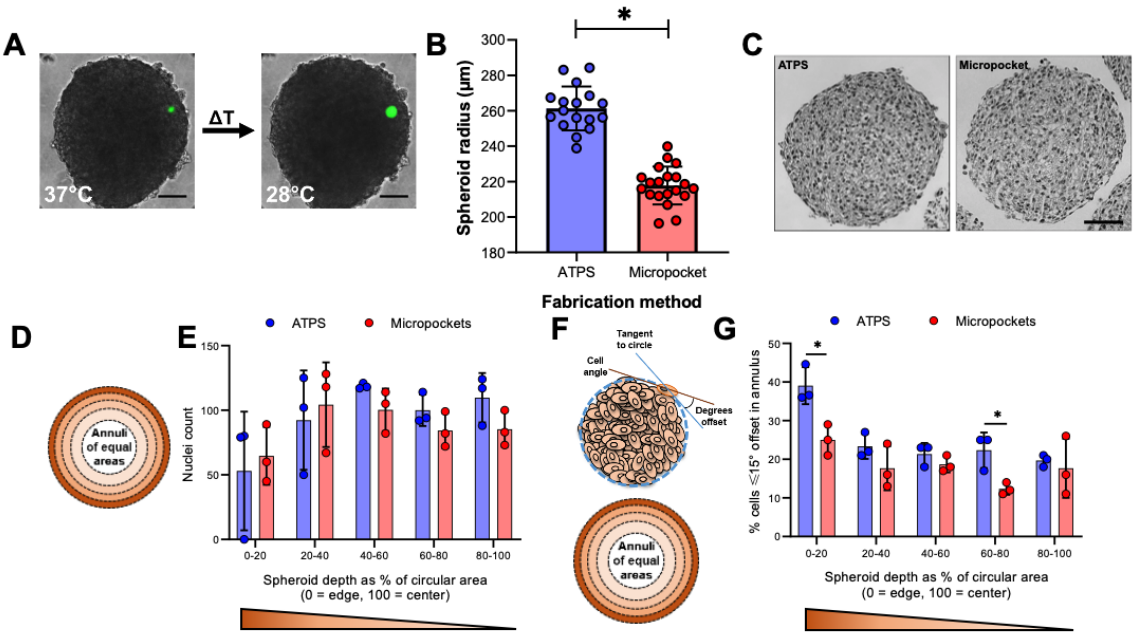

Supplementary Figure 5. Cell count and orientation in ATPS and micropocket spheroids. (A) Spheroids are formed and maintained at 37 °C, where μTAMs remain compacted. Measurements of residual stiffness can be made by reducing the temperature and expanding the μTAMs. Scale bar = 100 μm. (B) Characterization of spheroid dimensions formed in ATPS and micropocket systems. ATPS spheroids are slightly but significantly larger in radius than micropocket spheroids by 44 ± 4 μm (unpaired two-tailed t-test, $p < 0.0001$ for $n = 20$ and 17 respectively). (C) Representative images of H&E stained sections show that at the edge, ATPS spheroids preferentially align along the circumference of the spheroid in contrast to micropocket spheroids. Scale bar = 100 μm. (D, E) Nuclei count between the two spheroid generation methods in each annuli representing equal areas show no significant differences. (n = 3). (F, G) Cell orientation analysis show that cells along the periphery of ATPS spheroids preferentially elongate along the circumference of the spheroid significantly more than their micropocket counterparts. Asterisks denotes significance at $p = 0.0022$ by two-ANOVA with a Bonferroni test. (n = 3 spheroids for both ATPS and micropocket methods). Representative images show one example out of hundreds of spheroids generated with μTAMs incorporated over at least 6 independent HS-5 spheroid generation experiments for each method. Data for panels B, E and G are presented as mean +/- SD.

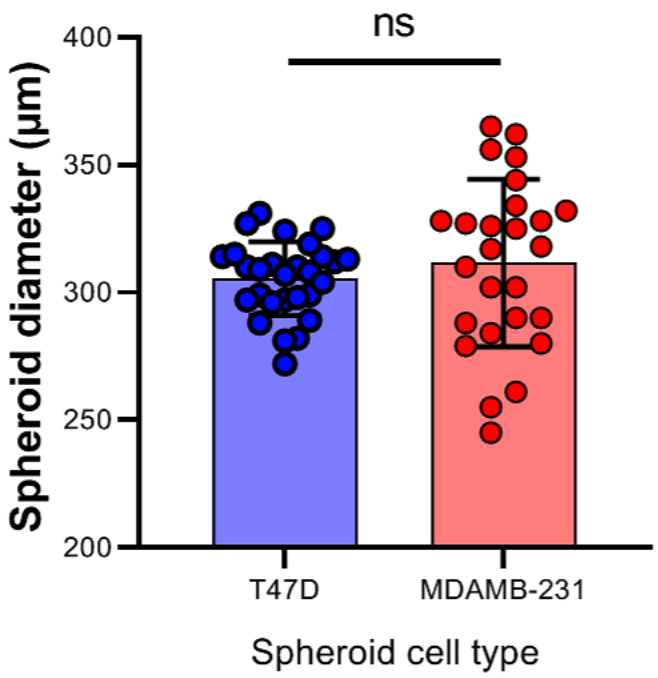

Supplementary Figure 6. Diameter of breast cancer cell line spheroids generated using polyacrylamide micropockets. No significant difference in spheroid size between the two cell types (unpaired two-tailed t-test with Welch's correction; n.s. $p = 0.383$, $n = 28$ and 26 for T47D and MDA-MB-231 spheroids respectively). Data are presented as mean values +/- SD.

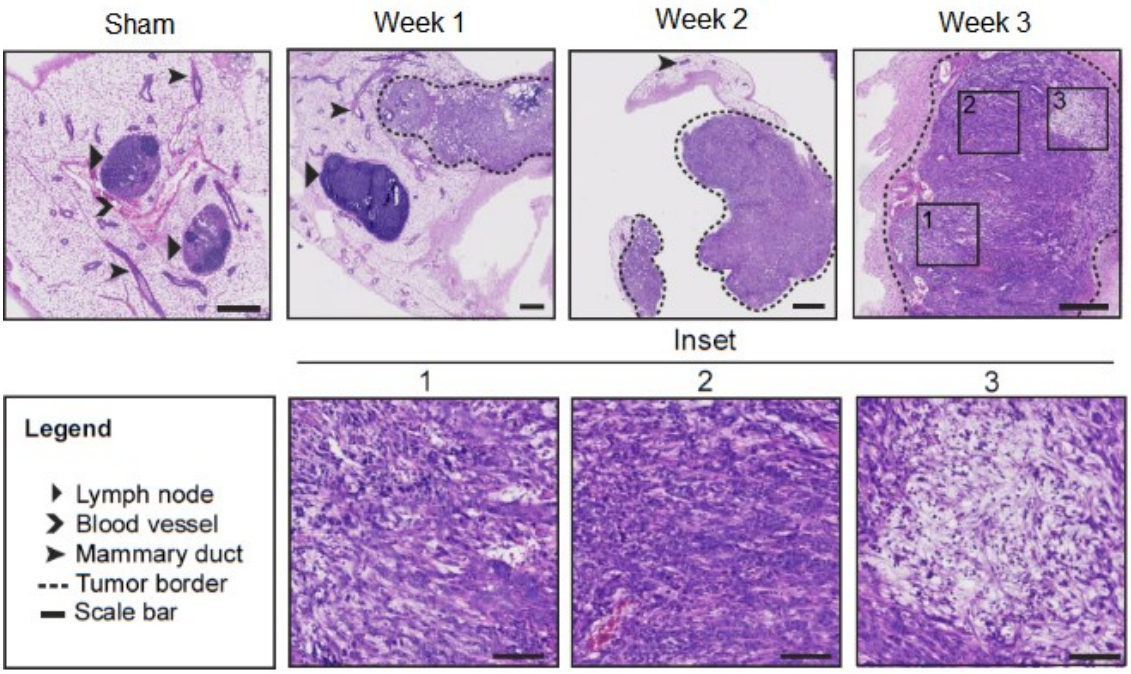

Supplementary Figure 7. Tumour development over three weeks. Representative images of T41 tumour growth within the mammary fat pad of immunocompetent BALB/c mice. Scale bars = 500 µm. Inset scale bars 100 µm. Representative images showing consistent sightings among 6 BALB/c mice injected with 4T1 cancer cells + µTAMs in both left and right mammary ducts and 6 sham mice injected with PBS + µTAMs.

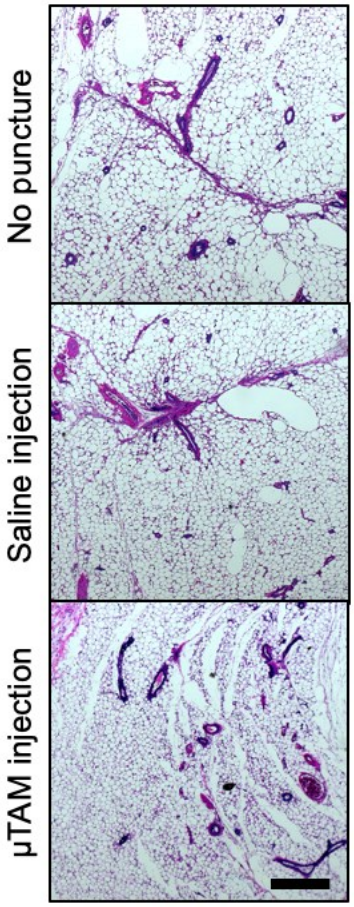

Supplementary Figure 8. Comparative histology in mouse mammary fat pads subjected to needle injection. Representative images of mammary fat pads that were injected with saline or µTAMs using a 22G needle compared to fat pads that were not punctured show no visual differences in histology with an H&E stain. Seen in these sections are normal fat cells with occasional cross and longitudinal sections of mammary duct structures and blood vessels. Fibrotic tissue would appear as dense areas of collagen which would stain pink. Scale bar = 500 µm. Two mice were tested in both left and right mammary ducts for n = 4 for each condition.

2.8.2 Supplementary Tables

Supplementary Table 1. PNiPAAM microgel formulations. Highlighted row in yellow indicates formulation used for all in vitro and in vivo experiments.

NiPAAM (%)	Bis-acrylamide (%)	Formula shorthand	20% (w/v) NiPAAM in PBS (µL)	2% Bis-acrylmide (µL)	PBS (µL)	TEMED (µL)	Fluorescein o-methacrylate in DMSO (100 mg/mL)	1% (w/v) APS in PBS (µL)
9	0.6	9N/0.6B	450	300	147.5	1.5	1	100
6	0.3	6N/0.3B	300	150	447.5	1.5	1	100
6	0.1	6N/0.1B	300	50	547.5	1.5	1	100
3	0.2	3N/0.2B	150	100	647.5	1.5	1	100
3	0.1	3N/0.1B	150	50	697.5	1.5	1	100

Supplementary Table 2. Tissue phantom formulations of stiffness-tunable polyacrylamide.

Acrylamide (%)	Bis-acrylamide (%)	40 % Acrylamide (µL)	2% Bis-acrylmide (µL)	PBS (µL)	TEMED (µL)	1 or 10% (w/v) APS in PBS (µL)	Young's Modulus based on shear rheology (Pa)
3	0.05	75	24.5	799	1.5	100 (1%)	150
3	0.11	75	53.5	770	1.5	100 (1%)	400
7.5	0.05	187.5	27	694	1.5	100 (1%)	4250
7.5	0.24	187.5	118	593	1.5	100 (1%)	9200
12	0.24	300	120.5	478	1.5	100 (1%)	19500
20	2	490	300	304.5	0.5	5 (10%)	245000
20	3	485	200	204.5	0.5	5 (10%)	271000

Supplementary Table 3. Best fit values for PNiPAAM expansion model. Asterisks show empirically measured values. Bolded values are iterated best fits

Polyacrylamide Formulation	$E_{microgel}$ (kPa) Expanded - Contracted	Free expansion ratio	B coefficient	R^2 fit
3N0.2B	0.48 * - 98 *	2.72*	N/A	N/A
	12.45	**2.52**	**0.91**	**0.94**
9N0.6B	18.6* - 125*	1.92*	0.34	0.86
	21.60	**1.78**	**0.514**	**0.91**

Chapter 3

Mechanical stiffness is an important correlate of tumor metastasis, but little is known about the highly localized mechanical properties of surrounding individual cells during tumor development. Using the cell-sized thermoresponsive microgel sensors I previously developed, I analyzed stiffness profiles present within tumor spheroids formed from two human breast cancer cell lines with distinct levels of aggressiveness as well as one engineered breast cancer cell line under inducible oncogenic gene expression. Here we find that mechanical heterogeneity develops over time in spheroids with invasive potential. Furthermore cells immediately adjacent to microregions of different rigidities have distinct morphological responses based on invasive potential. Interestingly, the variations in stiffness within spheroids can be stabilized through growth in confined conditions, suggesting a novel regulatory mechanism between internal and external tumor mechanics during tumor growth.

3 Time and growth evolution of stiffness in cancer tumor models

3.1 Abstract

The mechanical microenvironment evolves with the development of cancer and metastasis. The literature is divided over whether cancer cells stiffen or soften over time, and whether growth under confinement drives metastatic behavior. To characterize tumor stiffness at the "meso" length scale between the sub-cellular and tissue length scales, we recently developed cell-sized thermoresponsive microgel sensors that can be incorporated within a living tissue to measure residual elasticity at highly localized regions within 3D tissues. Using these sensors in spheroids generated from cancer cell lines as a model for avascular solid tumors, we analyzed stiffness profiles present within tumor spheroids formed from human breast cancer cell lines with distinct metastatic potential. We first demonstrate that stiffness at distinct sites within spheroids do evolve, and in T47D spheroids generally stiffen over time. We then compared the internal tumor residual elasticity profiles of spheroids generated from invasive (MDAMB-231) and non-invasive cancer cell (T47D) lines, under unconfined and confined growth conditions. Conversely, we then asked whether the presence of regions of high stiffness influences internal tumor architecture, and examined the histological features of the cells surrounding different microregions of controlled stiffness. Cell arrangements immediately adjacent to these microregions show distinct morphologies depending on whether the local area is soft or stiff. Overall, these studies demonstrate that mechanical heterogeneity develops over time in spheroids and these local differences may provide both the mechanical activation cues and intrinsic mechanical properties that create a feedback loop between stiffened regions and cell organization required for metastasis.

3.2 Introduction

Invasion and metastatic events are the main cause of death for individuals with cancer. Mechanical stiffness correlate to metastasis but conflicting results make it difficult to understand how it evolves over time [15,53]. Initial tumor cells are stiffer than normal tissues to displace local tissue [196]. Stromal cells near the tumor react by laying dense fibrotic tissue around the growth to confine it which increases the stiffness of the overall tumor [37]. Continued uncontrolled proliferation of cancer cells within this environment creates solid and compressive stresses [197,198]. In some instances, compressive stresses stabilize tumor growth through the induction of apoptosis to balance proliferation [173,197,198]. In others, this confinement increases invasive behavior. Mechanical compression of breast cancer cells has been shown to induce cytoskeletal changes and increase migration rates [58,59]. This compression-induced phenotype may be time-dependent: individual cells from a previously confined cancer spheroid readily escape and migrate away from the tumor location [60]. Increasing tensile stresses have also been shown to contribute towards invasive potential [199]. Furthermore, at some point during disease progression, cancer cells must soften to navigate through extracellular matrix barriers and invasive cancer cells tend to be softer than their benign counterparts [51,200–202]. The exact timeline of these cellular, tumoral, and stromal stiffness changes is unclear; but these seemingly disparate findings suggest that to achieve metastasis, cells need to be initially stiff enough to displace tissue for growth, mechanically stimulated to invade through increased stiffness, and then themselves become soft enough to escape the tumor boundaries.

Characterizing the mechanical properties within the cellular microenvironment is difficult especially within cancer tissues and 3D cancer models. Spheroids are good models for avascular solid tumors as they share structural and functional similarities [203,204]. However, these samples tend to be dense and highly heterogeneous in structure and composition. There are limited options available to study cell-length mechanics within this type of intact 3D tissue. Current gold standards for these mechanical tests rely on mechanical indentation of an exposed or cut surface, but this has been shown to

significantly influence mechanical properties near the cut region [35,37]. Recently, injectable magnetic oil droplets have been used in zebrafish embryos to measure stiffness within specific parts of the organism by measuring the deformations generated by directional magnetic actuation of the ferromagnetic fluid [134]. However, these incompressible oil droplets are not suitable for extended long term culture or within larger complex tissues. Cell movement can lead to droplet splitting within the tissue over time making it difficult to observe or generate enough actuation forces within the magnetic field to probe local mechanics. Furthermore magnetic techniques require customized equipment and careful calibration to generate the specific magnetic fields to actuate the ferromagnetic oil microdroplets. Recently, we have developed microscale temperature-actuated mechanosensors (μTAMs) for measuring cell scale stiffness and successfully used them within cancer spheroids [205]. These measurements represent residual stiffness after all the viscous behaviors of the tissue have dissipated. The sensors actuate by temperature control and are biocompatible over long term incorporation in animal models. In this study, we aim to quantify and characterize the mechanical changes that occur over time within extended cultures of differentially invasive breast cancer spheroids.

3.3 Results

3.3.1 Tracked microregions show fluctuations in residual stiffness throughout tumor growth

We first looked at how T47D breast cancer spheroids changed over extended spheroid culture. From previous experience, these spheroids readily form well-defined borders within spherical micropocket wells (Figure 3.1A & Figure 3.2A) [171]. Furthermore, they exhibit a benign tumor phenotype as they are unable to migrate into encapsulating matrices including collagen I hydrogels. Individual spheroids and the μTAM sensors within them were tracked over 6 days after initial spheroid formation (Figure 3.1A). Sensors were randomly incorporated throughout the tissue during initial formation and stabilized once the spheroid was formed. Unsurprisingly the spheroid grew larger over time, likely due to proliferation of the cancer cells, and confirming cell and tissue viability (Figure 3.1B). Interestingly, mechanical measurements by μTAMs within the spheroids show varied changes, where some regions stiffen while other soften; with an overall trend towards increased stiffness. Since these readings are from the same individual sensors, the observed stiffness changes are happening at the same location over time and demonstrates that the spheroid architecture at individual locations within the spheroid are evolving over time (Figure 3.1C).

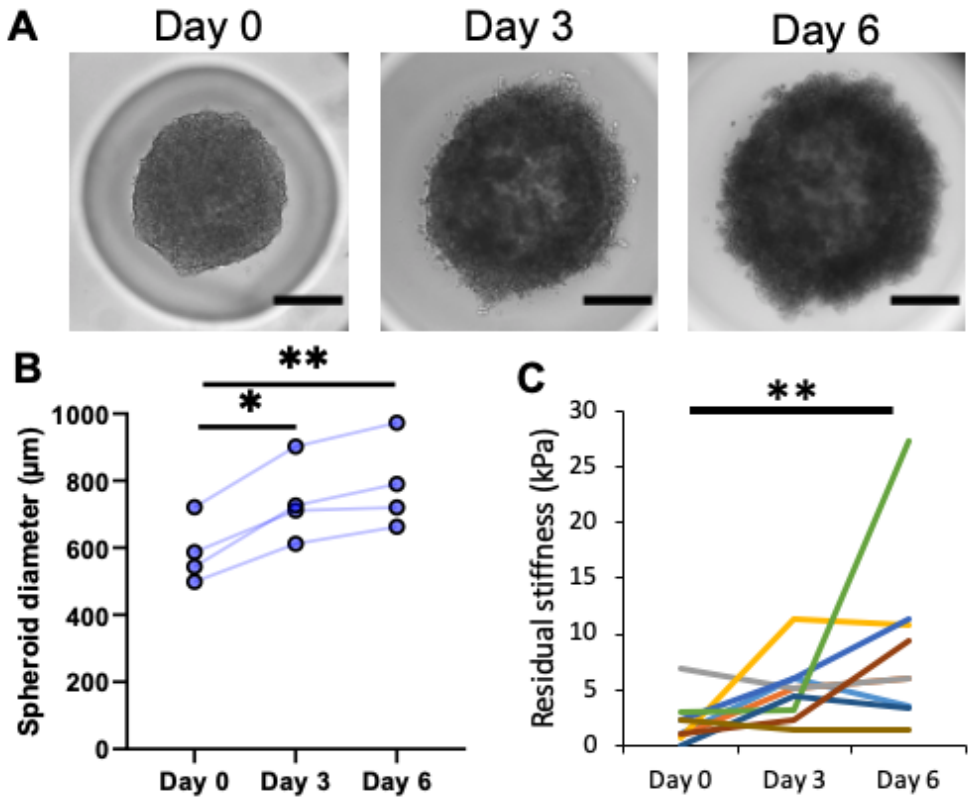

Figure 3.1. Tracking individual spheroids and sensor measurements over extended culture.
(A) Representative images of a T47D spheroid tracked over 6 days. Scale bars = 250 µm. Individually tracked T47D spheroids show significant increases in spheroid diameter (B) and in residual stiffness and variation (C) over time. Different colored lines in panel C represent individual sensors. * $p = 0.0078$ and ** $p = 0.0139$ in panel B and **$p = 0.0031$ in panel C from a one-way ANOVA with Tukey's post-hoc test. n = 4 spheroids and 20 matched stiffness measurements at each timepoint.

When we studied a greater population of T47D spheroids without rigorous tracking, these residual stiffness trends were no longer significant. Although spheroid diameter increased as expected, the average residual stiffness measurements did not show significant differences over time. Similar trends can be seen in spheroids generated from MDAMB-231 cells which show more invasive phenotypes in regular cell culture as they will readily remodel and migrate into collagen I hydrogels. Consistent with our previous studies [205],

MDAMB-231 spheroids have areas of extreme stiffness magnitude that do not appear in the less invasive T47D spheroids (Figure 3.2B&C).

3.3.2 Confinement stabilizes spheroid growth in invasive spheroids

In the previous experiments, the spheroids had enough space to grow within the micropocket wells and can be considered as being allowed to expand freely without constraint. However, tumors in vivo tend to grow in confined conditions due to a desmoplastic response in neighboring tissue from stromal cells reacting and interacting with the tumor. As confined growth has previously been implicated in the metastatic cascade [58,59], we replicated confined growth conditions, by embedding the spheroids in 2% alginate hydrogels cast over on the micropocket devices. The alginate was applied two days after initial spheroid formation (labelled day 0 to indicate the start of confined culture) and filled in the gaps between the well and the tissue (Figure 3.2A). Alginate hydrogels are a validated, non-toxic material permissive for cell culture growth [206–208]. Mammalian cells lack the ability to form adhesions to alginate and thus cannot remodel or invade through alginate hydrogels. Shear rheology confirmed this alginate hydrogel formulation produced samples with shear storage modulus of 1.7 ± 0.05 kPa. While there were no appreciable differences in changes of spheroid size and stiffness evolution in T47D spheroids grown in confinement compared to unconfined controls, considerable changes were observed in MDAMB-231 spheroids between the confined and unconfined growth conditions (Figure 3.2B&C). First, MDAMB-231 spheroid sizes seem to stabilize with confinement as spheroid size changes over time are no longer significant. Second, although the residual stiffnesses do not change, there is a stabilization of stiffness values such that the stiffness ranges narrow over time in confinement. This suggests that confinement in more aggressive cancer cells results in less spatial variations in stiffness.

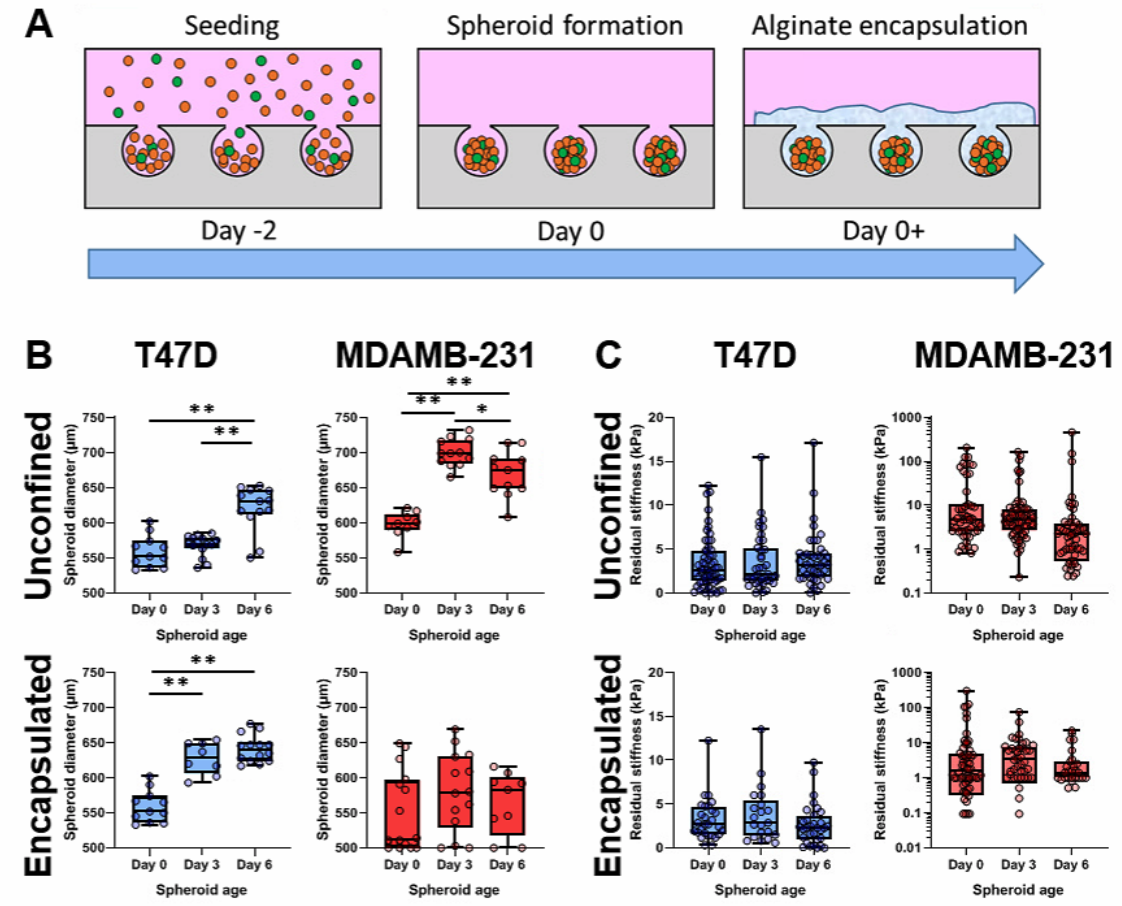

Figure 3.2. Comparing growth and stiffness measurements between different spheroids generated from different breast cancer cell lines confined in alginate or unconfined.

(A) Schematic overview of spheroid life cycle. Micropocket devices were seeded with a suspension of single cells (orange) and collagen I coated µTAMs (green) for spheroid formation by day 0. Baseline spheroid stiffness measurements were done on day 0 before spheroids were conditioned for confinement or left unconfined. Additional stiffness measurements were taken 3 and 6 days after encapsulation. (B)T47D spheroids grow larger over time whether or not it is encapsulated whereas MDA spheroids will also increase in size over time unless they are grown in confinement. (C) Mean and median stiffness values for both spheroid types do not differ significantly but in MDAMB-231 spheroids, standard deviations do differ significantly between time points according to Barlett's test for variance. ** denotes $p < 0.0001$ and * denotes $p = 0.0158$.

3.3.3 Mechanical heterogeneity is stabilized through confinement

To make a more direct comparison between non-aggressive and aggressive cells from similar biological backgrounds, we used an altered MCF7 cell line with a doxycycline-inducible expression of the Src oncogene. Src is normally a regulator of cell proliferation, but its over expression is common within aggressive cancers and has been shown to alter signaling pathways related to migration, invasion, and survival implicated in disease progression [209,210]. Although both T47D and MDBMB-231 cell lines are derived from breast cancers, they are fundamentally different cells with different oncogenic drivers, growth rates, and responses to external stresses [211]. This system offers the most direct comparison between behavioral differences in aggressive and non-aggressive cancer cell states because the control and induced conditions will only differ between Src overexpression. Src expression was only activated after initial spheroid formation from day 0 onwards. The trends in non-induced MCF7 spheroids matches with the other cell line behaviors where spheroid diameter increases with no change in averaged residual stiffness with time. When Src is expressed in these cells, they show sufficiently rapid proliferation to fill the entire cavity of the microwell space. By day 3, the spheroids can be considered growing under mechanical confinement (Figure 3.3A). Although spheroid sizes between control and Src activated conditions are significantly different, their final mean sizes were reasonably comparable at 845 ± 14 μm and 924 ± 39 μm respectively. During this growth, a clear increase in residual stiffness between day 0 and 3 can be seen, which is then reduced after extended confinement over the subsequent 3 days. Consistent with our studies in MDA-MB-231 cells, this suggests that external mechanical confinement acts to reduce the heterogeneity within tissues (Figure 3.3B). Furthermore, during the rapid growth phase between day 0 and 3, a broad range of stiffnesses are observed similar to MDAMB-231 unconfined growth. Since Src expression is induced at day 0, these spheroids required time to build up these stiffness variations which subsequently settle because of confined conditions. These results confirm our previous studies demonstrating differential mechanical characteristics in spheroids of different invasive potential, and also

demonstrate that this evolution of mechanical features is time- and environment-dependent.

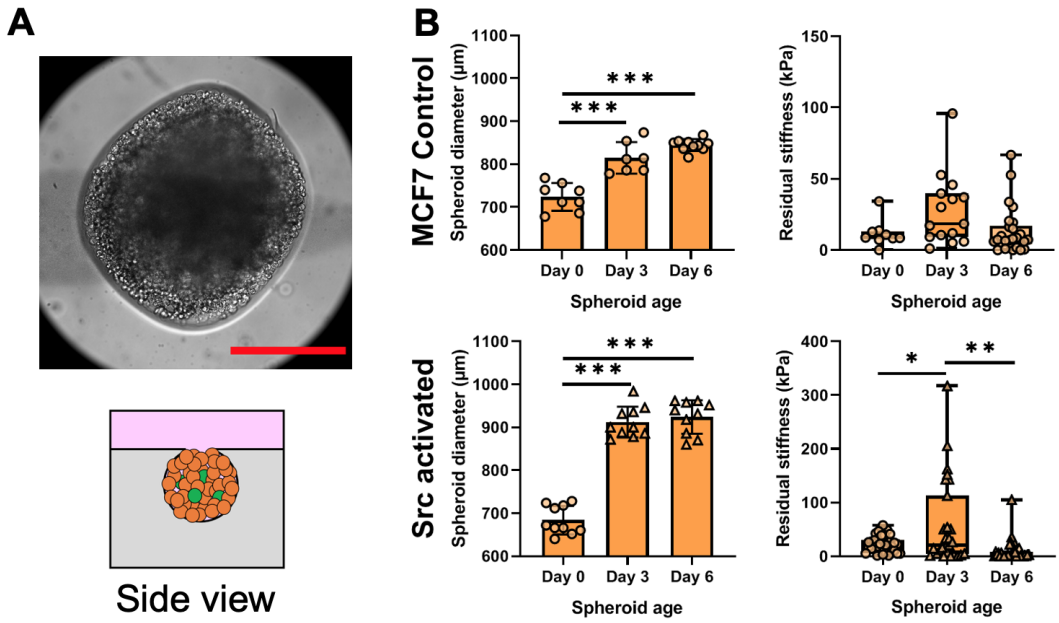

Figure 3.3. MCF7-Src inducible spheroids offer a direct comparison between aggressive and non-aggressive cancer phenotypes.
(A) After 3 days of Src oncogene expression, spheroids have occupied the entire space of the microwell and are confined. Scale bar = 500 µm. (B) Spheroid diameter and residual stiffness measurements over time. * p = 0.0094, ** p = 0.0003, *** p = <0.0001 from an ordinary one-way ANOVA with Tukey's post hoc test.

3.3.4 Differentially stiff microregions show distinct local tissue morphology

As these regions of different stiffness likely result in differences in cell behavior and morphology, we then wondered whether these regions of stiffness were causing phenotypic changes in the cells around them. However, our sensor measurements may disturb the local tissue structure when they expand for stiffness measurements. Furthermore, it is very challenging to see what the cells are doing at these regions and simultaneously assay

stiffness. Therefore, to recreate defined regions of soft and stiff areas within spheroids that were observed, we incorporated soft or stiff polyacrylamide microgels within the spheroids and examined the local architecture in these regions. These formulations were validated to be differently stiff through shear rheology with Young's moduli of 238 Pa for soft gels and 9.2 kPa for stiff gels. T47D spheroids form cuboidal shapes around embedded soft microgels with nuclear elongation towards the microgel that is lost away from the hydrogel (Figure 3.4A&B). In MDAMB-231 spheroids, cells around soft embedded microgels showed similar round cell morphologies whereas cells around stiff microgels had a distinctly different stretched and elongated shape (Figure 3.4C). These distinct morphologies suggest differences in cell tensional states occur in response to local stiffness variations within the spheroid. Tensile forces promote cancer cell invasion, suggesting that these architectural patterns may precede early and local transformative events within the tissue.

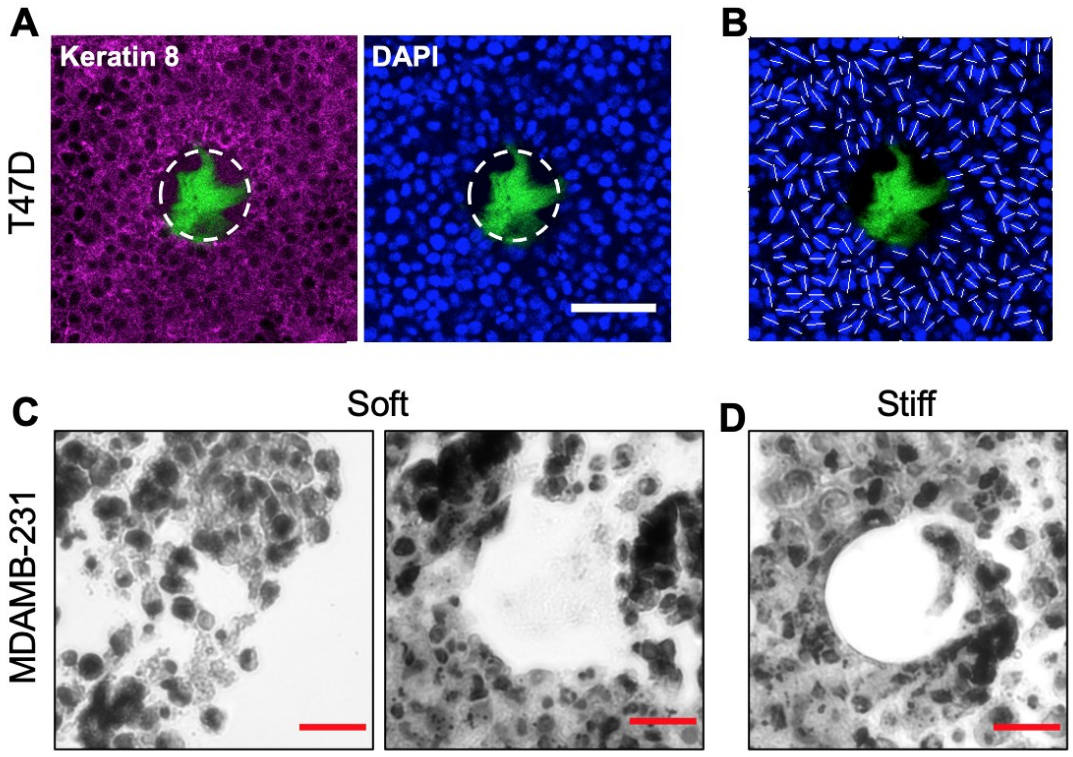

Figure 3.4. Polyacrylamide microgel doped spheroids show unique tissue organization around soft versus stiff microgels mimicking local stiffness heterogeneity.
(A) T47D cells within a spheroid organize around a soft (200G) fluorescein labelled polyacrylamide microsphere with (B) radial nuclear alignment. Colors shown are magenta for keratin 8 for overall cell shape, blue for DAPI, and green for the polyacrylamide bead that has dehydrated and deformed during histological processing. White scale bar = 50 µm. (C) Cells within MDAMB-231 spheroids doped with soft microgels are round and circular in stark contrast to (D) cells around stiff microgels which are elongated and spread tightly around it. Red scale bar = 25 µm.

3.4 Discussion

At a given location within the spheroid local stiffness can increase or decrease over time. Local differences in proliferation may account for some of this variation as growth has been shown to contribute to the accumulation of solid stresses within the tissue but do not account for drops in stiffness [54]. Epithelial tissues in 2D and 3D display jamming transition behavior depending on cell shape, adhesion, and motility [212]. Jammed cells are densely packed with stabilized adhesions that prevent them from moving or flowing over one another within the tissue and behave as a collective [213]. In contrast, unjammed cells tend to move freely and individually dissociate from other cells within the tissue [214]. Fluidization within the tissue may better explain these stiffness fluctuations measured in the tracked sensor readings as random disordered movement within the tissue [215]. Furthermore, the evolution of mechanical heterogeneity within spheroids over time and the stabilization after confinement may be explained by jamming transition behavior. Cells within the spheroid display individualized, unjammed behavior when there is space to move and grow [216]. Localized heterogeneity within tumors correlated with metastatic potential during unconfined growth. MDAMB-231 and Src-activated MCF-7 cells have invasive capability to contract and move individually within the tissue to create more local variances whereas T47D cells are natively quite jammed due to their strong cell-cell adhesions through E-cadherin expression and show more uniform stiffness profiles [217,218]. Confinement imposes jamming upon all cells as they are crowded together and this reduced individualized cell movement may explain the mechanical stabilization in confined spheroids as jamming reduces variability in cell shapes [214,219].

Mechanical stabilization might underlie other changes happening within the tissue during confinement to maintain mechanical uniformity. Jamming is important in growth, plateau, and migration progression in tumors [212,215]. The density changes during confined growth can trigger cell extrusion mechanisms which are supposed to be a tumor suppressive mechanism to manage overcrowding under normal circumstances [220]. Pathologically, cell extrusion has been implicated as a way for cells to escape a confined region [221] and possibly facilitate epithelial to mesenchymal transition [222]. Cell

extrusion is driven by a purse-string closure mechanism achieved through collective cell dynamics where neighboring cells around the cell-to-be-ejected form an actin ring and physically push the center cell out [223]. Different morphological responses observed in soft versus stiff polyacrylamide microgels implanted within spheroid tissues could support signs of this underlying mechanical action which could be revealed through a f-actin or p-myosin stains for tension and contractility. These micro-regional patterns within cancer spheroids revealed through histology could precede transformative or early invasive events.

Overall, these findings resolve contradictory paradigms that tumors both soften and stiffen during metastasis. Heterogeneity develops as tumors have space grow and these local changes result in different tissue architectures that contribute to the development of metastasis. Stabilization due to confinement may trigger biophysical mechanisms to facilitate tumor invasion. Monitoring the mechanical progression of cancer cells through tumor growth and metastasis may provide insight into their underlying mechanisms, and thus aid in the development of novel prognostic indicators and therapeutic targets.

3.5 Methods

Unless otherwise stated, all cell culture materials and supplies were purchased from Fisher Scientific (Ottawa, ON), and chemicals from Sigma Aldrich (Oakville, ON).

Cell lines

T47D, MDAMB-231 and MCF7-Src inducible human breast cancer cell lines were cultured in DMEM supplemented with 10% FBS and 1% anti-anti. Cells were passaged when 80% confluent using trypsin-EDTA and seeded in a new vessel at a 1:10 dilution to maintain lines. Leftover cells were used for spheroid formation.

Spheroid forming in micropocket devices

Spheroids were formed using polyacrylamide micropocket devices previously described [171]. Briefly, polyacrylamide hydrogels with spherical pockets 1 mm in diameter were fabricated using a 3D printed inverse mold. Hydrogels were cast on a 18 mm silanized glass coverslip for easier device manipulation. Newly fabricated devices were submerged and stored in PBS with 1% anti-anti overnight after 3 PBS washes before further use.

Cells were seeded on the device by carefully pipetting 100 uL of a 10^7 cell/mL suspension on the device. To measure cell-scale internal stiffness within the spheroids, 2-3 uL of a μTAM suspension was added to the 100 uL of concentrated cell suspension prior to device overlay. The cell suspension was left for at least 5 minutes to allow cells to settle and fill the micropockets. Afterwards, the well was filled with 2 mL with complete media. Stable spheroids were formed 2 days post-seeding.

Extended culture and growth confinement

Freely grown spheroids were left in situ within the device with daily media changes for as long as 6 days after spheroid formation. Confined spheroids were restricted by embedding the entire device in alginate gelled with calcium chloride. This was done by partially submerging the device with 1 mL of a 4% (w/v) alginate solution dissolved in complete media and adding 1 mL of a 1% (w/v) calcium chloride solution for 30 seconds. The entire embedded device was extensively rinsed with PBS and then topped off with 1 mL of complete media. Media changes were done daily.

Internal stiffness measurement analysis

Local residual stiffness was measured by observing μTAM size change through a temperature cycle from 37C to 28C over 30 minutes under a fluorescent microscope and stage warmer [205]. Measurements were taken at initial spheroid formation (two days after device seeding) were considered day 0. After these baseline measurements, the spheroids were either left to grow unconfined or confined within alginate. Additional stiffness measurements with temperature cycling were done every 3 days afterwards.

Polyacrylamide microgel fabrication

Microgels were generated within a stirred emulsion by mixing the pre-gel mixture within an oil phase under an oxygen free system as previously described [139]. 1 mL of pre-gel solution for soft microgels consisted of: 75 μL of 40% acrylamide, 29.5 μL of 2% bisacrylamide, 794 μL of phosphate buffered saline (PBS), 1.5 μL of tetramethylethylenediamaine (TEMED), and 100 μL of 1% (w/v) ammonium persulfate (APS) in PBS. 1 mL of stiff microgel pre-gel solution consisted of: 300 μL of 40% acrylamide, 1205 μL of 2% bisacrylamide, 478 μL PBS, 1.5 μL TEMED, and 100 μL of 1% (w/v) ammonium persulfate (APS) in PBS.

Spheroid tissue processing and Staining

Spheroids were fixed in situ with the device with 4% paraformaldehyde in PBS for 24 hours. The entire device was embedded in 1% agarose and scraped off its glass into a cassette. Sponges were also placed within the cassette to prevent the polyacrylamide hydrogel device from curling up during the paraffin embedding process. Spheroids were sectioned at 6 μm thickness and mounted on charged glass slides for histology.

Sections were deparaffinized using xylene for hematoxylin and eosin staining or Histo-Clear II (CA101412-884, VWR) for immunostaining for 10 minutes. The sections were then rehydrated in sequential soakings of 100%, 90%, then 75% ethanol solutions for 3 minutes in each before two PBS washes for 5 minutes.

For hematoxylin and eosin stains, Mayer's hematoxylin solution (MHS1-100ML, Sigma) was applied to cover the tissue for 5 minutes and subsequently washed with two changes of RO water. The section was then placed under running tap water for 30 seconds as a bluing reagent. Afterwards, the slide was dipped in 100% ethanol before an application of enough eosin Y solution (HT110316-500ML, Sigma) to cover the tissue for 2 minutes. The slide was rinsed in 100% ethanol and dehydrated through a reverse sequence of the rehydrating solutions described above. The slide was fully dehydrated in xylene before mounting with a glass coverslip using DPX new synthetic mounting media (1005790507, Sigma).

For immunostaining, rehydrated slides were immersed in Tris/EDTA buffer for heat induced epitope retrieval using a pressure cooker (Instapot, Amazon.ca) set to a 10 minute cook time under the porridge cook setting. Slides were left to cool and renature for 20 minutes before three 5 minute PBS washes. Tissue sections were blocked using 5% donkey serum for 30 minutes. Primary antibody (rat anti-cytokeratin 8, 1:250, Developmental Studies Hybridoma Bank, TROMA-1-C) was applied for overnight incubation at 4°C. After three PBS washes, the secondary antibody solution (donkey anti-rat IgG Alexa Fluor 647, 1:750, Abcam, ab150155) was applied for 1 hour at room

temperature. The sections were counterstained with 2 μg/mL of DAPI in PBS for 10 minutes before two final PBS washes. The slides were coverslip mounted using Fluoromount Aqueous mounting media (F4680-25ML, Sigma) and the edges were sealed with generic clear nail polish.

Image acquisition and analysis

Images were taken on an Olympus IX-73 microscope under epifluorescence (Olympus, X-CITE 120 LED), with an sCMOS Flash 4.0 Camera and Metamorph software (version 7.8.13.0), and automated stage (Zaber) to record and return to specified positions. All image analyses were performed using FIJI.[193] All statistical analyses were performed using GraphPad Prism v8.0.2 (San Diego, CA).

Chapter 4

Tissues are complex materials that can exhibit nonlinear viscoelastic behavior. In this chapter, I asked whether we could extend the use of μTAMs to characterize local viscoelasticity of the tissue microenvironment as well residual stiffness. To do this, I studied the temporal evolution of μTAM expansion within linear elastic polyacrylamide matrices and characterized the force-stroke length curve generated by the sensor to describe the amount of force μTAMs generate at a given strain for a given size of μTAM. Using this force-stroke length curve, which related μTAM force generation to sensor size and strain, we simulated the expansion of a sensor in a viscoelastic Kelvin-Voight model material and ran parameter sweeps for combinations of viscoelastic parameters to create strain versus time curves for each condition. By matching simulated curves to experimental time-expansion profiles of μTAMs within tissues, we were able to determine their viscoelastic properties.

4 Local viscoelastic measurements using thermoreponsive mechanosensors within cancer spheroids

4.1 Abstract

Matrix stiffness has been shown to influence a number of cell behaviors and determine cell fates during development. These studies focused on cells cultured on linear elastic substrates, but the cellular microenvironment is neither linear nor purely elastic. Biological tissues are viscoelastic materials that exhibit time dependent responses to stress and strain. When cells mechanically probe their local environment, they exert traction forces to gauge the stiffness of their environment. Therefore the apparent stiffness a cell initially experiences may differ from the material stiffness of the matrix. Few techniques exist capable of measuring cell scale viscoelasticity without probing an exposed surface of the tissue. Here, we adapted the use of fluorescently-labelled swellable mechanosensors to characterize microscale viscoelasticity within complex 3D tissues. These cell-sized sensors were previously used to measure local stiffness based on equilibrated sensor size changes. To further the technology for viscoelastic measurements, we characterized stresses generated by the sensors at various expansions, and found that this depends on the expansional state and on the size of the sensor. We then used the force-stroke curve to inverse finite element method to model strain time curves experimentally obtained from cancer spheroids. As a first application, we evaluated the viscoelastic properties of invasive and non-invasive tumor models, and demonstrate a significant difference in viscous behavior at the cellular length scale within these realistic tissue models. This technique provides the means to characterize viscoelasticity with cell-scale resolution at unprecedented tissue depths. Bridging the gap between viscoelasticity and cell behavior can enrich our understanding of how mechanical characteristics of the local environment influence cell behavior.

4.2 Introduction

Cells sense and respond to their mechanical microenvironment, which can vary considerably between and within tissues [224,225,1]. While the effects of elastic substrate stiffness are quite dramatic on cell spread area [226,227], generated traction forces [228], cell motility [229], and stem cell differentiation [24], viscoelastic characteristics of the material have recently emerged as potent regulators of cell function. Viscoelasticity describes materials that simultaneously display both instantaneous elasticity and time-dependent viscous behaviors in response to stress, resulting in stress relaxation and viscous creep occurring under load. Biological viscoelastic responses to stress arise due to protein unfolding, crosslink rearrangements between macromolecules, and the release of entangled molecules [65]. Cells generating forces to test their local microenvironment realistically experience some opposing stress that relaxes with time in a viscoelastic material. Indeed, both substrate stress relaxation and creep have been shown to affect cell spreading as well as stem cell growth and differentiation [230–232]. Tissue viscoelasticity, much like stiffness, changes with disease, and magnetic resonance elastography have demonstrated broad differences in viscoelasticity exist between malignant and benign tumors [233]. Single cell mechanical testing reveal normal and benign cancer cells exhibit higher viscous behaviors compared to invasive cells [234,235] However, these findings were done on isolated cells and whether these local strain behavior differences at cell scale resolutions still exist within intact 3D tumors is unknown. Dimensionality alters cell signalling, adhesion and structure and preserving the 3D architecture through the use of more realistic 3D systems represents the best way to replicate more physiologically relevant higher-order structures [30].

Characterizing local viscoelastic behavior within intact biological samples is difficult. Traditional mechanical tests require large sample volumes that may be difficult to obtain, handle, and can provide only a macroscopic material description, whereas cells may experience distinct localized time-dependent matrix responses [122,236,237]. Current tools adapted to measure cell-scale material viscoelasticity do exist through micro-indentation or nanoscale cantilever AFM stress relaxation tests to cell or tissue surfaces

[238–240]. Other methods rely on culturing cells on viscoelastic 2D substrates or observing tissue margin retraction after dissection [241,242]. However, these techniques are not suited to measure properties within 3D tissue samples and cannot do so without sectioning or damaging the sample. To address some of these limitations, we previously developed cell-sized mechanosensors to measure long term residual stiffnesses with a high dynamic range within complex 3D tissues [205]. These mechanosensors actuate based on temperature and expand to exert forces, locally deforming the tissue it is within in the process. Residual stiffness measurements can be determined based on sensor size changes between its initial state and at equilibrium.

Recently, Serwane et al. developed ferrofluid-based magnetic oil droplets, that can be injected intracellularly within an 8-cell zebrafish embryo to make local viscoelastic measurements [134]. Magnetic stresses were applied to the deform the oil droplet into an ellipsoid shape within a cell and strain response over time was observed to model viscoelastic behavior. However, this magnetic actuation produces very low forces that would not be able to deform stiff tissues and has limiting the probing depths based on by the area established by the magnetic field.

We were inspired by this idea of tracking time dependent deformations within a tissue and asked whether our microscale temperature actuated mechanosensors (μTAMs) could be extended into the time domain to make similar measurements within cancer spheroids. Taking measurements within these representative cancer tissue models present its own unique challenges as they tend stiff and require deeper probing depths that cannot be accessed with magnetic actuation. Our sensors are remotely actuated by temperature, have a high dynamic range, and can also be used for long term studies. We expect that sensor expansion within a linear elastic material to be instantaneous and follow a step function, but within viscoelastic materials, to be gradual, only reaching a plateau over time (Figure 4.1A). We developed simulations based on the Kelvin-Voigt model (Figure 4.1B) for viscoelasticity to infer viscoelastic parameters observed when these sensors are

embedded within cancer spheroids generated from cell lines with different invasive potential to reveal potential differences in the viscoelastic behavior.

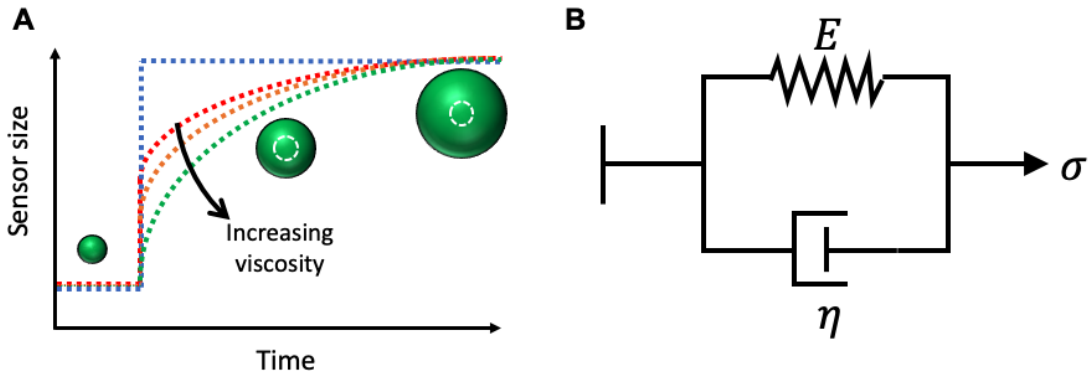

Figure 4.1. Schematic concept of using μTAMs to characterize local viscoelasticity. (A) A μTAM sensor expands rapidly when taken from 37°C to <30°C and can be approximated as an ideal step function when embedded in an ideal elastic material (blue line). Sensors embedded in less (red line) versus more (green line) viscoelastic matrices will show time delay to reach equilibrium size. (B) Schematic representation Kelvin-Voigt model for viscoelasticity where E is the elastic modulus, h is viscosity, and s represents stress.

4.3 Results

4.3.1 Developing force-stroke length curves of μTAM expansion

Adapting μTAMs for time-based measurements presents its own problems that need to be addressed. Unlike conventional constant force applications used to study viscoelastic strain behavior, we suspected that as μTAM expansion occurs, its spring constant would be reduced and as a result, forces generated by the μTAM would change over its stroke length. Therefore, to begin characterizing local viscoelastic properties within tissues, we needed to characterize the stresses generated by an individual sensor, at different degrees of expansion by developing the force-stroke curve of a μTAM sensor. This curve would predict what forces are generated by the sensor at a given point over the entire expansion until the sensor is fully expanded.

Previous force measurements on expanding N-isopropylacrylamide hydrogels confirmed that force decreases with increasing stroke length [243]. However, in that study, large mL volume samples were used and a cylindrical geometry, which is not relevant to μTAM in both size and geometry. Therefore, it is important to specifically measure μTAM expansion forces. We embedded μTAMs in linear elastic matrices designed to constrain μTAM expansion to different degrees. It is expected that when the sensor fully expands within the polyacrylamide hydrogel and reaches an equilibrium, there is a balance of forces between the sensor deformation into the hydrogel matrix and the forces generated by the sensor at that sensor strain. As a result, the stresses generated by the sensor can be obtained from the material properties of the polyacrylamide hydrogel (Figure 4.2A). Equilibrated sensor expansion data within different polyacrylamide hydrogels of different stiffness was generated to relate μTAM size to local stiffness. All the polyacrylamide stiffness formulations were confirmed to have linear elastic behavior up to 10% strain of the global hydrogel corresponding to ~1.2 mm of displacement within the matrix – far greater than any displacement generated by sensor expansion (Figure 4.2B).

The sensors did not expand to the same degree, even within the same hydrogel. We therefore asked whether sensor size changed the level of stress that is applied. Sensor stress

was normalized by its initial radius to reveal a linear relationship between sensor stress and matrix strain for each stiffness of polyacrylamide gel formulation, as expected (Figure 4.2C). We modelled the relationship between sensor size and applied stress using a 2D axisymmetric geometry in COMSOL and found that it changes for different initial sensor size (Figure 4.2D). For larger sensor sizes (>20 µm), the surface plot was extrapolated based on stress and sensor size scaling linearly as force scales linearly with displacement according to Hooke's law. Stress and strain appear to follow an exponential trend, which is characteristic of a first-order system such as diffusion and damping phenomenon. These trends appear to be conserved for all initial sensor sizes as forces generated by the sensor are expected to be the highest at low sensor strains during initial expansion and decay with further strain as a fully expanded sensor is not expected to exert any stress (Figure 4.2E).

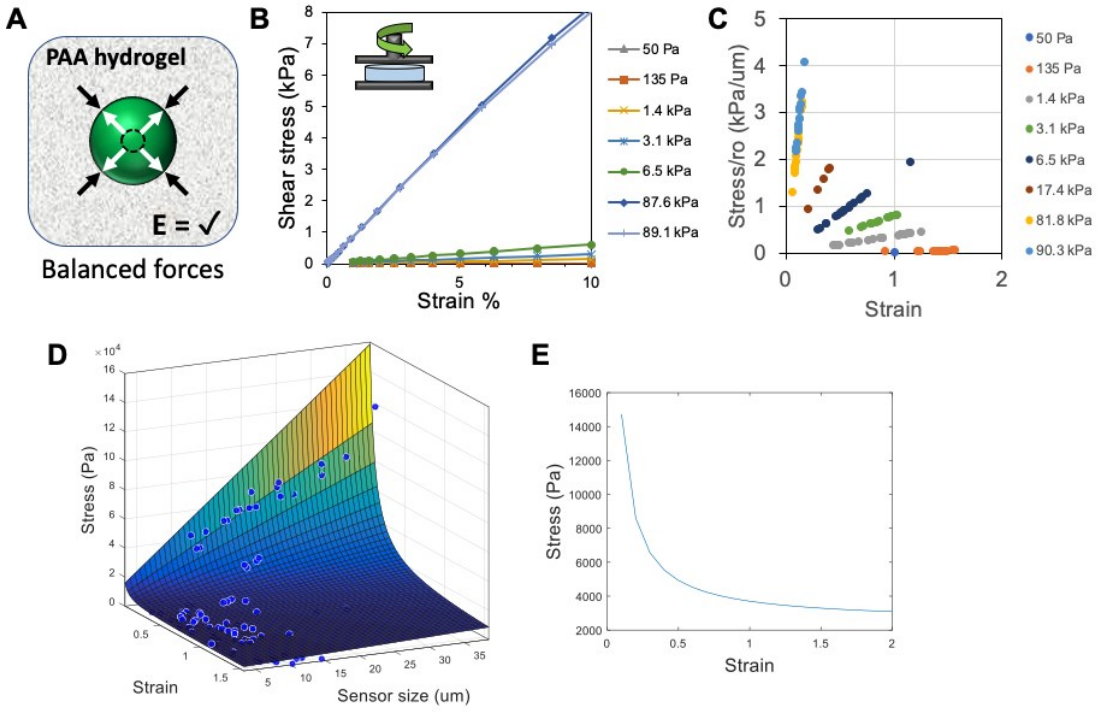

Figure 4.2. Stress-strain characterization of µTAM sensor expansion.
(A) Microgel expansion within polyacrylamide hydrogels of different stiffnesses provides the resistive force to measure sensor stress outputs at given sensor strains when expansion reaches equilibrium. (B) Shear rheometer characterization of polyacrylamide hydrogels

used to embed μTAMs to measure sensor force generation. (C) Stress generated by expanding sensor with polyacrylamide matrix normalized by initial compressed sensor radius shows linear relationship. (D) Relationship between sensor size and applied stress with strain. (E) Representative stress strain curve for an individual sensor size.

4.3.2 Relative time independent expansion of μTAMs in linear elastic matrices

In order to make viscoelastic measurements using the μTAM sensors, we also had to confirm that sensor expansion rate within a linear elastic matrix was faster than its rate within viscoelastic tissues. Having quantitatively established the stresses are generated by a sensor given its size, we studied the rate of sensor expansion immediately following a temperature shift below its lower critical solution temperature (LCST) which corresponds to 34ºC for these microgels. To trigger an immediate sensor expansion, pre-compressed sensors kept at 37ºC within an incubator were cold shocked by dropping ice into the liquid submerging the sensor laden polyacrylamide hydrogels. This resulted in immediate cooling of the system at a faster rate than what was previously done when using μTAMs to measure residual stiffness. (Figure 4.3A). Sensor expansion was rapid and immediate, and full expansion was achieved within a few seconds with μTAMS embedded in a linear elastic polyacrylamide phantom tissue (Figure 4.3B). We then modelled sensor expansion within a matrix based on the Kelvin-Voigt model for viscoelastic materials. In this model, materials are represented by a single dashpot and spring connected in parallel to represent the viscous and elastic behaviors of the material respectively (Figure 4.1B). Parameter sweep simulations show that in general, increases in the elastic component result in smaller amplitude strains while increasing viscosity leads to longer time scales to reach a given strain (Figure 4.4B&C). This makes sense as μTAM expansion in a soft, low viscosity material should have a faster expansion rate. In contrast, expansion within a stiff material with high viscosity which would result in less overall expansion over a longer duration.

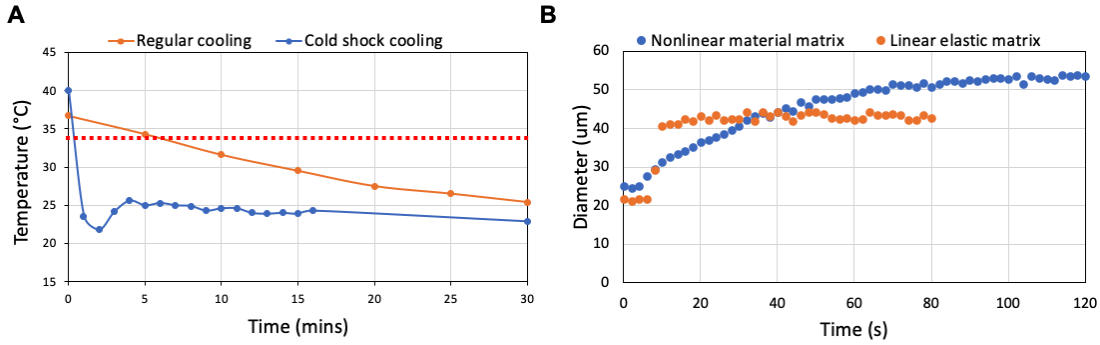

Figure 4.3. Sensor conditions for viscoelastic characterization.
(A) Temperature versus time profile between regular cool down and ice shocked cool down eliminates the temperature time dependency for local viscoelastic characterization. Dashed red line marks the temperature at which sensor size change occurs. (B) Time versus expansion profiles between sensor expansion within linear elastic polyacrylamide matrix compared to expansion with a spheroid.

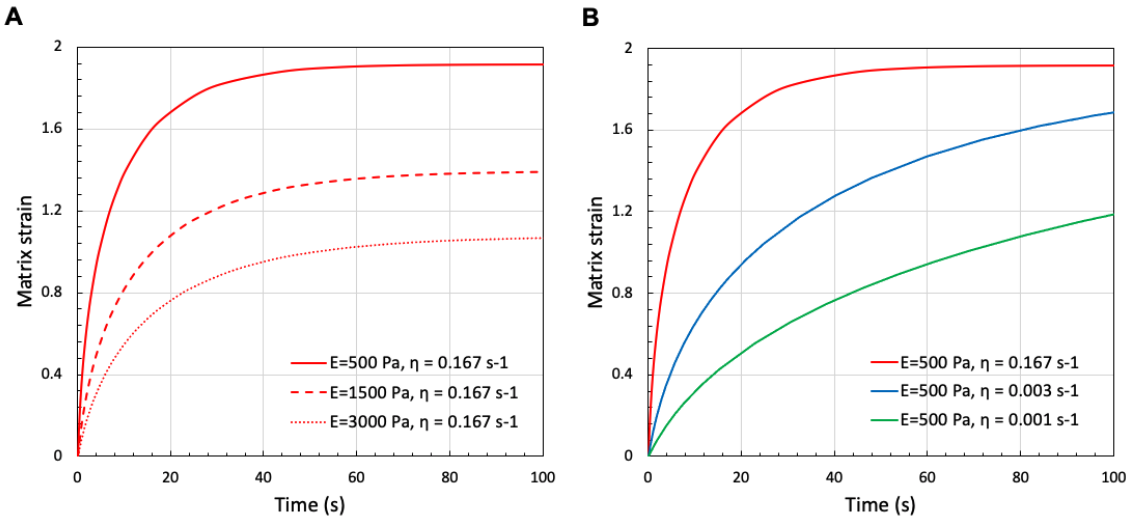

Figure 4.4. Finite element modelling of sensor expansion within viscoelastic matrices.
Expansion time curves for different moduli (A) and viscosity (B) values obtained from parameter sweeps of the Kelvin-Voigt model for viscoelasticity.

4.3.3 Inverse finite element modeling viscoelastic behavior in cancer spheroids

To study cellular length scale viscoelasticity within a biological sample, spheroids were generated using the micropocket device method [171]. Two breast cancer cell lines with different invasive capabilities were used to generate spheroids. MDAMB-231 cells are highly invasive within collagen gels whereas T47D cells do not migrate [171]. μTAM sensors were incorporated into the spheroids for viscoelastic measurements (Figure 4.5A). Cold shocked sensors within MDAMB-231 spheroids expansion reached an equilibrium faster than T47D spheroids (Figure 4.5B&C). Viscoelastic parameters were obtained by fitting simulated and experimental time expansion profiles for each condition (Figure 4.5D&E). MDAMB-231 spheroids exhibit significantly less time delayed response than T47D spheroids, suggesting that they exhibit more elastic behavior with faster responses to strain while T47D spheroids tend to be more viscous and take more time to deform. In contrast, T47D with their high cell-cell adhesions display a coordinated whole tissue response to stress by slowly dissipating strains through the tissue resulting in longer strain rates.

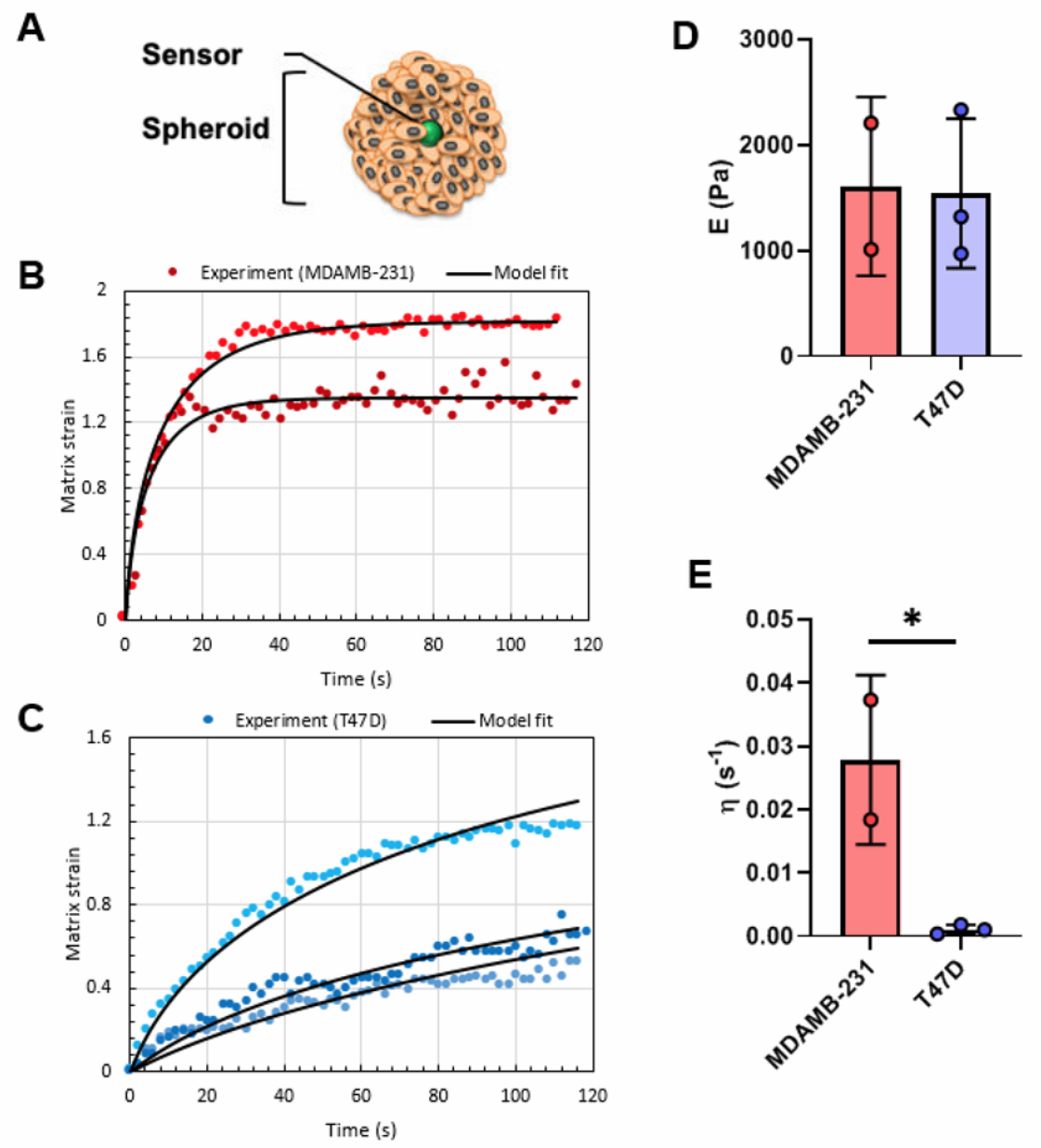

Figure 4.5. Cellular-length scale viscoelasticity in cancer spheroids.
(A) μTAMs are incorporated within spheroids by mixing them in the initial single cell suspension prior to formation. (B and C) Time course of μTAM expansion within spheroids of different breast cancer cell lines with model fitting. (D and E) Values for the elastic and viscous components of the Kelvin-Voigt model as obtained by fitting simulated time expansion profiles to those experimentally obtained.

4.4 Discussion

Here, we demonstrate the use of μTAMs to characterize viscoelastic behavior within microregions of MDAMB-231 and T47D cancer spheroids. These cell-sized mechanosensors demonstrate that spheroids with different invasive potentials showed highly distinctive internal viscoelastic characteristics, where invasive MDAMB-231 spheroids display rapid strain responses to stress, compared to less aggressive T47D spheroids which have a slower, more viscous deformation profile. Interestingly, these distinct viscous properties arise even at sites with very similar elastic moduli. Other viscoelastic studies on individual cells using AFM have also found invasive cancer cells exhibit significantly less viscous behaviors and their normal or benign equivalent cells [234,235], and these findings demonstrate that this phenotype is maintained even in spheroid cultures, where viscoelasticity can arise from multiple features of the three-dimensional tissue context. Similar results using shear wave and ultrasound elastography in humans tissue further support these findings as being translational to the in vivo human context, as malignant lesions have had lower time retardance suggesting higher eta values as well [244,245].

Viscous behavior arises from different sources within the tissue. T47D cells express E-cadherin proteins [217], which allows tightly coupled attachments and close cell-to-cell contact between neighboring cells within the spheroid. This mechanical cell-cell coupling may facilitate stress dissipation throughout the tissue to elicit a cohesive and collective overall fluid-like time delayed strain response as observed [246]. As phenotypically invasive cells, MDAMB-231 cells within the spheroid do not express these cell-cell adhesions [247], and thus respond to local deformations with immediate local strains. Fluid movement may also contribute to viscoelastic behavioral differences. Cells and cellular aggregates have been described and modeled by poroelastic theory that describes a fluid phase that permeates through a solid phase [248,249]. As sensor expansion is also reliant on fluid flow into the sensor and time delays between spheroid types may reflect differences in extracellular fluid flow within the spheroids, which is tightly coupled to local solid deformation. Delayed sensor expansion in T47D spheroids may be due to impaired

fluid flow to the sensor. These cells have been shown to express intercellular tight junctions that normally function to create molecularly water tight barriers which could result in intercellular fluid flow resistance [250,251]. In contrast, MDAMB-231 cells within the spheroid are not as densely packed or closely adhered to one another and so fluid movement between the cells is faster and sensor expansion can happen faster. However, this is unlikely the case because mammalian cell membranes are highly permeable to water. Changes in osmotic pressure has been show be capable of driving large changes in cell volume [252,253]. Furthermore, μTAM sensor sizes average 27±11 μm in radius [205], and since T47D cells specifically have been reported to have a water permeability of 20 μm/s [254], it seems unlikely that fluid flow to the sensor is the cause of the time delays observed. Instead, delays in fluid flow are likely due to delayed reorganization of the tissue. The motile MDAMB-231 cells may display faster strain responses because they exhibit more movement within the tissue for an overall fluidized behavior [114,255].

Changes in viscoelastic responses affect how cells perceive their mechanical environment over time. This tool provides the ability to characterize viscoelastic microenvironment at the cell scale resolution better understand how time dependent mechanics can influence or change with cell behavior. Mechanical changes within the cellular microenvironment are associated with disease states and these cues can promote further dysfunctional cell behavior [53,256]. Thus, the ability to measure and quantify viscoelasticity provide the means to measure subtle time dependent differences of mechanical behaviors within the cellular microenvironment that a cell would experience.

4.5 Methods

Unless otherwise stated, all cell culture materials and supplies were purchased from Fisher Scientific (Ottawa, ON), and chemicals from Sigma Aldrich (Oakville, ON).

Polyacrylamide gel fabrication and mechanical testing

Polyacrylamide hydrogel solutions were prepared as previously described [205]. Pure hydrogels were cast between two (Trimethoxysilyl) propyl methacrylate (MPS) coverslips for parallel plate shear rheometry testing (Anton-Paar, MCR 302). Hydrogels with μTAMs mixed in the pre-gel solution were cast between a silanized 18 mm coverslip and a Rain-X treated glass slide. The μTAM laden hydrogels were casted on a slide warmer set to 40ºC to maintain compacted sensor state. After gelation, the gels cast on 18 mm the coverslips were carefully released off the Rain-X treated glass slide. All newly casted gels were submerged in PBS and soaked overnight. Blank hydrogels were store in the fridge, but μTAM laden hydrogels were kept in an incubator set at 37ºC to maintain sensor compaction.

Cell culture

T47D and MDAMB-231 breast cancer cells were cultured in DMEM supplemented with 10% FBS and 1% anti-anti. Cells were subcultured at 80% confluency with 0.25% trypsin-EDTA and reseeded at a 1:10 dilution. The remaining suspension was used to form spheroids spheroid formation.

Spheroid formation with μTAMs

Spheroids were made by passive confinement in polyacrylamide micropockets as previously described [171]. The pocket size used were 1 mm diameter spheres with a 400 um opening. The polyacrylamide pre-gel solution was filter sterilized before use and the micropocket devices were cast onto a MPS treated 18 mm coverslip for ease of handling. Devices were washed with PBS and stored in PBS with 1% anti-anti minimally overnight before use.

A $17x10^6$ cell/mL suspension was prepared to load the micropocket devices. Each device was loaded with 100 uL of cell suspension plus 1-3 µL of a collagen I coated µTAM suspension. The device was left undisturbed for 5 minutes to allow cells to settle into the micropockets, after which the device was submerged in complete media. Spheroids were left to form over 2 days.

µTAM size measurements

All samples were mounted on Chamlide imaging chamber and submerged with 500 µL of PBS which was then placed on a controlled stage warmer (Ibidi). Image acquisition was done on an Olympus IX-73 microscope under epifluorescence (Olympus, X-CITE 120 LED), with an sCMOS Flash 4.0 Camera and Metamorph software (version 7.8.13.0). Samples were maintained at 37°C until cool down was initiated. Cool down was achieved by either releasing temperature control and allowing the system to naturally equilibrate to room temperature or by dropping ice into the Chamlide chamber to cold shock the system.

Finite element modeling of µTAM expansion within linear elastic and viscoelastic matrices

µTAM expansion was computationally simulated as an expanding hole within a defined nearly-infinite matrix using a two-dimensional axisymmetric finite element model built with COMSOL v.5.3.1.201 (Comsol Inc., Burlington, MA, USA). To obtain the µTAM force-stroke length

relationship, the model was first used to quantify the steady-state stresses associated with experimentally-observed μTAM expansion in well-characterized polyacrylamide matrices (Figure 2). The known stiffness of these hydrogels was used to define the Young's modulus of the linear elastic material model while experimental bead size measurements were used to set up the initial bead radius and the displacement boundary condition. The resulting stress values (σ) were then compiled in MATLAB R2018b (The MathWorks, Inc.) and fitted to obtain the following stress-strain relationship for a given initial bead radius, r, (in m).

$$\sigma = Ar\left(\exp\left(\frac{B}{1+\varepsilon}\right) - 1\right) - C$$

$$where\ A = 414.9\frac{Pa}{m}, B = 2.194\ and\ C = 3334\ Pa$$

This relationship was ultimately implemented as a pressure boundary condition in a time-dependent study to simulate μTAM expansion within viscoelastic matrices as defined by the Kelvin-Voigt model (Figure 4). To estimate the viscoelastic Kelvin-Voigt parameters characteristic of breast cancer spheroids, parameter estimation was performed by matching simulated sensor expansion profiles with those obtained experimentally under an optimality tolerance of 0.0001 (Figure 5). For all studies, a free triangular mesh was used and optimized to ensure a coefficient of variation of less than 1% with mesh element quality larger than 0.9 at all time points.

Statistics

All statistical analyses were performed using GraphPad Prism v8.0.2 (San Diego, CA).

Chapter 5

5 Final Remarks

5.1 Original Contributions to Knowledge

1. I developed a new method to measure tissue mechanics with a spatial resolution close to the size of a cell that can be broadly applied to any existing in vitro 3D systems like spheroids and in vivo animal models. I validated its use for residual stiffness measurements over a range of expected from biological soft tissues by calibrating the system in mechanically defined phantom biomaterials. This system can be used to measure residual stiffness within intact 3D tissues to characterize the mechanical microenvironment that cells experience within a physiologically relevant condition. More importantly, this technique can uniquely be used for long-term, deep tissue imaging.

2. Using this technique, I discovered areas of unexpectedly high and low stiffness exist simultaneously within a given tissue, reconciling variations observed with different existing techniques attempting similar measurements. Statistical averaging the localized measurements across the whole tissue would mask these small regions and diminish their importance especially within diseases like cancer where one or a small cluster of highly aggressive cells drive pathogenesis further.

3. I found localized mechanical heterogeneity develops within spheroids generated from highly aggressive breast cancer cells lines over time, provided that there was space to grow. In contrast, under confined growth, these mechanical variations stabilized over time suggesting that internal mechanical conditions respond to external mechanical conditions.

4. I showed that cells differentially arrange themselves around defined soft versus stiff microregions. These morphological differences could be the cause or the effect of

local stiffness variations within tissues and underly other cell behavioral changes in response to stiffness.

5. I further developed the mechanosensory system to readout local viscoelasticity, recognizing its importance as a material trait of biological tissues. Using this new capability, I discovered that spheroids derived from benign cancer cell lines exhibit more viscous, time delayed behaviors in response to stress compared to invasive cell lines. These findings may reflect changes in cell movement and resultant fluid flow within the issue.

5.2 Comprehensive Discussion

The original motivation behind these works was to characterize the mechanics within the cellular microenvironment. However at the time, there were no tools available that could do this within intact tissues and at a cell scale resolution. In the first chapter, I reviewed the current knowledge on how cells respond to their physical microenvironment, emphasizing the need to recognize and measure the heterogeneity within biological samples [1,257]. This was exemplified within the context of the cancer microenvironment, where the disease can be driven by a few aggressive cells [258]. Changes in mechanical state of the tissue accompany the changes in disease progression [259]. Mechanical differences were reported between normal and diseased whole tissues [244,260], and benign versus malignant cancer cells [51]. The altered cancer microenvironment may provide physical cues to control or promote further disease outcomes [42,259]. Initial mechanobiology studies at the microscale level were typically done on single cells or 2D cultures – platforms that are physiologically and mechanically far removed from its native environment within the body [30]. I recognized the need to preserve the physical context of the cellular microenvironment to gain a more accurate mechanical readout of the physical conditions a cell would realistically experience. However at the time there were no tools available that could make these measurements within 3D tissues at a spatial resolution of a cell. Therefore, I developed μTAM sensors that could be incorporated into any existing 3D cell culture or animal model systems to probe the internal mechanics within complex tissue structures to address this need.

In the second chapter, I outlined the design principles, characterization, and validation of the μTAMs to measure cell-scale residual stiffness over a broad mechanical range that would be encountered within soft tissues. Then in chapter 4, I adapted the μTAM to be able to characterize viscoelastic behaviors of the local environment as well. These two applications represent a novel method with the potential to study living cell mechanics throughout their growth and without disrupting tissue architecture or killing the cells. This also provided the means to mechanically study of internal tumor stiffness and viscoelasticity with cell sized resolution and sensitivity over time. Measurements made

using μTAMs cannot be compared to other methods as it probes mechanics at the micro length scale within 3D tissue samples whereas comparable techniques either rely on cutting the tissue to expose surfaces and inadvertently release internal stresses, thus altering the internal mechanics, or are not comparable in spatial resolution [14,35,37].

In chapters 2, 3, and 4, I demonstrated the broad application of μTAMs by applying them within model 3D culture systems and animal models for breast cancer to make internal mechanical measurements. In doing so, I quantified the range of mechanical heterogeneity that exists within these tissues and showed that stiffness in local areas fluctuate over time and growth. This heterogeneity only appeared in tissues derived from cells with high invasive potential (established 4T1 tumors, and MDAMB-231 and induced MCF7-Src) suggesting these changes in local stiffness were related to cell movement or changes in local cell arrangement. Interestingly, differences in viscoelastic behavior may also be explained by cell mobility within the tissue as MDAMB-231 spheroids strain faster to applied stresses than benign T47D spheroids. Genetic instability may also contribute to the mechanical variations seen in the MDAMB-231 spheroids [261] as chromosomal instability and aneuploidy are hallmarks of cancer that contribute to tumor evolution [262]. This would result in genetically varied population of cells within the spheroid as errors in chromosomal segregation during cell division accumulate during tissue growth leading to phenotypic variations as well. Histological spheroid sections showed that cells around areas of high stiffness are stretched and elongated whereas cells around soft regions remain rounded within spheroids. This morphological response is similar to what has been observed on soft versus stiff 2D substrates [227] but represents the first time it is observed within 3D tissues. Furthermore, these findings are the first to show local structural differences do exist around microregions of different stiffnesses in 3D cultures. At the same time, the elongated morphology are similar to the contractile phenotype either for individual cell movement or collective cell activity for cell extrusion and may be the source of high stiffness [218,222]. Therefore, initial variations of stiffness within a tissue may be due to changes in cell movement and microregions of high stiffness may result in reactive local cell contractions which can lead to greater apparent stiffnesses. Currently, the results

are consistent with the idea that high fluidity within tissues prevent accumulation of microregions of stiffness because local reorganization continually alters the mechanical environment. Cell-cell adhesions are not as permanent or fixed and cells can move and flow around each other.

Interestingly, mechanical heterogeneity appears to stabilize within confined growth. These measured changes in internal mechanics during this confinement have never been reported before. However, compressive forces have been reported to stabilize tumor growth but promote more invasive capability once compression is released [60,263]. Histological observations from chapter 3 could be visual representation of cell extrusion occurring. This could be the means of early metastatic cell dissemination.

5.3 Future Directions

Future directions for the works presented in this thesis include studies exploring the underlying biology for the observations made, as well as additional technological developments expanding the usage of μTAMs. The collective findings thus far suggest the following mechanical timeline in tumor development and progression towards metastasis: (1) early proliferation of benign cells have a uniform mechanical landscape, (2) transformative events conferring cell mobility within the tissue creates areas of mechanical heterogeneity, (3) continued tumor growth leads to eventual confinement that reduces internal cell mobility and mechanical variation, (4) localized areas of immobilized high stiffness may trigger cell extrusion mechanisms to promote invasion and metastasis. Procedures could be developed to assay mechanics and then match those findings with immunostaining to find correlations between biological and mechanical signals. For example, in the current works markers of contraction or cell mechanical activity such as f-actin or p-myosin to confirm contractile arrangement of cells around local areas of stiff and soft spots. Furthermore, to reinforce that cell movement is truly the cause of mechanical heterogeneity, cell mobility in invasive cells can be modulated with pharmacologic compounds targeting different regulators of actin-myosin contractility to determine whether they influence appearance of this heterogeneity [264].

The mechanobiological basis linking these mechanical observations and behavioral cell phenotypes has not been explored in depth in the current works but presents an additional avenue of study. Defining the signaling pathways that are affected or that contribute to the phenotypes observed helps to define causation from correlation. The Hippo-YAP/TAZ tumor suppressor pathway is an obvious first choice to extend the current work [265,266]. YAP and TAZ are transcription factors downstream the Hippo signaling pathway and there is a correlation between high nuclear levels of these transcription factors in cancer with tumor progression [267,268]. Interestingly, although the Hippo pathway appears to drive tumor growth in cancer cells, its activity within normal healthy cells appears to have a tumor suppressor effect [269]. Nuclear localization of YAP/TAZ is influenced by mechanical cues from the cytoskeleton to drive changes in gene expression

influencing proliferation and cell survival [270]. Perhaps the oncogenic switch for this pathway is mechanically dependent. This pathway also cross talks with other mechanotransduction pathways such as Wnt/β-catenin signaling further implicating a role for mechanics in driving cell behavior [271,272]. Biomarkers suggesting activity in these pathways around microregions of stiffness could be observed through further histological analysis and then manipulated through selective inhibitors in future experiments to correlate cause and effects. Alternatively, various omics analysis could be used to uncover other regulatory pathways linking these phenotypes back to cell biology. These analysis would involve universally detecting differences in genes, mRNA expression, and protein production between different cell populations, in this case cells from defined soft or stiff microregions compared to cells from the rest of the spheroid [273].

The full size ranges of the μTAMs achievable has yet to be explored in further depth. Although sensor design for this thesis was aimed towards smaller, cell-length sizes, this does not necessarily limit the technology to these length scales. It is possible to generate hydrogels of larger sizes and even different geometries to probe other mechanical features within tissues like anisotropy. These changes would require additional hydrogel characterization as well as considerations with temporal, temperature dependent, and solvent diffusion dynamics involved in pNiPAAM hydrogel expansion.

Although the sensors were used in spheroid models, μTAMs are broadly applicable to a wide variety of model systems that could not be mechanically assayed by conventional or existing methods. These sensors are particularly suitable within 3D sealed systems or inside microfluidic organ on a chip systems involving 3D hydrogels [274]. Recent developments in 3D cultures have produced self-organizing organoid structures representing different tissues from stem cells to model development and disease [275]. Tissue development and remodeling is influenced by mechanobiology [146]. Organoids are closed tissue systems surrounded by ECM. μTAMs can seamlessly be incorporated within either component to provide mechanical readouts of supracellular stiffness within the tissue and track mechanical changes during morphogenesis. Surface functionalization

on the μTAM sensors can be altered as well to promote tissue cohesion and uptake or even test local biochemical or phenotypic response to different ligands.

The current understanding provided by the μTAMs suggest that the tissues themselves are in a constant mechanical flux at the microscale level. Macroscale properties of the tissues alone are not enough to describe tissue conditions and may be a long-term outcome of microscale events that happen earlier. In the context of cancer, discrete microregions of highly varied stiffness could be the manifestation of cell movement within the tissue revealing early transformative events have occurred. This could be a predictive marker for metastatic competence and future disease progression.

5.4 Summary and Conclusion

In this thesis, I have engineered a new technique to monitor local stiffness within engineered tumors by using N-isopropylacrylamide microgels as a mechanosensory that can be broadly utilized across existing 3D culture platforms and animal models in chapter 2. I measured and tracked the stiffness evolution within 3D models of breast cancer by mixing these sensors with the cells prior to spheroid formation, and measured residual stiffness using sensor size change as a proxy in chapter 3. Finally, I further characterized temporal behavior of μTAM expansion to measure viscoelastic behavior between invasive and non-invasive cancer spheroids in chapter 4.

Together, these works provide demonstrate that it is now possible to study cell-scale mechanics within complex tissues over time. Irregular changes in tissue mechanics at spatial resolution of a cell may provide early indicators for deviations of normal physiology and health. In developing the μTAMs, these mechanics can be characterized to determine whether these changes can be used as potential prognostic markers linking tissue stiffness to disease progression. Although the thesis focuses heavily on using these sensors in the context of cancer in this thesis, there other physiological events where changes in tissue mechanics provide a guiding factor like in early development, and wound healing, that can be explored.

Tissue and cells are active materials that apply and transmit forces, adapting to physical cues from their environment. The recent development of tools to measure tissue material properties and the stresses in 3D at the nano and microscale gives us the opportunity to isolate the mechanical contributions of every component within tissues. By recognizing the complex and varied mechanics involved at the cell scale, we have a better understanding of how local matrix material properties affect cell signaling and gene expression, which in turn influence cellular interactions with their environment. Despite current progress, there remain many unexplored opportunities to further understand the role of physical cues within the cellular microenvironment. It is also important to highlight that the cellular microenvironment is greater than the sum of its individual parts. The tools

and techniques described in this thesis will aid in the transition from testing simple cell monolayer cultures to more complex 3D systems and in vivo animal models. Ultimately, this will provide better physiological context to understand microscale mechanical behaviors in tissues and refine the applicability of such knowledge to elucidate mechanisms for tissue development, homeostasis, and disease progression. Furthermore, combining different techniques within the same experiment can further provide a more complete understanding of the interactive nature of mechanical behavior. The differing mechanics measured by a plethora of techniques used to measure differing mechanics within and across the length scales suggests that the physical experience within biological tissues is a subjective one based on time, space, and location.

Complete References

[1] Discher DE, Janmey P, Wang Y. Tissue Cells Feel and Respond to the Stiffness of Their Substrate. Science 2005;310:1139–43. https://doi.org/10.1126/science.1116995.

[2] Hoffman BD, Crocker JC. Cell Mechanics: Dissecting the Physical Responses of Cells to Force. Annu Rev Biomed Eng 2009;11:259–88. https://doi.org/10.1146/annurev.bioeng.10.061807.160511.

[3] Janmey PA, Miller RT. Mechanisms of mechanical signaling in development and disease. J Cell Sci 2011;124:9–18. https://doi.org/10.1242/jcs.071001.

[4] Merten O-W. Advances in cell culture: anchorage dependence. Philos Trans R Soc B Biol Sci 2015;370. https://doi.org/10.1098/rstb.2014.0040.

[5] Wei Q, Hariharan V, Huang H. Cell-Cell Contact Preserves Cell Viability via Plakoglobin. PLOS ONE 2011;6:e27064. https://doi.org/10.1371/journal.pone.0027064.

[6] Chen J, Irianto J, Inamdar S, Pravincumar P, Lee DA, Bader DL, et al. Cell Mechanics, Structure, and Function Are Regulated by the Stiffness of the Three-Dimensional Microenvironment. Biophys J 2012;103:1188–97. https://doi.org/10.1016/j.bpj.2012.07.054.

[7] Ingber DE, Wang N, Stamenović D. Tensegrity, cellular biophysics, and the mechanics of living systems. Rep Prog Phys Phys Soc G B 2014;77:046603. https://doi.org/10.1088/0034-4885/77/4/046603.

[8] Spagnol ST, Armiger TJ, Dahl KN. Mechanobiology of Chromatin and the Nuclear Interior. Cell Mol Bioeng 2016:1–9. https://doi.org/10.1007/s12195-016-0444-9.

[9] Takaki T, Montagner M, Serres MP, Berre ML, Russell M, Collinson L, et al. Actomyosin drives cancer cell nuclear dysmorphia and threatens genome stability. Nat Commun 2017;8:16013. https://doi.org/10.1038/ncomms16013.

[10] Stowers RS, Shcherbina A, Israeli J, Gruber JJ, Chang J, Nam S, et al. Matrix stiffness induces a tumorigenic phenotype in mammary epithelium through changes in chromatin accessibility. Nat Biomed Eng 2019:1–11. https://doi.org/10.1038/s41551-019-0420-5.

[11] Swift J, Discher DE. The nuclear lamina is mechano-responsive to ECM elasticity in mature tissue. J Cell Sci 2014;127:3005–15. https://doi.org/10.1242/jcs.149203.

[12] Elosegui-Artola A, Oria R, Chen Y, Kosmalska A, Pérez-González C, Castro N, et al. Mechanical regulation of a molecular clutch defines force transmission and transduction in response to matrix rigidity. Nat Cell Biol 2016;18:540–8. https://doi.org/10.1038/ncb3336.

[13] Wang X, Ha T. Defining Single Molecular Forces Required to Activate Integrin and Notch Signaling. Science 2013;340:991–4. https://doi.org/10.1126/science.1231041.

[14] Guimarães CF, Gasperini L, Marques AP, Reis RL. The stiffness of living tissues and its implications for tissue engineering. Nat Rev Mater 2020:1–20. https://doi.org/10.1038/s41578-019-0169-1.

[15] Butcher DT, Alliston T, Weaver VM. A tense situation: forcing tumour progression. Nat Rev Cancer 2009;9:108–22. https://doi.org/10.1038/nrc2544.
[16] McKee CT, Last JA, Russell P, Murphy CJ. Indentation Versus Tensile Measurements of Young's Modulus for Soft Biological Tissues. Tissue Eng Part B Rev 2011;17:155–64. https://doi.org/10.1089/ten.teb.2010.0520.
[17] Janmey PA, Georges PC, Hvidt S. Basic rheology for biologists. Methods Cell Biol 2007;83:3–27. https://doi.org/10.1016/S0091-679X(07)83001-9.
[18] Lee GYH, Lim CT. Biomechanics approaches to studying human diseases. Trends Biotechnol 2007;25:111–8. https://doi.org/10.1016/j.tibtech.2007.01.005.
[19] Bissell MJ, Radisky DC, Rizki A, Weaver VM, Petersen OW. The organizing principle: microenvironmental influences in the normal and malignant breast. Differentiation 2002;70:537–46. https://doi.org/10.1046/j.1432-0436.2002.700907.x.
[20] Kass L, Erler JT, Dembo M, Weaver VM. Mammary epithelial cell: Influence of extracellular matrix composition and organization during development and tumorigenesis. Int J Biochem Cell Biol 2007;39:1987–94. https://doi.org/10.1016/j.biocel.2007.06.025.
[21] Han YL, Pegoraro AF, Li H, Li K, Yuan Y, Xu G, et al. Cell swelling, softening and invasion in a three-dimensional breast cancer model. Nat Phys 2020;16:101–8. https://doi.org/10.1038/s41567-019-0680-8.
[22] Acerbi I, Cassereau L, Dean I, Shi Q, Au A, Park C, et al. Human breast cancer invasion and aggression correlates with ECM stiffening and immune cell infiltration. Integr Biol 2015;7:1120–34. https://doi.org/10.1039/C5IB00040H.
[23] Adams JC, Watt FM. Regulation of development and differentiation by the extracellular matrix. Development 1993;117:1183–98.
[24] Engler AJ, Sen S, Sweeney HL, Discher DE. Matrix Elasticity Directs Stem Cell Lineage Specification. Cell 2006;126:677–89. https://doi.org/10.1016/j.cell.2006.06.044.
[25] Ghibaudo M, Saez A, Trichet L, Xayaphoummine A, Browaeys J, Silberzan P, et al. Traction forces and rigidity sensing regulate cell functions. Soft Matter 2008;4:1836–43. https://doi.org/10.1039/B804103B.
[26] Baker BM, Trappmann B, Wang WY, Sakar MS, Kim IL, Shenoy VB, et al. Cell-mediated fibre recruitment drives extracellular matrix mechanosensing in engineered fibrillar microenvironments. Nat Mater 2015;14:1262–8. https://doi.org/10.1038/nmat4444.
[27] Bonnans C, Chou J, Werb Z. Remodelling the extracellular matrix in development and disease. Nat Rev Mol Cell Biol 2014;15:786–801. https://doi.org/10.1038/nrm3904.
[28] Pedersen JA, Swartz MA. Mechanobiology in the Third Dimension. Ann Biomed Eng 2005;33:1469–90. https://doi.org/10.1007/s10439-005-8159-4.
[29] Leung BM, Moraes C, Cavnar SP, Luker KE, Luker GD, Takayama S. Microscale 3D Collagen Cell Culture Assays in Conventional Flat-Bottom 384-Well Plates. J Lab Autom 2015;20:138–45. https://doi.org/10.1177/2211068214563793.

[30] Baker BM, Chen CS. Deconstructing the third dimension – how 3D culture microenvironments alter cellular cues. J Cell Sci 2012;125:3015–24. https://doi.org/10.1242/jcs.079509.
[31] Doxzen K, Vedula SRK, Leong MC, Hirata H, Gov NS, Kabla AJ, et al. Guidance of collective cell migration by substrate geometry. Integr Biol 2013;5:1026–35. https://doi.org/10.1039/c3ib40054a.
[32] Siedlik MJ, Manivannan S, Kevrekidis IG, Nelson CM. Cell Division Induces and Switches Coherent Angular Motion within Bounded Cellular Collectives. Biophys J 2017;112:2419–27. https://doi.org/10.1016/j.bpj.2017.05.001.
[33] Tanner K, Mori H, Mroue R, Bruni-Cardoso A, Bissell MJ. Coherent angular motion in the establishment of multicellular architecture of glandular tissues. Proc Natl Acad Sci 2012;109:1973–8. https://doi.org/10.1073/pnas.1119578109.
[34] Erdogan B, Ao M, White LM, Means AL, Brewer BM, Yang L, et al. Cancer-associated fibroblasts promote directional cancer cell migration by aligning fibronectin. J Cell Biol 2017;216:3799–816. https://doi.org/10.1083/jcb.201704053.
[35] Nia HT, Liu H, Seano G, Datta M, Jones D, Rahbari N, et al. Solid stress and elastic energy as measures of tumour mechanopathology. Nat Biomed Eng 2017;1:0004. https://doi.org/10.1038/s41551-016-0004.
[36] Plodinec M, Loparic M, Monnier CA, Obermann EC, Zanetti-Dallenbach R, Oertle P, et al. The nanomechanical signature of breast cancer. Nat Nanotechnol 2012;7:757–65. https://doi.org/10.1038/nnano.2012.167.
[37] Voutouri C, Stylianopoulos T. Accumulation of mechanical forces in tumors is related to hyaluronan content and tissue stiffness. PLOS ONE 2018;13:e0193801. https://doi.org/10.1371/journal.pone.0193801.
[38] Hanahan D, Weinberg RA. Hallmarks of Cancer: The Next Generation. Cell 2011;144:646–74. https://doi.org/10.1016/j.cell.2011.02.013.
[39] Sanders ME, Schuyler PA, Dupont WD, Page DL. The natural history of low-grade ductal carcinoma in situ of the breast in women treated by biopsy only revealed over 30 years of long-term follow-up. Cancer 2005;103:2481–4. https://doi.org/10.1002/cncr.21069.
[40] Margenthaler JA, Vaughan A. NO surgery for low-grade ductal carcinoma in situ? JAMA Surg 2015;150:746–746. https://doi.org/10.1001/jamasurg.2015.0895.
[41] Boghaert E, Gleghorn JP, Lee K, Gjorevski N, Radisky DC, Nelson CM. Host epithelial geometry regulates breast cancer cell invasiveness. Proc Natl Acad Sci 2012;109:19632–7. https://doi.org/10.1073/pnas.1118872109.
[42] Bissell MJ, Hines WC. Why don't we get more cancer? A proposed role of the microenvironment in restraining cancer progression. Nat Med 2011;17:320–9. https://doi.org/10.1038/nm.2328.
[43] Liu Z, Vunjak-Novakovic G. Modeling tumor microenvironments using custom-designed biomaterial scaffolds. Curr Opin Chem Eng 2016;11:94–105. https://doi.org/10.1016/j.coche.2016.01.012.
[44] I. Lopez J, Kang I, You W-K, M. McDonald D, M. Weaver V. In situ force mapping of mammary gland transformation. Integr Biol 2011;3:910–21. https://doi.org/10.1039/C1IB00043H.

[45] Hoyt K, Castaneda B, Zhang M, Nigwekar P, di Sant'Agnese PA, Joseph JV, et al. Tissue elasticity properties as biomarkers for prostate cancer. Cancer Biomark Sect Dis Markers 2008;4:213–25.
[46] McDonald DM, Baluk P. Significance of Blood Vessel Leakiness in Cancer. Cancer Res 2002;62:5381–5.
[47] Jain RK, Martin JD, Stylianopoulos T. The Role of Mechanical Forces in Tumor Growth and Therapy. Annu Rev Biomed Eng 2014;16:321–46. https://doi.org/10.1146/annurev-bioeng-071813-105259.
[48] Wells RG. Tissue mechanics and fibrosis. Biochim Biophys Acta BBA - Mol Basis Dis 2013;1832:884–90. https://doi.org/10.1016/j.bbadis.2013.02.007.
[49] Fenner J, Stacer AC, Winterroth F, Johnson TD, Luker KE, Luker GD. Macroscopic Stiffness of Breast Tumors Predicts Metastasis. Sci Rep 2014;4. https://doi.org/10.1038/srep05512.
[50] Xu W, Mezencev R, Kim B, Wang L, McDonald J, Sulchek T. Cell Stiffness Is a Biomarker of the Metastatic Potential of Ovarian Cancer Cells. PLOS ONE 2012;7:e46609. https://doi.org/10.1371/journal.pone.0046609.
[51] Swaminathan V, Mythreye K, O'Brien ET, Berchuck A, Blobe GC, Superfine R. Mechanical Stiffness Grades Metastatic Potential in Patient Tumor Cells and in Cancer Cell Lines. Cancer Res 2011;71:5075–80. https://doi.org/10.1158/0008-5472.CAN-11-0247.
[52] Levental KR, Yu H, Kass L, Lakins JN, Egeblad M, Erler JT, et al. Matrix Crosslinking Forces Tumor Progression by Enhancing Integrin Signaling. Cell 2009;139:891–906. https://doi.org/10.1016/j.cell.2009.10.027.
[53] Paszek MJ, Zahir N, Johnson KR, Lakins JN, Rozenberg GI, Gefen A, et al. Tensional homeostasis and the malignant phenotype. Cancer Cell 2005;8:241–54. https://doi.org/10.1016/j.ccr.2005.08.010.
[54] Stylianopoulos T, Martin JD, Snuderl M, Mpekris F, Jain SR, Jain RK. Coevolution of Solid Stress and Interstitial Fluid Pressure in Tumors During Progression: Implications for Vascular Collapse. Cancer Res 2013;73:3833–41. https://doi.org/10.1158/0008-5472.CAN-12-4521.
[55] Stylianopoulos T, Martin JD, Chauhan VP, Jain SR, Diop-Frimpong B, Bardeesy N, et al. Causes, consequences, and remedies for growth-induced solid stress in murine and human tumors. Proc Natl Acad Sci U S A 2012;109:15101–8. https://doi.org/10.1073/pnas.1213353109.
[56] Solon J, Levental I, Sengupta K, Georges PC, Janmey PA. Fibroblast Adaptation and Stiffness Matching to Soft Elastic Substrates. Biophys J 2007;93:4453–61. https://doi.org/10.1529/biophysj.106.101386.
[57] Xu J, Tseng Y, Wirtz D. Strain Hardening of Actin Filament Networks REGULATION BY THE DYNAMIC CROSS-LINKING PROTEIN α-ACTININ. J Biol Chem 2000;275:35886–92. https://doi.org/10.1074/jbc.M002377200.
[58] Tse JM, Cheng G, Tyrrell JA, Wilcox-Adelman SA, Boucher Y, Jain RK, et al. Mechanical compression drives cancer cells toward invasive phenotype. Proc Natl Acad Sci 2012;109:911–6. https://doi.org/10.1073/pnas.1118910109.

[59] Demou ZN. Gene Expression Profiles in 3D Tumor Analogs Indicate Compressive Strain Differentially Enhances Metastatic Potential. Ann Biomed Eng 2010;38:3509–20. https://doi.org/10.1007/s10439-010-0097-0.
[60] Alessandri K, Sarangi BR, Gurchenkov VV, Sinha B, Kießling TR, Fetler L, et al. Cellular capsules as a tool for multicellular spheroid production and for investigating the mechanics of tumor progression in vitro. Proc Natl Acad Sci 2013;110:14843–8. https://doi.org/10.1073/pnas.1309482110.
[61] Baker EL, Lu J, Yu D, Bonnecaze RT, Zaman MH. Cancer Cell Stiffness: Integrated Roles of Three-Dimensional Matrix Stiffness and Transforming Potential. Biophys J 2010;99:2048–57. https://doi.org/10.1016/j.bpj.2010.07.051.
[62] Yamazaki D, Kurisu S, Takenawa T. Regulation of cancer cell motility through actin reorganization. Cancer Sci 2005;96:379–86. https://doi.org/10.1111/j.1349-7006.2005.00062.x.
[63] Cross SE, Jin Y-S, Rao J, Gimzewski JK. Nanomechanical analysis of cells from cancer patients. Nat Nanotechnol 2007;2:780–3. https://doi.org/10.1038/nnano.2007.388.
[64] Taloni A, Ben Amar M, Zapperi S, La Porta CAM. The role of pressure in cancer growth. Eur Phys J Plus 2015;130:224. https://doi.org/10.1140/epjp/i2015-15224-0.
[65] Chaudhuri O, Cooper-White J, Janmey PA, Mooney DJ, Shenoy VB. Effects of extracellular matrix viscoelasticity on cellular behaviour. Nature 2020;584:535–46. https://doi.org/10.1038/s41586-020-2612-2.
[66] Chang S-W, Buehler MJ. Molecular biomechanics of collagen molecules. Mater Today 2014;17:70–6. https://doi.org/10.1016/j.mattod.2014.01.019.
[67] Bancelin S, Aimé C, Gusachenko I, Kowalczuk L, Latour G, Coradin T, et al. Determination of collagen fibril size via absolute measurements of second-harmonic generation signals. Nat Commun 2014;5:4920. https://doi.org/10.1038/ncomms5920.
[68] Hulmes DJS. Building Collagen Molecules, Fibrils, and Suprafibrillar Structures. J Struct Biol 2002;137:2–10. https://doi.org/10.1006/jsbi.2002.4450.
[69] Mouw JK, Ou G, Weaver VM. Extracellular matrix assembly: a multiscale deconstruction. Nat Rev Mol Cell Biol 2014;15:771–85. https://doi.org/10.1038/nrm3902.
[70] Yanagishita M. Function of proteoglycans in the extracellular matrix. Acta Pathol Jpn 1993;43:283–93. https://doi.org/10.1111/j.1440-1827.1993.tb02569.x.
[71] Kechagia JZ, Ivaska J, Roca-Cusachs P. Integrins as biomechanical sensors of the microenvironment. Nat Rev Mol Cell Biol 2019;20:457–73. https://doi.org/10.1038/s41580-019-0134-2.
[72] Chowdhury F, Li ITS, Leslie BJ, Doğanay S, Singh R, Wang X, et al. Single molecular force across single integrins dictates cell spreading. Integr Biol 2015;7:1265–71. https://doi.org/10.1039/C5IB00080G.
[73] Wang X, Sun J, Xu Q, Chowdhury F, Roein-Peikar M, Wang Y, et al. Integrin Molecular Tension within Motile Focal Adhesions. Biophys J 2015;109:2259–67. https://doi.org/10.1016/j.bpj.2015.10.029.

[74] Wehrle-Haller B. Structure and function of focal adhesions. Curr Opin Cell Biol 2012;24:116–24. https://doi.org/10.1016/j.ceb.2011.11.001.
[75] Pegoraro AF, Janmey P, Weitz DA. Mechanical Properties of the Cytoskeleton and Cells. Cold Spring Harb Perspect Biol 2017;9. https://doi.org/10.1101/cshperspect.a022038.
[76] Svitkina TM. Actin Cell Cortex: Structure and Molecular Organization. Trends Cell Biol 2020;30:556–65. https://doi.org/10.1016/j.tcb.2020.03.005.
[77] Schwayer C, Sikora M, Slováková J, Kardos R, Heisenberg C-P. Actin Rings of Power. Dev Cell 2016;37:493–506. https://doi.org/10.1016/j.devcel.2016.05.024.
[78] Cooper GM. Actin, Myosin, and Cell Movement. Cell Mol Approach 2nd Ed 2000.
[79] Blanchoin L, Boujemaa-Paterski R, Sykes C, Plastino J. Actin Dynamics, Architecture, and Mechanics in Cell Motility. Physiol Rev 2014;94:235–63. https://doi.org/10.1152/physrev.00018.2013.
[80] Sanghvi-Shah R, Weber GF. Intermediate Filaments at the Junction of Mechanotransduction, Migration, and Development. Front Cell Dev Biol 2017;5. https://doi.org/10.3389/fcell.2017.00081.
[81] Galou M, Gao J, Humbert J, Mericskay M, Li Z, Paulin D, et al. The importance of intermediate filaments in the adaptation of tissues to mechanical stress: evidence from gene knockout studies. Biol Cell 1997;89:85–97.
[82] Charrier EE, Janmey PA. Mechanical properties of intermediate filament proteins. Methods Enzymol 2016;568:35–57. https://doi.org/10.1016/bs.mie.2015.09.009.
[83] Holthöfer B, Windoffer R, Troyanovsky S, Leube RE. Structure and function of desmosomes. Int Rev Cytol 2007;264:65–163. https://doi.org/10.1016/S0074-7696(07)64003-0.
[84] Green KJ, Jones JCR. Desmosomes and hemidesmosomes: structure and function of molecular components. FASEB J 1996;10:871–81. https://doi.org/10.1096/fasebj.10.8.8666164.
[85] Hawkins T, Mirigian M, Selcuk Yasar M, Ross JL. Mechanics of microtubules. J Biomech 2010;43:23–30. https://doi.org/10.1016/j.jbiomech.2009.09.005.
[86] Tolić-Nørrelykke IM. Push-me-pull-you: how microtubules organize the cell interior. Eur Biophys J 2008;37:1271–8. https://doi.org/10.1007/s00249-008-0321-0.
[87] Singh A, Saha T, Begemann I, Ricker A, Nüsse H, Thorn-Seshold O, et al. Polarized microtubule dynamics directs cell mechanics and coordinates forces during epithelial morphogenesis. Nat Cell Biol 2018;20:1126–33. https://doi.org/10.1038/s41556-018-0193-1.
[88] Vleugel M, Kok M, Dogterom M. Understanding force-generating microtubule systems through in vitro reconstitution. Cell Adhes Migr 2016;10:475–94. https://doi.org/10.1080/19336918.2016.1241923.
[89] Matis M. The Mechanical Role of Microtubules in Tissue Remodeling. BioEssays 2020;42:1900244. https://doi.org/10.1002/bies.201900244.
[90] Bose P, Eyckmans J, Nguyen TD, Chen CS, Reich DH. Effects of Geometry on the Mechanics and Alignment of Three-Dimensional Engineered Microtissues. ACS Biomater Sci Eng 2018. https://doi.org/10.1021/acsbiomaterials.8b01183.

[91] Campàs O, Mammoto T, Hasso S, Sperling RA, O'Connell D, Bischof AG, et al. Quantifying cell-generated mechanical forces within living embryonic tissues. Nat Methods 2014;11:183–9. https://doi.org/10.1038/nmeth.2761.
[92] Legant WR, Pathak A, Yang MT, Deshpande VS, McMeeking RM, Chen CS. Microfabricated tissue gauges to measure and manipulate forces from 3D microtissues. Proc Natl Acad Sci 2009;106:10097–102. https://doi.org/10.1073/pnas.0900174106.
[93] Aoun L, Larnier S, Weiss P, Cazales M, Herbulot A, Ducommun B, et al. Measure and characterization of the forces exerted by growing multicellular spheroids using microdevice arrays. PLOS ONE 2019;14:e0217227. https://doi.org/10.1371/journal.pone.0217227.
[94] Wisdom KM, Adebowale K, Chang J, Lee JY, Nam S, Desai R, et al. Matrix mechanical plasticity regulates cancer cell migration through confining microenvironments. Nat Commun 2018;9:4144. https://doi.org/10.1038/s41467-018-06641-z.
[95] Guillou L, Babataheri A, Puech P-H, Barakat AI, Husson J. Dynamic monitoring of cell mechanical properties using profile microindentation. Sci Rep 2016;6:21529. https://doi.org/10.1038/srep21529.
[96] Beekmans SV, Emanuel KS, Smit TH, Iannuzzi D. Minimally Invasive Micro-Indentation: mapping tissue mechanics at the tip of an 18G needle. Sci Rep 2017;7:11364. https://doi.org/10.1038/s41598-017-10526-4.
[97] Chen SH, Soh AK. The capillary force in micro- and nano-indentation with different indenter shapes. Int J Solids Struct 2008;45:3122–37. https://doi.org/10.1016/j.ijsolstr.2008.01.014.
[98] Braunsmann C, Seifert J, Rheinlaender J, Schäffer TE. High-speed force mapping on living cells with a small cantilever atomic force microscope. Rev Sci Instrum 2014;85:073703. https://doi.org/10.1063/1.4885464.
[99] Lekka M, Gil D, Pogoda K, Dulińska-Litewka J, Jach R, Gostek J, et al. Cancer cell detection in tissue sections using AFM. Arch Biochem Biophys 2012;518:151–6. https://doi.org/10.1016/j.abb.2011.12.013.
[100] Stylianopoulos T. The Solid Mechanics of Cancer and Strategies for Improved Therapy. J Biomech Eng 2017;139. https://doi.org/10.1115/1.4034991.
[101] Vogel A, Venugopalan V. Mechanisms of Pulsed Laser Ablation of Biological Tissues. Chem Rev 2003;103:577–644. https://doi.org/10.1021/cr010379n.
[102] González-Bermúdez B, Guinea GV, Plaza GR. Advances in Micropipette Aspiration: Applications in Cell Biomechanics, Models, and Extended Studies. Biophys J 2019;116:587–94. https://doi.org/10.1016/j.bpj.2019.01.004.
[103] Sawicka A, Babataheri A, Dogniaux S, Barakat AI, Gonzalez-Rodriguez D, Hivroz C, et al. Micropipette force probe to quantify single-cell force generation: Application to T-cell activation. Mol Biol Cell 2017;28:3229–39. https://doi.org/10.1091/mbc.E17-06-0385.
[104] Hogan B, Babataheri A, Hwang Y, Barakat AI, Husson J. Characterizing Cell Adhesion by Using Micropipette Aspiration. Biophys J 2015;109:209–19. https://doi.org/10.1016/j.bpj.2015.06.015.

[105] Biro M, Maître J-L. Chapter 14 - Dual pipette aspiration: A unique tool for studying intercellular adhesion. In: Paluch EK, editor. Methods Cell Biol., vol. 125, Academic Press; 2015, p. 255–67. https://doi.org/10.1016/bs.mcb.2014.10.007.
[106] Chu Y-S, Thomas WA, Eder O, Pincet F, Perez E, Thiery JP, et al. Force measurements in E-cadherin–mediated cell doublets reveal rapid adhesion strengthened by actin cytoskeleton remodeling through Rac and Cdc42. J Cell Biol 2004;167:1183–94. https://doi.org/10.1083/jcb.200403043.
[107] Maître J-L, Berthoumieux H, Krens SFG, Salbreux G, Jülicher F, Paluch E, et al. Adhesion Functions in Cell Sorting by Mechanically Coupling the Cortices of Adhering Cells. Science 2012;338:253–6. https://doi.org/10.1126/science.1225399.
[108] Lee LM, Lee JW, Chase D, Gebrezgiabhier D, Liu AP. Development of an advanced microfluidic micropipette aspiration device for single cell mechanics studies. Biomicrofluidics 2016;10:054105. https://doi.org/10.1063/1.4962968.
[109] Capitanio M, Pavone FS. Interrogating Biology with Force: Single Molecule High-Resolution Measurements with Optical Tweezers. Biophys J 2013;105:1293–303. https://doi.org/10.1016/j.bpj.2013.08.007.
[110] Svoboda K, Block SM. Force and velocity measured for single kinesin molecules. Cell 1994;77:773–84. https://doi.org/10.1016/0092-8674(94)90060-4.
[111] Staunton JR, Vieira W, Fung KL, Lake R, Devine A, Tanner K. Mechanical properties of the tumor stromal microenvironment probed in vitro and ex vivo by in situ-calibrated optical trap-based active microrheology. Cell Mol Bioeng 2016;9:398–417. https://doi.org/10.1007/s12195-016-0460-9.
[112] Wottawah F, Schinkinger S, Lincoln B, Ebert S, Müller K, Sauer F, et al. Characterizing single suspended cells by optorheology. Acta Biomater 2005;1:263–71. https://doi.org/10.1016/j.actbio.2005.02.010.
[113] Guck J, Schinkinger S, Lincoln B, Wottawah F, Ebert S, Romeyke M, et al. Optical Deformability as an Inherent Cell Marker for Testing Malignant Transformation and Metastatic Competence. Biophys J 2005;88:3689–98. https://doi.org/10.1529/biophysj.104.045476.
[114] Coughlin MF, Bielenberg DR, Lenormand G, Marinkovic M, Waghorne CG, Zetter BR, et al. Cytoskeletal stiffness, friction, and fluidity of cancer cell lines with different metastatic potential. Clin Exp Metastasis 2013;30:237–50. https://doi.org/10.1007/s10585-012-9531-z.
[115] Kasza KE, Vader D, Köster S, Wang N, Weitz DA. Magnetic Twisting Cytometry. Cold Spring Harb Protoc 2011;2011:pdb.prot5599. https://doi.org/10.1101/pdb.prot5599.
[116] Zhang Y, Wei F, Poh Y-C, Jia Q, Chen J, Chen J, et al. Interfacing 3D magnetic twisting cytometry with confocal fluorescence microscopy to image force responses in living cells. Nat Protoc 2017;12:1437–50. https://doi.org/10.1038/nprot.2017.042.
[117] Guo F, Mao Z, Chen Y, Xie Z, Lata JP, Li P, et al. Three-dimensional manipulation of single cells using surface acoustic waves. Proc Natl Acad Sci 2016;113:1522–7. https://doi.org/10.1073/pnas.1524813113.

[118] Ozcelik A, Rufo J, Guo F, Gu Y, Li P, Lata J, et al. Acoustic tweezers for the life sciences. Nat Methods 2018;15:1021–8. https://doi.org/10.1038/s41592-018-0222-9.
[119] Sitters G, Kamsma D, Thalhammer G, Ritsch-Marte M, Peterman EJG, Wuite GJL. Acoustic force spectroscopy. Nat Methods 2015;12:47–50. https://doi.org/10.1038/nmeth.3183.
[120] Kamsma D, Creyghton R, Sitters G, Wuite GJL, Peterman EJG. Tuning the Music: Acoustic Force Spectroscopy (AFS) 2.0. Methods 2016;105:26–33. https://doi.org/10.1016/j.ymeth.2016.05.002.
[121] Tassieri M, Giudice FD, Robertson EJ, Jain N, Fries B, Wilson R, et al. Microrheology with Optical Tweezers: Measuring the relative viscosity of solutions ' at a glance .' Sci Rep 2015;5:8831. https://doi.org/10.1038/srep08831.
[122] Insana MF, Pellot-Barakat C, Sridhar M, Lindfors KK. Viscoelastic Imaging of Breast Tumor Microenvironment With Ultrasound. J Mammary Gland Biol Neoplasia 2004;9:393–404. https://doi.org/10.1007/s10911-004-1409-5.
[123] Fovargue D, Fiorito M, Capilnasiu A, Nordsletten D, Lee J, Sinkus R. Towards noninvasive estimation of tumour pressure by utilising MR elastography and nonlinear biomechanical models: a simulation and phantom study. Sci Rep 2020;10:5588. https://doi.org/10.1038/s41598-020-62367-3.
[124] Kennedy BF, Wijesinghe P, Sampson DD. The emergence of optical elastography in biomedicine. Nat Photonics 2017;11:215–21. https://doi.org/10.1038/nphoton.2017.6.
[125] Kennedy KM, Chin L, McLaughlin RA, Latham B, Saunders CM, Sampson DD, et al. Quantitative micro-elastography: imaging of tissue elasticity using compression optical coherence elastography. Sci Rep 2015;5:15538. https://doi.org/10.1038/srep15538.
[126] Prevedel R, Diz-Muñoz A, Ruocco G, Antonacci G. Brillouin microscopy: an emerging tool for mechanobiology. Nat Methods 2019;16:969–77. https://doi.org/10.1038/s41592-019-0543-3.
[127] Scarcelli G, Polacheck WJ, Nia HT, Patel K, Grodzinsky AJ, Kamm RD, et al. Noncontact three-dimensional mapping of intracellular hydromechanical properties by Brillouin microscopy. Nat Methods 2015;12:1132–4. https://doi.org/10.1038/nmeth.3616.
[128] Tan JL, Tien J, Pirone DM, Gray DS, Bhadriraju K, Chen CS. Cells lying on a bed of microneedles: An approach to isolate mechanical force. Proc Natl Acad Sci 2003;100:1484–9. https://doi.org/10.1073/pnas.0235407100.
[129] Trichet L, Digabel JL, Hawkins RJ, Vedula SRK, Gupta M, Ribrault C, et al. Evidence of a large-scale mechanosensing mechanism for cellular adaptation to substrate stiffness. Proc Natl Acad Sci 2012;109:6933–8. https://doi.org/10.1073/pnas.1117810109.
[130] Zhao R, Boudou T, Wang W, Chen CS, Reich DH. Decoupling cell and matrix mechanics in engineered microtissues using magnetically actuated microcantilevers. Adv Mater Deerfield Beach Fla 2013;25:1699–705. https://doi.org/10.1002/adma.201203585.

[131] Zhao R, Chen CS, Reich DH. Force-driven evolution of mesoscale structure in engineered 3D microtissues and the modulation of tissue stiffening. Biomaterials 2014;35:5056–64. https://doi.org/10.1016/j.biomaterials.2014.02.020.
[132] Walker M, Rizzuto P, Godin M, Pelling AE. Structural and mechanical remodeling of the cytoskeleton maintains tensional homeostasis in 3D microtissues under acute dynamic stretch. Sci Rep 2020;10:7696. https://doi.org/10.1038/s41598-020-64725-7.
[133] Walker M, Godin M, Pelling AE. A vacuum-actuated microtissue stretcher for long-term exposure to oscillatory strain within a 3D matrix. Biomed Microdevices 2018;20:43. https://doi.org/10.1007/s10544-018-0286-4.
[134] Serwane F, Mongera A, Rowghanian P, Kealhofer DA, Lucio AA, Hockenbery ZM, et al. In vivo quantification of spatially varying mechanical properties in developing tissues. Nat Methods 2017;14:181–6. https://doi.org/10.1038/nmeth.4101.
[135] Lucio AA, Mongera A, Shelton E, Chen R, Doyle AM, Campàs O. Spatiotemporal variation of endogenous cell-generated stresses within 3D multicellular spheroids. Sci Rep 2017;7:12022. https://doi.org/10.1038/s41598-017-12363-x.
[136] Dolega ME, Delarue M, Ingremeau F, Prost J, Delon A, Cappello G. Cell-like pressure sensors reveal increase of mechanical stress towards the core of multicellular spheroids under compression. Nat Commun 2017;8:ncomms14056. https://doi.org/10.1038/ncomms14056.
[137] Mohagheghian E, Luo J, Chen J, Chaudhary G, Chen J, Sun J, et al. Quantifying compressive forces between living cell layers and within tissues using elastic round microgels. Nat Commun 2018;9:1878. https://doi.org/10.1038/s41467-018-04245-1.
[138] Alshehri AM, Wilson OC, Dahal B, Philip J, Luo X, Raub CB. Magnetic nanoparticle-loaded alginate beads for local micro-actuation of in vitro tissue constructs. Colloids Surf B Biointerfaces 2017;159:945–55. https://doi.org/10.1016/j.colsurfb.2017.08.062.
[139] Lee W, Kalashnikov N, Mok S, Halaoui R, Kuzmin E, Putnam AJ, et al. Dispersible hydrogel force sensors reveal patterns of solid mechanical stress in multicellular spheroid cultures. Nat Commun 2019;10:144. https://doi.org/10.1038/s41467-018-07967-4.
[140] Wu P-H, Aroush DR-B, Asnacios A, Chen W-C, Dokukin ME, Doss BL, et al. A comparison of methods to assess cell mechanical properties. Nat Methods 2018;15:491. https://doi.org/10.1038/s41592-018-0015-1.
[141] Moeendarbary E, Harris AR. Cell mechanics: principles, practices, and prospects. Wiley Interdiscip Rev Syst Biol Med 2014;6:371–88. https://doi.org/10.1002/wsbm.1275.
[142] Solnica-Krezel L, Eaton S. Embryo morphogenesis: getting down to cells and molecules. Development 2003;130:4229–33. https://doi.org/10.1242/dev.00693.
[143] Nelson CM, Tien J. Microstructured extracellular matrices in tissue engineering and development. Curr Opin Biotechnol 2006;17:518–23. https://doi.org/10.1016/j.copbio.2006.08.011.

[144] Discher DE, Mooney DJ, Zandstra PW. Growth Factors, Matrices, and Forces Combine and Control Stem Cells. Science 2009;324:1673–7. https://doi.org/10.1126/science.1171643.
[145] Keung AJ, Kumar S, Schaffer DV. Presentation Counts: Microenvironmental Regulation of Stem Cells by Biophysical and Material Cues. Annu Rev Cell Dev Biol 2010;26:533–56. https://doi.org/10.1146/annurev-cellbio-100109-104042.
[146] Eyckmans J, Boudou T, Yu X, Chen CS. A Hitchhiker's Guide to Mechanobiology. Dev Cell 2011;21:35–47. https://doi.org/10.1016/j.devcel.2011.06.015.
[147] Nelson CM, Gleghorn JP. Sculpting Organs: Mechanical Regulation of Tissue Development. Annu Rev Biomed Eng 2012;14:129–54. https://doi.org/10.1146/annurev-bioeng-071811-150043.
[148] Mammoto T, Mammoto A, Ingber DE. Mechanobiology and Developmental Control. Annu Rev Cell Dev Biol 2013;29:27–61. https://doi.org/10.1146/annurev-cellbio-101512-122340.
[149] Sinha R, Verdonschot N, Koopman B, Rouwkema J. Tuning Cell and Tissue Development by Combining Multiple Mechanical Signals. Tissue Eng Part B Rev 2017;23:494–504. https://doi.org/10.1089/ten.teb.2016.0500.
[150] Heer NC, Martin AC. Tension, contraction and tissue morphogenesis. Development 2017;144:4249–60. https://doi.org/10.1242/dev.151282.
[151] Maechler FA, Allier C, Roux A, Tomba C. Curvature-dependent constraints drive remodeling of epithelia. J Cell Sci 2019;132. https://doi.org/10.1242/jcs.222372.
[152] Huebsch N, Arany PR, Mao AS, Shvartsman D, Ali OA, Bencherif SA, et al. Harnessing traction-mediated manipulation of the cell/matrix interface to control stem-cell fate. Nat Mater 2010;9:518–26. https://doi.org/10.1038/nmat2732.
[153] Gkretsi V, Stylianopoulos T. Cell Adhesion and Matrix Stiffness: Coordinating Cancer Cell Invasion and Metastasis. Front Oncol 2018;8. https://doi.org/10.3389/fonc.2018.00145.
[154] Najafi M, Farhood B, Mortezaee K. Extracellular matrix (ECM) stiffness and degradation as cancer drivers. J Cell Biochem 2019;120:2782–90. https://doi.org/10.1002/jcb.27681.
[155] Li Y, Fanous MJ, Kilian KA, Popescu G. Quantitative phase imaging reveals matrix stiffness-dependent growth and migration of cancer cells. Sci Rep 2019;9:248. https://doi.org/10.1038/s41598-018-36551-5.
[156] Sridharan R, Cavanagh B, Cameron AR, Kelly DJ, O'Brien FJ. Material stiffness influences the polarization state, function and migration mode of macrophages. Acta Biomater 2019. https://doi.org/10.1016/j.actbio.2019.02.048.
[157] Zahn JT, Louban I, Jungbauer S, Bissinger M, Kaufmann D, Kemkemer R, et al. Age-Dependent Changes in Microscale Stiffness and Mechanoresponses of Cells. Small 2011;7:1480–7. https://doi.org/10.1002/smll.201100146.
[158] Kohn JC, Chen A, Cheng S, Kowal DR, King MR, Reinhart-King CA. Mechanical heterogeneities in the subendothelial matrix develop with age and decrease with exercise. J Biomech 2016;49:1447–53. https://doi.org/10.1016/j.jbiomech.2016.03.016.

[159] Proestaki M, Ogren A, Burkel B, Notbohm J. Modulus of Fibrous Collagen at the Length Scale of a Cell. Exp Mech 2019. https://doi.org/10.1007/s11340-018-00453-4.
[160] Wang N, Ingber DE. Probing transmembrane mechanical coupling and cytomechanics using magnetic twisting cytometry. Biochem Cell Biol 1995;73:327–35. https://doi.org/10.1139/o95-041.
[161] Yamada S, Wirtz D, Kuo SC. Mechanics of Living Cells Measured by Laser Tracking Microrheology. Biophys J 2000;78:1736–47. https://doi.org/10.1016/S0006-3495(00)76725-7.
[162] Ashkin A. Optical trapping and manipulation of neutral particles using lasers. Proc Natl Acad Sci 1997;94:4853–60. https://doi.org/10.1073/pnas.94.10.4853.
[163] Buxboim A, Rajagopal K, Brown AEX, Discher DE. How deeply cells feel: methods for thin gels. J Phys Condens Matter Inst Phys J 2010;22. https://doi.org/10.1088/0953-8984/22/19/194116.
[164] Pelton R. Poly(N-isopropylacrylamide) (PNIPAM) is never hydrophobic. J Colloid Interface Sci 2010;348:673–4. https://doi.org/10.1016/j.jcis.2010.05.034.
[165] Ward MA, Georgiou TK. Thermoresponsive Polymers for Biomedical Applications. Polymers 2011;3:1215–42. https://doi.org/10.3390/polym3031215.
[166] Ma X, Schickel ME, Stevenson MD, Sarang-Sieminski AL, Gooch KJ, Ghadiali SN, et al. Fibers in the Extracellular Matrix Enable Long-Range Stress Transmission between Cells. Biophys J 2013;104:1410–8. https://doi.org/10.1016/j.bpj.2013.02.017.
[167] Gancheva T, Virgilio N. Enhancing and Tuning the Response of Environmentally Sensitive Hydrogels With Embedded and Interconnected Pore Networks. Macromolecules 2016;49:5866–76. https://doi.org/10.1021/acs.macromol.6b01411.
[168] Bhan C, Mandlewala R, Gebregeorgis A, Raghavan D. Adsorption–Desorption Study of BSA Conjugated Silver Nanoparticles (Ag/BSA NPs) on Collagen Immobilized Substrates. Langmuir 2012;28:17043–52. https://doi.org/10.1021/la303539n.
[169] Ellmerer M, Schaupp L, Brunner GA, Sendlhofer G, Wutte A, Wach P, et al. Measurement of interstitial albumin in human skeletal muscle and adipose tissue by open-flow microperfusion. Am J Physiol Endocrinol Metab 2000;278:E352-356. https://doi.org/10.1152/ajpendo.2000.278.2.E352.
[170] Tevis KM, Colson YL, Grinstaff MW. Embedded Spheroids as Models of the Cancer Microenvironment. Adv Biosyst 2017;1. https://doi.org/10.1002/adbi.201700083.
[171] Zhao L, Mok S, Moraes C. Micropocket hydrogel devices for all-in-one formation, assembly, and analysis of aggregate-based tissues. Biofabrication 2019. https://doi.org/10.1088/1758-5090/ab30b4.
[172] Atefi E, Lemmo S, Fyffe D, Luker GD, Tavana H. High Throughput, Polymeric Aqueous Two-Phase Printing of Tumor Spheroids. Adv Funct Mater 2014;24:6509–15. https://doi.org/10.1002/adfm.201401302.

[173] Montel F, Delarue M, Elgeti J, Malaquin L, Basan M, Risler T, et al. Stress Clamp Experiments on Multicellular Tumor Spheroids. Phys Rev Lett 2011;107:188102. https://doi.org/10.1103/PhysRevLett.107.188102.
[174] Cisneros Castillo LR, Oancea A-D, Stüllein C, Régnier-Vigouroux A. Evaluation of Consistency in Spheroid Invasion Assays. Sci Rep 2016;6. https://doi.org/10.1038/srep28375.
[175] Boyd NF, Li Q, Melnichouk O, Huszti E, Martin LJ, Gunasekara A, et al. Evidence That Breast Tissue Stiffness Is Associated with Risk of Breast Cancer. PLOS ONE 2014;9:e100937. https://doi.org/10.1371/journal.pone.0100937.
[176] Lang NR, Skodzek K, Hurst S, Mainka A, Steinwachs J, Schneider J, et al. Biphasic response of cell invasion to matrix stiffness in three-dimensional biopolymer networks. Acta Biomater 2015;13:61–7. https://doi.org/10.1016/j.actbio.2014.11.003.
[177] Wang WY, Davidson CD, Lin D, Baker BM. Actomyosin contractility-dependent matrix stretch and recoil induces rapid cell migration. Nat Commun 2019;10:1186. https://doi.org/10.1038/s41467-019-09121-0.
[178] Liu H, Wen J, Xiao Y, Liu J, Hopyan S, Radisic M, et al. In Situ Mechanical Characterization of the Cell Nucleus by Atomic Force Microscopy. ACS Nano 2014;8:3821–8. https://doi.org/10.1021/nn500553z.
[179] Kasza KE, Rowat AC, Liu J, Angelini TE, Brangwynne CP, Koenderink GH, et al. The cell as a material. Curr Opin Cell Biol 2007;19:101–7. https://doi.org/10.1016/j.ceb.2006.12.002.
[180] Chang JM, Park IA, Lee SH, Kim WH, Bae MS, Koo HR, et al. Stiffness of tumours measured by shear-wave elastography correlated with subtypes of breast cancer. Eur Radiol 2013;23:2450–8. https://doi.org/10.1007/s00330-013-2866-2.
[181] Pulaski BA, Ostrand- Rosenberg S. Mouse 4T1 Breast Tumor Model. Curr Protoc Immunol 2000;39:20.2.1-20.2.16. https://doi.org/10.1002/0471142735.im2002s39.
[182] Agus DB, Alexander JF, Arap W, Ashili S, Aslan JE, Austin RH, et al. A physical sciences network characterization of non-tumorigenic and metastatic cells. Sci Rep 2013;3. https://doi.org/10.1038/srep01449.
[183] Han YL, Pegoraro AF, Li H, Li K, Yuan Y, Xu G, et al. Cell swelling, softening and invasion in a three-dimensional breast cancer model. Nat Phys 2019:1–8. https://doi.org/10.1038/s41567-019-0680-8.
[184] Paszek MJ, Zahir N, Johnson KR, Lakins JN, Rozenberg GI, Gefen A, et al. Tensional homeostasis and the malignant phenotype. Cancer Cell 2005;8:241–54. https://doi.org/10.1016/j.ccr.2005.08.010.
[185] Chaudhuri O, Gu L, Klumpers D, Darnell M, Bencherif SA, Weaver JC, et al. Hydrogels with tunable stress relaxation regulate stem cell fate and activity. Nat Mater 2016;15:326–34. https://doi.org/10.1038/nmat4489.
[186] Pei Y, Chen J, Yang L, Shi L, Tao Q, Hui B, et al. The effect of pH on the LCST of poly(N-isopropylacrylamide) and poly(N-isopropylacrylamide-co-acrylic acid). J Biomater Sci Polym Ed 2004;15:585–94. https://doi.org/10.1163/156856204323046852.

[187] Zhang X, Lin Y, Gillies RJ. Tumor pH and its measurement. J Nucl Med Off Publ Soc Nucl Med 2010;51:1167–70. https://doi.org/10.2967/jnumed.109.068981.
[188] Sunyer R, Trepat X, Fredberg JJ, Farré R, Navajas D. The temperature dependence of cell mechanics measured by atomic force microscopy. Phys Biol 2009;6:025009. https://doi.org/10.1088/1478-3975/6/2/025009.
[189] Demetri-Lewis A, Slanetz PJ, Eisenberg RL. Breast Calcifications: The Focal Group. Am J Roentgenol 2012;198:W325–43. https://doi.org/10.2214/AJR.10.5732.
[190] Ham SL, Atefi E, Fyffe D, Tavana H. Robotic Production of Cancer Cell Spheroids with an Aqueous Two-phase System for Drug Testing. JoVE J Vis Exp 2015:e52754. https://doi.org/10.3791/52754.
[191] Dougherty R. Extensions of DAMAS and Benefits and Limitations of Deconvolution in Beamforming. 11th AIAACEAS Aeroacoustics Conf., American Institute of Aeronautics and Astronautics; 2005. https://doi.org/10.2514/6.2005-2961.
[192] Takigawa T, Morino Y, Urayama K, Masuda T. Poisson's ratio of polyacrylamide (PAAm) gels. Polym Gels Netw 1996;4:1–5. https://doi.org/10.1016/0966-7822(95)00013-5.
[193] Schindelin J, Arganda-Carreras I, Frise E, Kaynig V, Longair M, Pietzsch T, et al. Fiji: an open-source platform for biological-image analysis. Nat Methods 2012;9:676–82. https://doi.org/10.1038/nmeth.2019.
[194] Maas SA, Ellis BJ, Ateshian GA, Weiss JA. FEBio: Finite Elements for Biomechanics. J Biomech Eng 2012;134:11005-NaN. https://doi.org/10.1115/1.4005694.
[195] Maas SA, Erdemir A, Halloran JP, Weiss JA. A general framework for application of prestrain to computational models of biological materials. J Mech Behav Biomed Mater 2016;61:499–510. https://doi.org/10.1016/j.jmbbm.2016.04.012.
[196] Voutouri C, Mpekris F, Papageorgis P, Odysseos AD, Stylianopoulos T. Role of Constitutive Behavior and Tumor-Host Mechanical Interactions in the State of Stress and Growth of Solid Tumors. PLoS ONE 2014;9. https://doi.org/10.1371/journal.pone.0104717.
[197] Cheng G, Tse J, Jain RK, Munn LL. Micro-environmental mechanical stress controls tumor spheroid size and morphology by suppressing proliferation and inducing apoptosis in cancer cells. PloS One 2009;4:e4632. https://doi.org/10.1371/journal.pone.0004632.
[198] Helmlinger G, Netti PA, Lichtenbeld HC, Melder RJ, Jain RK. Solid stress inhibits the growth of multicellular tumor spheroids. Nat Biotechnol 1997;15:778–83. https://doi.org/10.1038/nbt0897-778.
[199] Kopanska KS, Alcheikh Y, Staneva R, Vignjevic D, Betz T. Tensile Forces Originating from Cancer Spheroids Facilitate Tumor Invasion. PLOS ONE 2016;11:e0156442. https://doi.org/10.1371/journal.pone.0156442.
[200] Nikkhah M, Strobl JS, Schmelz EM, Agah M. Evaluation of the influence of growth medium composition on cell elasticity. J Biomech 2011;44:762–6. https://doi.org/10.1016/j.jbiomech.2010.11.002.

[201] Li QS, Lee GYH, Ong CN, Lim CT. AFM indentation study of breast cancer cells. Biochem Biophys Res Commun 2008;374:609–13. https://doi.org/10.1016/j.bbrc.2008.07.078.
[202] Hayashi K, Iwata M. Stiffness of cancer cells measured with an AFM indentation method. J Mech Behav Biomed Mater 2015;49:105–11. https://doi.org/10.1016/j.jmbbm.2015.04.030.
[203] Costa EC, Moreira AF, de Melo-Diogo D, Gaspar VM, Carvalho MP, Correia IJ. 3D tumor spheroids: an overview on the tools and techniques used for their analysis. Biotechnol Adv 2016;34:1427–41. https://doi.org/10.1016/j.biotechadv.2016.11.002.
[204] Nunes AS, Barros AS, Costa EC, Moreira AF, Correia IJ. 3D tumor spheroids as in vitro models to mimic in vivo human solid tumors resistance to therapeutic drugs. Biotechnol Bioeng 2019;116:206–26. https://doi.org/10.1002/bit.26845.
[205] Mok S, Al Habyan S, Ledoux C, Lee W, MacDonald KN, McCaffrey L, et al. Mapping cellular-scale internal mechanics in 3D tissues with thermally responsive hydrogel probes. Nat Commun 2020;11:4757. https://doi.org/10.1038/s41467-020-18469-7.
[206] Augst AD, Kong HJ, Mooney DJ. Alginate Hydrogels as Biomaterials. Macromol Biosci 2006;6:623–33. https://doi.org/10.1002/mabi.200600069.
[207] Cao N. Fabrication of alginate hydrogel scaffolds and cell viability in calcium-crosslinked alginate hydrogel, 2011.
[208] Lee KY, Mooney DJ. Alginate: properties and biomedical applications. Prog Polym Sci 2012;37:106–26. https://doi.org/10.1016/j.progpolymsci.2011.06.003.
[209] Irby RB, Yeatman TJ. Role of Src expression and activation in human cancer. Oncogene 2000;19:5636–42. https://doi.org/10.1038/sj.onc.1203912.
[210] Frame MC. Newest findings on the oldest oncogene; how activated src does it. J Cell Sci 2004;117:989–98. https://doi.org/10.1242/jcs.01111.
[211] Holliday DL, Speirs V. Choosing the right cell line for breast cancer research. Breast Cancer Res BCR 2011;13:215. https://doi.org/10.1186/bcr2889.
[212] Palamidessi A, Malinverno C, Frittoli E, Corallino S, Barbieri E, Sigismund S, et al. Unjamming overcomes kinetic and proliferation arrest in terminally differentiated cells and promotes collective motility of carcinoma. Nat Mater 2019;18:1252–63. https://doi.org/10.1038/s41563-019-0425-1.
[213] Garcia S, Hannezo E, Elgeti J, Joanny J-F, Silberzan P, Gov NS. Physics of active jamming during collective cellular motion in a monolayer. Proc Natl Acad Sci 2015;112:15314–9. https://doi.org/10.1073/pnas.1510973112.
[214] Sadati M, Taheri Qazvini N, Krishnan R, Park CY, Fredberg JJ. Collective migration and cell jamming. Differentiation 2013;86:121–5. https://doi.org/10.1016/j.diff.2013.02.005.
[215] Oswald L, Grosser S, Smith DM, Käs JA. Jamming transitions in cancer. J Phys Appl Phys 2017;50:483001. https://doi.org/10.1088/1361-6463/aa8e83.
[216] Ilina O, Gritsenko PG, Syga S, Lippoldt J, La Porta CAM, Chepizhko O, et al. Cell–cell adhesion and 3D matrix confinement determine jamming transitions in breast

cancer invasion. Nat Cell Biol 2020;22:1103–15. https://doi.org/10.1038/s41556-020-0552-6.

[217] Chekhun S, Bezdenezhnykh N, Shvets J, Lukianova N. Expression of biomarkers related to cell adhesion, metastasis and invasion of breast cancer cell lines of different molecular subtype. Exp Oncol 2013;35:174–9.

[218] Castro MG, Leggett SE, Wong IY. Clustering and jamming in epithelial–mesenchymal co-cultures. Soft Matter 2016;12:8327–37. https://doi.org/10.1039/C6SM01287F.

[219] Haeger A, Krause M, Wolf K, Friedl P. Cell jamming: Collective invasion of mesenchymal tumor cells imposed by tissue confinement. Biochim Biophys Acta BBA - Gen Subj 2014;1840:2386–95. https://doi.org/10.1016/j.bbagen.2014.03.020.

[220] Eisenhoffer GT, Loftus PD, Yoshigi M, Otsuna H, Chien C-B, Morcos PA, et al. Crowding induces live cell extrusion to maintain homeostatic cell numbers in epithelia. Nature 2012;484:546–9. https://doi.org/10.1038/nature10999.

[221] Slattum GM, Rosenblatt J. Tumour cell invasion: an emerging role for basal epithelial cell extrusion. Nat Rev Cancer 2014;14:495–501. https://doi.org/10.1038/nrc3767.

[222] Ohsawa S, Vaughen J, Igaki T. Cell Extrusion: A Stress-Responsive Force for Good or Evil in Epithelial Homeostasis. Dev Cell 2018;44:284–96. https://doi.org/10.1016/j.devcel.2018.01.009.

[223] Kocgozlu L, Saw TB, Le AP, Yow I, Shagirov M, Wong E, et al. Epithelial Cell Packing Induces Distinct Modes of Cell Extrusions. Curr Biol 2016;26:2942–50. https://doi.org/10.1016/j.cub.2016.08.057.

[224] Barriga EH, Mayor R. Adjustable viscoelasticity allows for efficient collective cell migration. Semin Cell Dev Biol 2019;93:55–68. https://doi.org/10.1016/j.semcdb.2018.05.027.

[225] Trappmann B, Chen CS. How cells sense extracellular matrix stiffness: a material's perspective. Curr Opin Biotechnol 2013;24:948–53. https://doi.org/10.1016/j.copbio.2013.03.020.

[226] Pelham RJ, Wang Y. Cell locomotion and focal adhesions are regulated by substrate flexibility. Proc Natl Acad Sci 1997;94:13661–5. https://doi.org/10.1073/pnas.94.25.13661.

[227] Yeung T, Georges PC, Flanagan LA, Marg B, Ortiz M, Funaki M, et al. Effects of substrate stiffness on cell morphology, cytoskeletal structure, and adhesion. Cell Motil 2005;60:24–34. https://doi.org/10.1002/cm.20041.

[228] Zhao R, Boudou T, Wang W-G, Chen CS, Reich DH. Decoupling Cell and Matrix Mechanics in Engineered Microtissues Using Magnetically Actuated Microcantilevers. Adv Mater 2013;25:1699–705. https://doi.org/10.1002/adma.201203585.

[229] Tzvetkova-Chevolleau T, Stéphanou A, Fuard D, Ohayon J, Schiavone P, Tracqui P. The motility of normal and cancer cells in response to the combined influence of the substrate rigidity and anisotropic microstructure. Biomaterials 2008;29:1541–51. https://doi.org/10.1016/j.biomaterials.2007.12.016.

[230] Chaudhuri O, Gu L, Darnell M, Klumpers D, Bencherif SA, Weaver JC, et al. Substrate stress relaxation regulates cell spreading. Nat Commun 2015;6:6365. https://doi.org/10.1038/ncomms7365.
[231] Cameron AndrewR, Frith JessicaE, Cooper-White JustinJ. The influence of substrate creep on mesenchymal stem cell behaviour and phenotype. Biomaterials 2011;32:5979–93. https://doi.org/10.1016/j.biomaterials.2011.04.003.
[232] Gong Z, Szczesny SE, Caliari SR, Charrier EE, Chaudhuri O, Cao X, et al. Matching material and cellular timescales maximizes cell spreading on viscoelastic substrates. Proc Natl Acad Sci 2018;115:E2686–95. https://doi.org/10.1073/pnas.1716620115.
[233] Sinkus R, Siegmann K, Xydeas T, Tanter M, Claussen C, Fink M. MR elastography of breast lesions: Understanding the solid/liquid duality can improve the specificity of contrast-enhanced MR mammography. Magn Reson Med 2007;58:1135–44. https://doi.org/10.1002/mrm.21404.
[234] Nematbakhsh Y, Pang KT, Lim CT. Correlating the viscoelasticity of breast cancer cells with their malignancy. Converg Sci Phys Oncol 2017;3:034003. https://doi.org/10.1088/2057-1739/aa7ffb.
[235] Xie Y, Wang M, Cheng M, Gao Z, Wang G. The viscoelastic behaviors of several kinds of cancer cells and normal cells. J Mech Behav Biomed Mater 2019;91:54–8. https://doi.org/10.1016/j.jmbbm.2018.11.029.
[236] Maccabi A, Shin A, Namiri NK, Bajwa N, John MS, Taylor ZD, et al. Quantitative characterization of viscoelastic behavior in tissue-mimicking phantoms and ex vivo animal tissues. PLOS ONE 2018;13:e0191919. https://doi.org/10.1371/journal.pone.0191919.
[237] Crichton ML, Donose BC, Chen X, Raphael AP, Huang H, Kendall MAF. The viscoelastic, hyperelastic and scale dependent behaviour of freshly excised individual skin layers. Biomaterials 2011;32:4670–81. https://doi.org/10.1016/j.biomaterials.2011.03.012.
[238] Shim S, Kim MG, Jo K, Kang YS, Lee B, Yang S, et al. Dynamic Characterization of Human Breast Cancer Cells Using a Piezoresistive Microcantilever. J Biomech Eng 2010;132. https://doi.org/10.1115/1.4002180.
[239] Carmichael B, Babahosseini H, Mahmoodi SN, Agah M. The fractional viscoelastic response of human breast tissue cells. Phys Biol 2015;12:046001. https://doi.org/10.1088/1478-3975/12/4/046001.
[240] Schierbaum N, Rheinlaender J, E. Schäffer T. Combined atomic force microscopy (AFM) and traction force microscopy (TFM) reveals a correlation between viscoelastic material properties and contractile prestress of living cells. Soft Matter 2019;15:1721–9. https://doi.org/10.1039/C8SM01585F.
[241] Darling EM, Zauscher S, Block JA, Guilak F. A Thin-Layer Model for Viscoelastic, Stress-Relaxation Testing of Cells Using Atomic Force Microscopy: Do Cell Properties Reflect Metastatic Potential? Biophys J 2007;92:1784–91. https://doi.org/10.1529/biophysj.106.083097.
[242] Kumar S, Maxwell IZ, Heisterkamp A, Polte TR, Lele TP, Salanga M, et al. Viscoelastic Retraction of Single Living Stress Fibers and Its Impact on Cell Shape,

Cytoskeletal Organization, and Extracellular Matrix Mechanics. Biophys J 2006;90:3762–73. https://doi.org/10.1529/biophysj.105.071506.
[243] Illeperuma WRK, Sun J-Y, Suo Z, Vlassak JJ. Force and stroke of a hydrogel actuator. Soft Matter 2013;9:8504–11. https://doi.org/10.1039/C3SM51617B.
[244] Kumar V, Denis M, Gregory A, Bayat M, Mehrmohammadi M, Fazzio R, et al. Viscoelastic parameters as discriminators of breast masses: Initial human study results. PLOS ONE 2018;13:e0205717. https://doi.org/10.1371/journal.pone.0205717.
[245] Qiu Y, Sridhar M, Tsou JK, Lindfors KK, Insana MF. Ultrasonic Viscoelasticity Imaging of Nonpalpable Breast Tumors: Preliminary Results. Acad Radiol 2008;15:1526–33. https://doi.org/10.1016/j.acra.2008.05.023.
[246] Charras G, Yap AS. Tensile Forces and Mechanotransduction at Cell–Cell Junctions. Curr Biol 2018;28:R445–57. https://doi.org/10.1016/j.cub.2018.02.003.
[247] Mbalaviele G, Dunstan CR, Sasaki A, Williams PJ, Mundy GR, Yoneda T. E-cadherin expression in human breast cancer cells suppresses the development of osteolytic bone metastases in an experimental metastasis model. Cancer Res 1996;56:4063–70.
[248] Ambrosi D, Pezzuto S, Riccobelli D, Stylianopoulos T, Ciarletta P. Solid tumors are poroelastic solids with a chemo–mechanical feedback on growth. J Elast 2017;129:107. https://doi.org/10.1007/s10659-016-9619-9.
[249] Moeendarbary E, Valon L, Fritzsche M, Harris AR, Moulding DA, Thrasher AJ, et al. The cytoplasm of living cells behaves as a poroelastic material. Nat Mater 2013;12:253–61. https://doi.org/10.1038/nmat3517.
[250] Jiménez-Salazar JE, Posadas-Rodríguez P, Lazzarini-Lechuga RC, Luna-López A, Zentella-Dehesa A, Gómez-Quiroz LE, et al. Membrane-Initiated Estradiol Signaling of Epithelial-Mesenchymal Transition-Associated Mechanisms Through Regulation of Tight Junctions in Human Breast Cancer Cells. Horm Cancer 2014;5:161–73. https://doi.org/10.1007/s12672-014-0180-3.
[251] Kovbasnjuk O, Leader JP, Weinstein AM, Spring KR. Water does not flow across the tight junctions of MDCK cell epithelium. Proc Natl Acad Sci 1998;95:6526–30. https://doi.org/10.1073/pnas.95.11.6526.
[252] Wang M, Yang Y, Han L, Xu F, Li F. Cell mechanical microenvironment for cell volume regulation. J Cell Physiol 2020;235:4070–81. https://doi.org/10.1002/jcp.29341.
[253] Monnier S, Delarue M, Brunel B, Dolega ME, Delon A, Cappello G. Effect of an osmotic stress on multicellular aggregates. Methods 2016;94:114–9. https://doi.org/10.1016/j.ymeth.2015.07.009.
[254] Hulikova A, Swietach P. Rapid CO2 permeation across biological membranes: implications for CO2 venting from tissue. FASEB J 2014;28:2762–74. https://doi.org/10.1096/fj.13-241752.
[255] Angelucci C, Maulucci G, Lama G, Proietti G, Colabianchi A, Papi M, et al. Epithelial-Stromal Interactions in Human Breast Cancer: Effects on Adhesion, Plasma Membrane Fluidity and Migration Speed and Directness. PLOS ONE 2012;7:e50804. https://doi.org/10.1371/journal.pone.0050804.

[256] Chaudhuri O, Koshy ST, Branco da Cunha C, Shin J-W, Verbeke CS, Allison KH, et al. Extracellular matrix stiffness and composition jointly regulate the induction of malignant phenotypes in mammary epithelium. Nat Mater 2014;13:970–8. https://doi.org/10.1038/nmat4009.
[257] Basoli F, Giannitelli SM, Gori M, Mozetic P, Bonfanti A, Trombetta M, et al. Biomechanical Characterization at the Cell Scale: Present and Prospects. Front Physiol 2018;9. https://doi.org/10.3389/fphys.2018.01449.
[258] Young EWK. Cells, tissues, and organs on chips: challenges and opportunities for the cancer tumor microenvironment. Integr Biol 2013;5:1096–109. https://doi.org/10.1039/C3IB40076J.
[259] Nagelkerke A, Bussink J, Rowan AE, Span PN. The mechanical microenvironment in cancer: How physics affects tumours. Semin Cancer Biol 2015;35:62–70. https://doi.org/10.1016/j.semcancer.2015.09.001.
[260] Handorf AM, Zhou Y, Halanski MA, Li W-J. Tissue Stiffness Dictates Development, Homeostasis, and Disease Progression. Organogenesis 2015;11:1–15. https://doi.org/10.1080/15476278.2015.1019687.
[261] Yoon D-S, Wersto RP, Zhou W, Chrest FJ, Garrett ES, Kwon TK, et al. Variable Levels of Chromosomal Instability and Mitotic Spindle Checkpoint Defects in Breast Cancer. Am J Pathol 2002;161:391–7.
[262] Bakhoum SF, Cantley LC. The Multifaceted Role of Chromosomal Instability in Cancer and Its Microenvironment. Cell 2018;174:1347–60. https://doi.org/10.1016/j.cell.2018.08.027.
[263] Taubenberger AV, Girardo S, Träber N, Fischer- Friedrich E, Kräter M, Wagner K, et al. 3D Microenvironment Stiffness Regulates Tumor Spheroid Growth and Mechanics via p21 and ROCK. Adv Biosyst 2019;3:1900128. https://doi.org/10.1002/adbi.201900128.
[264] Gandalovičová A, Rosel D, Fernandes M, Veselý P, Heneberg P, Čermák V, et al. Migrastatics—Anti-metastatic and Anti-invasion Drugs: Promises and Challenges. Trends Cancer 2017;3:391–406. https://doi.org/10.1016/j.trecan.2017.04.008.
[265] Low BC, Pan CQ, Shivashankar GV, Bershadsky A, Sudol M, Sheetz M. YAP/TAZ as mechanosensors and mechanotransducers in regulating organ size and tumor growth. FEBS Lett 2014;588:2663–70. https://doi.org/10.1016/j.febslet.2014.04.012.
[266] Calses PC, Crawford JJ, Lill JR, Dey A. Hippo Pathway in Cancer: Aberrant Regulation and Therapeutic Opportunities. Trends Cancer 2019;5:297–307. https://doi.org/10.1016/j.trecan.2019.04.001.
[267] Thompson BJ. YAP/TAZ: Drivers of Tumor Growth, Metastasis, and Resistance to Therapy. BioEssays 2020;42:1900162. https://doi.org/10.1002/bies.201900162.
[268] Han Y. Analysis of the role of the Hippo pathway in cancer. J Transl Med 2019;17:116. https://doi.org/10.1186/s12967-019-1869-4.
[269] Moya IM, Castaldo SA, Mooter LV den, Soheily S, Sansores-Garcia L, Jacobs J, et al. Peritumoral activation of the Hippo pathway effectors YAP and TAZ suppresses liver cancer in mice. Science 2019;366:1029–34. https://doi.org/10.1126/science.aaw9886.

[270] Gaspar P, Tapon N. Sensing the local environment: actin architecture and Hippo signalling. Curr Opin Cell Biol 2014;31:74–83. https://doi.org/10.1016/j.ceb.2014.09.003.
[271] Azzolin L, Zanconato F, Bresolin S, Forcato M, Basso G, Bicciato S, et al. Role of TAZ as mediator of Wnt signaling. Cell 2012;151:1443–56. https://doi.org/10.1016/j.cell.2012.11.027.
[272] Imajo M, Miyatake K, Iimura A, Miyamoto A, Nishida E. A molecular mechanism that links Hippo signalling to the inhibition of Wnt/β-catenin signalling. EMBO J 2012;31:1109–22. https://doi.org/10.1038/emboj.2011.487.
[273] Wang J, Lü D, Mao D, Long M. Mechanomics: an emerging field between biology and biomechanics. Protein Cell 2014;5:518–31. https://doi.org/10.1007/s13238-014-0057-9.
[274] Ingber DE. Is it Time for Reviewer 3 to Request Human Organ Chip Experiments Instead of Animal Validation Studies? Adv Sci 2020;n/a:2002030. https://doi.org/10.1002/advs.202002030.
[275] Clevers H. Modeling Development and Disease with Organoids. Cell 2016;165:1586–97. https://doi.org/10.1016/j.cell.2016.05.082.